

1 **Evaluating Nitrogen Cycling in Terrestrial Biosphere Models: Implications for a Disconnect**  
2 **between the Future Terrestrial Carbon Sink and Nitrogen Cycles**

3 Sian Kou-Giesbrecht<sup>1,2</sup>, Vivek K. Arora<sup>1</sup>, Christian Seiler<sup>2</sup>Seiler<sup>3</sup>, Almut Arneeth<sup>3</sup>Arneeth<sup>4</sup>,  
4 Stefanie Falk<sup>4</sup>Falk<sup>5</sup>, Atul Jain<sup>5</sup>K. Jain<sup>6</sup>, Fortunat Joos<sup>6</sup>Joos<sup>7</sup>, Daniel Kennedy<sup>7</sup>Kennedy<sup>8</sup>, Jürgen  
5 Knauer<sup>8</sup>Knauer<sup>9</sup>, Stephen Sitch<sup>9</sup>Sitch<sup>10</sup>, Michael O'Sullivan<sup>9</sup>O'Sullivan<sup>10</sup>, Naiqing Pan<sup>10</sup>Pan<sup>11</sup>,  
6 Qing Sun<sup>6</sup>Sun<sup>7</sup>, Hanqin Tian<sup>10</sup>Tian<sup>11</sup>, Nicolas Vuichard<sup>11</sup>Vuichard<sup>12</sup>, and Sönke  
7 Zaehle<sup>12</sup>Zaehle<sup>13</sup>

8 <sup>1</sup>Canadian Centre for Climate Modelling and Analysis, Climate Research Division, Environment  
9 Canada, Victoria, Canada

10 <sup>2</sup>School<sup>2</sup>Department of Earth and Environmental Sciences, Dalhousie University, Halifax,  
11 Canada

12 <sup>3</sup>School of Environmental Studies, Queen's University, Kingston, Canada

13 <sup>3</sup>Karlsruhe<sup>4</sup>Karlsruhe Institute of Technology, Atmospheric Environmental Research, Garmisch-  
14 Partenkirchen, Germany

15 <sup>4</sup>Department<sup>5</sup>Department für Geographie, Ludwig-Maximilians-Universität Munich, München,  
16 Germany

17 <sup>5</sup>Department<sup>6</sup>Department of Atmospheric Sciences, University of Illinois Urbana-Champaign,  
18 Urbana, USA

19 <sup>6</sup>Climate<sup>7</sup>Climate and Environmental Physics, Physics Institute and Oeschger Centre for Climate  
20 Change Research, University of Bern, Bern, Switzerland

21 <sup>7</sup>National<sup>8</sup>National Center for Atmospheric Research, Climate and Global Dynamics, Terrestrial  
22 Sciences Section, Boulder, USA

23 <sup>8</sup>Hawkesbury<sup>9</sup>Hawkesbury Institute for the Environment, Western Sydney University, Penrith,  
24 Australia

25 <sup>9</sup>Faculty<sup>10</sup>Faculty of Environment, Science and Economy, University of Exeter, Exeter, UK

26 <sup>10</sup>Schiller<sup>11</sup>Schiller Institute for Integrated Science and Society, Department of Earth and  
27 Environmental Sciences, Boston College, Chestnut Hill, USA

28 <sup>11</sup>Laboratoire<sup>12</sup>Laboratoire des Sciences du Climat et de l'Environnement, LSCE-IPSL (CEA-  
29 CNRS-UVSQ), Université Paris-Saclay, Gif-sur-Yvette, France

30 <sup>12</sup>Max<sup>13</sup>Max Planck Institute for Biogeochemistry, Jena, Germany

31 *Correspondence to:* Sian Kou-Giesbrecht (sian.kougiesbrecht@ec.gc.ca)

32  
33 **Abstract**

34 Terrestrial carbon (C) sequestration is limited by nitrogen (N), ~~an empirically~~  
35 established constraint that could intensify under CO<sub>2</sub> fertilisation and future global change. The  
36 terrestrial C sink is estimated to currently sequester approximately a third of annual  
37 anthropogenic CO<sub>2</sub> emissions based on an ensemble of terrestrial biosphere models, which have  
38 been evaluated in their ability to reproduce observations of the C, water, and energy cycles.  
39 However, their ability to reproduce observations of N cycling and thus the regulation of  
40 terrestrial C sequestration by N has been largely unexplored. Here, we evaluate an ensemble of  
41 terrestrial biosphere models with coupled C-N cycling and their performance at simulating N  
42 cycling, outlining a framework for evaluating N cycling that can be applied across terrestrial  
43 biosphere models. We find that models exhibit significant variability across N pools and fluxes,  
44 simulating different magnitudes and trends over the historical period, despite their ability to  
45 generally reproduce the historical terrestrial C sink. Furthermore, there are no significant  
46 correlations between model performance in simulating N cycling and model performance in  
47 simulating C cycling, nor are there significant differences in model performance between models  
48 with different representations of fundamental N cycling processes. This suggests that the  
49 underlying N processes that regulate terrestrial C sequestration operate differently across models  
50 and ~~may not be fully captured. Furthermore, models tended to appear to be disconnected from C~~  
51 cycling. Models tend to overestimate tropical biological N fixation, vegetation C:N ratio, and soil  
52 C:N ratio but underestimate temperate biological N fixation relative to observations. However,  
53 there is significant uncertainty associated with measurements of N cycling processes given their  
54 scarcity (especially relative to those of C cycling processes) and their high spatiotemporal  
55 variability. Overall, our results suggest that terrestrial biosphere models that represent coupled C-  
56 N cycling (~~let alone those without a representation of N cycling~~) could be overestimating C  
57 storage per unit N, which could lead to biases in projections of the future terrestrial C sink under  
58 CO<sub>2</sub> fertilisation and future global change. (~~let alone those without a representation of N~~  
59 cycling). More extensive observations of N cycling processes and comparisons against  
60 experimental manipulations are crucial to evaluate N cycling and its impact on C cycling as well  
61 as guide its development in terrestrial biosphere models.

## 63 Plain Language Summary

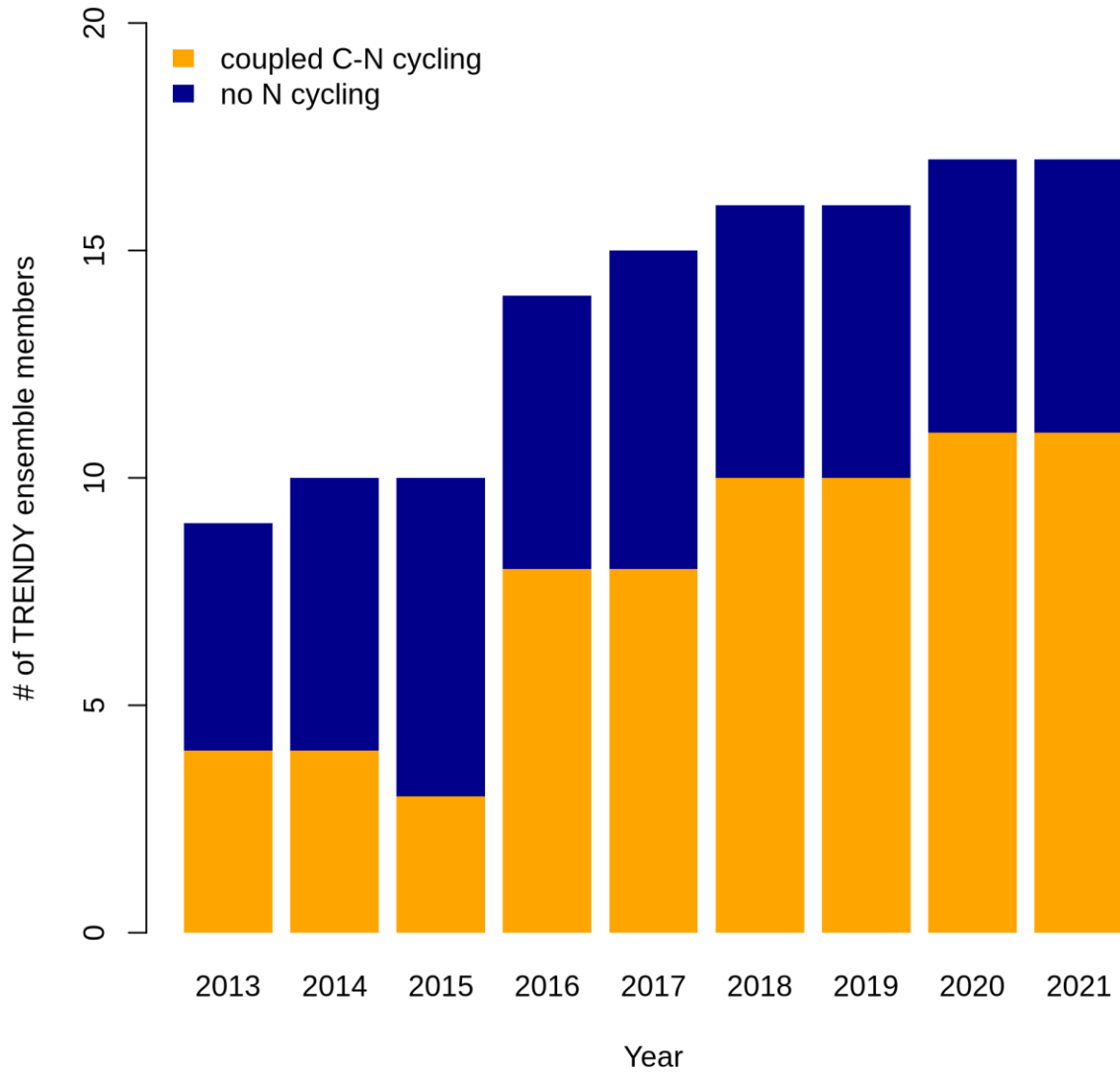
64 Nitrogen (N) is an essential limiting nutrient to terrestrial carbon (C) sequestration. We  
65 evaluate N cycling in an ensemble of terrestrial biosphere models. We find that ~~they simulate~~  
66 significant variability in N processes across models is large. Models tended to overestimate C  
67 storage per unit N in vegetation and soil, which could have consequences for projecting the  
68 future terrestrial C sink. However, N cycling measurements are highly uncertain, and more are  
69 necessary to guide the development of N cycling in models.

## 71 1 Introduction

72 The terrestrial biosphere is estimated to currently sequester approximately a third of  
73 anthropogenic CO<sub>2</sub> emissions by the Global Carbon Project (GCP) (Friedlingstein et al., 2022).  
74 The GCP annually reports an estimate of the global carbon (C) budget which includes an  
75 estimate of the atmosphere-land CO<sub>2</sub> flux, ~~i.e., the terrestrial C sink~~, based on simulations of an

76 ensemble of terrestrial biosphere models – the trends in the land carbon cycle project (TRENDY)  
77 ensemble. In recent years, the majority of the models within the TRENDY ensemble have  
78 incorporated a representation of coupled C and nitrogen (N) cycling given the empirically  
79 established importance of N limitation of vegetation growth (Elser et al., 2007; LeBauer and  
80 Treseder, 2008; Wright et al., 2018): whereas only ~~four~~<sup>4</sup> out of ~~nine~~<sup>9</sup> models represented  
81 coupled C-N cycling in the 2013 GCP, 11 out of 16 models represented coupled C-N cycling in  
82 the 2022 GCP (Figure 1). Capturing N constraints on C cycling is critical for realistically  
83 simulating the terrestrial C sink, which arises from the combined effects of concurrently acting  
84 global change drivers that are each modulated by N: CO<sub>2</sub> fertilisation is limited by N (Terrer et  
85 al., 2019; Wang et al., 2020a), intensifying N deposition increases N supply (O’Sullivan et al.,  
86 2019; Wang et al., 2017), rising temperature and varying precipitation modulate decomposition  
87 and soil N availability (Liu et al., 2017), and land use change and associated N fertilisation  
88 regimes determine N supply to crops.

89 Figure 1: ~~Inclusion of coupled C-N cycling in the~~Number of terrestrial biosphere models  
90 contributing to the Global Carbon Project, ~~i.e.,~~ (the TRENDY ensemble) ~~with and without~~  
91 ~~coupled C-N cycling.~~



92

93 The TRENDY ensemble has been extensively evaluated against observations of the C,  
94 water, and energy cycles (Collier et al., 2018; Friedlingstein et al., 2022; Seiler et al., 2022).  
95 Within the GCP itself, the primary simulated C pools, C fluxes, and water fluxes are evaluated  
96 using a skill score system developed by the International Land Model Benchmarking Project  
97 (ILAMB) that quantifies model performance by comparing model simulations to observations  
98 (Collier et al., 2018; Friedlingstein et al., 2022). ILAMB scores encompass the mean and  
99 variability of a given variable (pool or flux) over monthly to decadal temporal scales and over  
100 grid cell to global spatial scales. However, N cycling has not been explicitly evaluated despite its  
101 importance in regulating C cycling. This is in part due to the relatively recent incorporation of N  
102 cycling in terrestrial biosphere models (Figure 1) (Fisher and Koven, 2020; Hungate et al., 2003)  
103 but also due to the paucity of global observation-based datasets of N cycling: N exists in many  
104 forms and is lost from terrestrial ecosystems via numerous pathways (emissions of NH<sub>3</sub>, N<sub>2</sub>O,  
105 NO<sub>x</sub> and N<sub>2</sub> as well as NO<sub>3</sub><sup>-</sup> and NH<sub>4</sub><sup>+</sup> leaching), N processes are generally not measured in situ  
106 in networks such as FLUXNET, and remote sensing methodologies for measuring N processes  
107 are still in their infancy. Additionally, N processes exhibit extremely high spatial and temporal  
108 variabilities and are thus challenging to measure. As such, N cycling has commonly been  
109 evaluated by comparing simulated N pools and fluxes to global totals based on a small number of  
110 observations that have been scaled up or averaged to yield a value with wide confidence intervals  
111 (Davies-Barnard et al., 2020).

112 N cycling is implicitly evaluated by comparing terrestrial biosphere models without N  
113 cycling to those with coupled C-N cycling in reproducing observations of the C, water, and  
114 energy cycles in the absence of N cycle observations. Results suggest that there are only minor  
115 differences between the performance of models with and without N cycling. There is no  
116 significant difference between the terrestrial C sink simulated by the TRENDY models with and  
117 without N cycling (Friedlingstein et al., 2022) nor between the terrestrial C sink simulated by the  
118 models participating in the Multi-scale synthesis and Terrestrial Model Intercomparison Project  
119 (MsTMIP) with and without N cycling (Huntzinger et al., 2017). Comparing the mean score  
120 across all C, water, and energy cycle variables between TRENDY models with and without N  
121 cycling yielded no significant difference (Seiler et al., 2022). However, TRENDY models  
122 without N cycling had significantly higher scores for net biome productivity than TRENDY  
123 models with N cycling (although all other variables were not significantly different between  
124 TRENDY models with and without N cycling, including vegetation C, soil C, net biome  
125 productivity, leaf area index, latent heat flux, and runoff, among others) (Seiler et al., 2022).  
126 Despite this seeming absence of a difference between models with and without coupled C-N  
127 cycling in simulating the current terrestrial C sink, it is imperative that N constraints on C  
128 cycling are properly represented by terrestrial biosphere models in order to realistically simulate  
129 the terrestrial C sink under future global change, which modifies the C/N balance through N  
130 limitation of CO<sub>2</sub> fertilisation and intensifying N deposition among other effects of global  
131 change. As such, explicitly evaluating N cycling processes themselves is necessary to assess the  
132 ability of terrestrial biosphere models to capture the underlying mechanisms that determine  
133 terrestrial C sequestration and thus to realistically project the future terrestrial C sink under  
134 global change.

135 Here, we synthesise the N pools and fluxes simulated by 11 terrestrial biosphere models  
136 in the TRENDY ensemble that participated in the 2022 GCP. We evaluate their performance in  
137 reproducing observations of three key variables of the N cycle: biological N fixation, vegetation  
138 C:N ratio, and soil C:N ratio. These three variables are critical to C cycling because (1)  
139 biological N fixation is the dominant natural N supply to terrestrial ecosystems, influencing the  
140 degree of N limitation of plant growth and thus terrestrial C sequestration, and (2) vegetation and  
141 soil C:N ratios reflect assimilated C per unit N and thus terrestrial C storage.

142

## 143 **2 Methods**

### 144 **2.1 Simulation Protocol**

145 For the 2022 GCP (version 11), the TRENDY ensemble consisted of 16 terrestrial  
146 biosphere models, 11 of which represent N cycling (CABLE-POP, CLM5.0, DLEM, ISAM,  
147 JSBACH, JULES-ES, LPJ-GUESS, LPX-Bern, OCNv2, ORCHIDEEv3, and SDGVM).  
148 Although SDGVM includes a representation of N cycling, its representation is simplistic and was  
149 therefore not included. Additionally, CLASSIC contributed to the 2022 GCP without coupled C-  
150 N cycling; the S3 simulation [from the TRENDY protocol](#) was repeated by CLASSIC with  
151 coupled C-N cycling following the 2022 GCP protocol and was used here. Overall, we analysed  
152 eleven models with coupled C-N cycling (Table 1).

153 Table 1: Terrestrial biosphere models in the TRENDY-N ensemble and descriptions of their  
 154 representations of N limitation of vegetation growth, biological N fixation, vegetation response  
 155 to N limitation (i.e., strategies in which vegetation invests C to increase N supply in N-limited  
 156 conditions), and N limitation of decomposition.

	Reference	N limitation of vegetation growth	Biological N fixation	Vegetation response to N limitation	N limitation of decomposition
CABLE-POP	(Haverd et al., 2018)	$V_{cmax} = f(N)$ flexible C:N stoichiometry	Time-invariant	Static	N-invariant
CLASSIC	(Melton et al., 2020)	$V_{cmax} = f(N)$ flexible C:N stoichiometry	f(N limitation of vegetation growth)	Dynamic (biological N fixation)	N-invariant
CLM5.0	(Lawrence et al., 2019)	$V_{cmax} = f(N)$ flexible C:N stoichiometry	f(N limitation of vegetation growth)	Dynamic (biological N fixation, mycorrhizae, retranslocation)	f(soil N)
DLEM	(Tian et al., 2015)	$GPP = f(N)$	f(soil T, soil H <sub>2</sub> O, soil C, soil N)	Dynamic (root allocation)	f(soil N)
ISAM	(Shu et al., 2020)	$GPP = f(N)$	f(ET)	Static	f(soil N)
JSBACH	(Reick et al., 2021)	$NPP = f(N)$	f(NPP)	Static	f(soil N)
JULES-ES	(Wiltshire et al., 2021)	$NPP = f(N)$	f(NPP)	Static	f(soil N)
LPJ-GUESS	(Smith et al., 2014)	$V_{cmax} = f(N)$ flexible C:N stoichiometry	f(ET)	Dynamic (root allocation)	N-invariant
LPX-Bern	(Lienert and Joos, 2018)	$NPP = f(N)$	Derived post hoc to simulate a closed N cycle	Static	N-invariant
OCNv2	(Zaehle and Friend, 2010)	$V_{cmax} = f(N)$ flexible C:N stoichiometry	f(N limitation of vegetation growth)	Dynamic (root allocation)	f(soil N)

ORCHIDEEv3	(Vuichard et al., 2019)	$V_{\text{cmax}} = f(\text{N})$ flexible C:N stoichiometry	Time-invariant	Static	N-invariant
------------	-------------------------	---	----------------	--------	-------------

157



158 We analysed the S3 simulation [from the TRENDY protocol](#) which includes historical  
159 changes in atmospheric CO<sub>2</sub>, climate, N deposition, N fertilisation, and land use from 1851 to  
160 2021 (see Friedlingstein et al. (2022) for a full description of the simulation protocol). Briefly,  
161 models were forced with atmospheric CO<sub>2</sub> from Dlugokencky and Tans (2022), the merged  
162 monthly Climate Research Unit (CRU) and 6-hourly Japanese 55-year Reanalysis (JRA-55)  
163 dataset or the monthly CRU dataset [from](#) Harris et al. (2020), N deposition from Hegglin et al.  
164 (2016) / Tian et al. (2022), N fertilisation from the global N<sub>2</sub>O Model Intercomparison Project  
165 (NMIP) (Tian et al., 2018), and land use from the LUH2-GCB2022 (Land-Use Harmonization 2)  
166 dataset (Chini et al., 2021; Hurtt et al., 2020; Klein Goldewijk et al., 2017a, b). We interpolated  
167 outputs from all models to a common resolution of 1° x 1° using bilinear interpolation.

## 168 2.2 Terrestrial biosphere model descriptions

169 The terrestrial biosphere models in the TRENDY ensemble employ a wide variety of  
170 assumptions and formulations of N cycling processes, reflecting knowledge gaps and divergent  
171 theories (Table 1). Here we describe four fundamental aspects of N cycling for each terrestrial  
172 biosphere model: N limitation of vegetation growth, biological N fixation, the response of  
173 vegetation to N limitation (i.e., strategies in which vegetation invests C to increase N supply in  
174 N-limited conditions), and N limitation of decomposition. These have been identified as  
175 important challenges for representing N cycling in terrestrial biosphere models (Meyerholt et al.,  
176 2020; Peng et al., 2020; Stocker et al., 2016; Wieder et al., 2015a; Zaehle et al., 2015; Zaehle and  
177 Dalmonech, 2011).

178 Terrestrial biosphere models differ in how N limitation of vegetation growth is  
179 represented (Thomas et al., 2015). Some TRENDY models represent flexible C:N stoichiometry  
180 and modelled maximum carboxylation rate of photosynthesis ( $V_{cmax}$ ) decreases with decreasing  
181 leaf N (CABLE-POP, CLASSIC, CLM5.0, LPJ-GUESS, OCNv2, ORCHIDEEv3) following  
182 empirical evidence (Walker et al., 2014). Other TRENDY models represent time-invariant C:N  
183 stoichiometry and modelled GPP or NPP decreases with N limitation (DLEM, ISAM, JSBACH,  
184 JULES-ES, and LPX-Bern). Importantly, flexible vs. time-invariant C:N stoichiometry  
185 determines terrestrial C storage per unit N.

186 Biological N fixation is the dominant natural N supply to terrestrial ecosystems (Vitousek  
187 et al., 2013). In terrestrial biosphere models, biological N fixation has generally been represented  
188 phenomenologically as a function of either net primary productivity (NPP) or evapotranspiration  
189 (ET) (Cleveland et al., 1999). More recently, representations of biological N fixation have been  
190 updated such that it is up-regulated in N-limited conditions following empirical evidence (Menge  
191 et al., 2015; Vitousek et al., 2013; Zheng et al., 2019). The majority of TRENDY models  
192 represent biological N fixation phenomenologically (ISAM, JSBACH, JULES-ES, and LPJ-  
193 GUESS). Three TRENDY models (CLASSIC, CLM5.0, and OCNv2) represent biological N  
194 fixation mechanistically such that it increases with N limitation of vegetation [and has an](#)  
195 [associated C cost per unit N fixed](#) (Kou-Giesbrecht and Arora, 2022; Lawrence et al., 2019;  
196 Meyerholt et al., 2016; Shi et al., 2016; Fisher et al., 2010). These representations separate free-  
197 living biological N fixation (via soil microbes, epiphytic microbes, lichens, bryophytes, etc.  
198 (Reed et al., 2011)) from symbiotic biological N fixation, which is regulated by N limitation of

199 vegetation. DLEM derives biological N fixation as a function of soil temperature, soil moisture,  
200 soil C, and soil N. LPX-Bern derives biological N fixation post hoc to simulate a closed N cycle,  
201 implicitly including rock N sources (Joos et al., 2020). Finally, CABLE-POP and ORCHIDEEv3  
202 represent biological N fixation as a specified time-invariant input over the historical period.  
203 Importantly, representing the regulation of biological N fixation by N limitation does not only  
204 determine biological N fixation itself but also modulates terrestrial C sequestration: it enables  
205 vegetation to increase N uptake in N-limited conditions, reduce N limitation, and thus sustain  
206 terrestrial C sequestration. Some TRENDY models (DLEM, LPJ-GUESS, and OCNv2) also  
207 represent increasing C allocation to roots with increasing N limitation (Smith et al., 2014; Zaehle  
208 and Friend, 2010) following empirical evidence (Poorter et al., 2012). This enables vegetation to  
209 increase root N uptake in N-limited conditions, reduce N limitation, and thus sustain terrestrial C  
210 sequestration. The response of vegetation to N limitation, which could also include increased C  
211 allocation to mycorrhizae (Phillips et al., 2013) (represented in CLM5.0) or increased  
212 retranslocation of N during tissue turnover (Du et al., 2020; Han et al., 2013; Kobe et al., 2005)  
213 (represented in CLM5.0) is important for determining terrestrial C sequestration.

214 Decomposition rate is controlled by soil temperature, soil moisture, and N content in  
215 litter, where increasing litter C:N ratio decreases decomposition rate (Cotrufo et al., 2013). Some  
216 TRENDY models represent this reduction in decomposition rate with increasing litter C:N ratio  
217 (CLM5.0, DLEM, ISAM, JSBACH, JULES-ES, and OCNv2) following empirical evidence.

## 218 **2.3 Observation-based datasets**

219 We interpolated observation-based datasets to a common resolution of  $1^\circ \times 1^\circ$  using  
220 bilinear interpolation for comparison against model outputs. To compare model outputs against  
221 observation-based datasets we averaged model outputs over 1980–2021, which spans the period  
222 in which most measurements were made.

### 223 **2.3.1 Biological N fixation**

224 A biological N fixation observation-based dataset was derived from Davies-Barnard and  
225 Friedlingstein (2020), a global meta-analysis of field measurements of natural biological N  
226 fixation (free-living and symbiotic) that scales biome-specific means onto the Collection 5  
227 MODIS Global Land Cover Type International Geosphere-Biosphere Programme (IGBP)  
228 product (Friedl et al., 2010). ~~To account for~~ This dataset includes agricultural biological N  
229 ~~fixation, we assumed and assumes that N-fixing crops account for 15.7% of global cropland area~~  
230 ~~and their crop~~ biological N fixation ~~rate as  $11.5 \text{ g N m}^{-2} \text{ yr}^{-1}$ . We assumed that N-fixing crops are~~  
231 ~~distributed evenly across all cropland. We amended the dataset from Davies-Barnard and~~  
232 ~~Friedlingstein (2020) to include agricultural biological N fixation (DBF-USDA); rates are~~  
233 ~~equivalent to those of grasses.~~

234 The score of LPX-Bern in simulating biological N fixation is not analysed because it  
235 implicitly includes rock N sources and is thus not directly comparable to the observation-based  
236 dataset.

### 237 **2.3.2 Vegetation C:N ratio**

238 A vegetation C:N ratio observation-based dataset was derived by scaling biome-specific  
239 means for vegetation C:N ratios from the TRY plant trait database (Kattge et al., 2020) onto the  
240 Collection 5 MODIS Global Land Cover Type IGBP product (Friedl et al., 2010) and combining  
241 it with the remote sensing leaf N content product from Moreno-Martínez et al. (2018). First, we  
242 obtained N content per dry mass for leaves, root, and stem, as well as C content per dry mass for  
243 leaves, root, and stem from the TRY plant trait database. We selected entries that reported  
244 species. Second, we obtained plant functional type (PFT) for each species from the TRY plant  
245 trait database. We categorised each PFT into the IGBP land cover types (Table A1) and then  
246 used this to categorise each entry into the IGBP land cover types- using species. We averaged  
247 across entries in each IGBP land cover type. Third, we divided mean tissue C content per tissue  
248 dry mass by mean tissue N content per tissue dry mass for each tissue and for each IGBP land  
249 cover type. Fourth, we weighed each tissue by its PFT-specific fraction of total biomass from  
250 Poorter et al. (2012) to obtain total vegetation C:N ratio for each IGBP land cover type.  
251 LastlyFifth, we scaled total vegetation C:N ratio and leaf N content per dry mass for each IGBP  
252 land cover type to the Collection 5 MODIS Global Land Cover Type IGBP product. Sixth, we  
253 multiplied derived total vegetation C:N ratio relative to leaf N content per dry mass by the  
254 remote sensing leaf N content per dry mass product (Moreno-Martínez et al., 2018) to obtain a  
255 vegetation C:N ratio observation-based dataset.

### 256 2.3.3 Soil C:N ratio

257 A soil C:N ratio observation-based dataset was derived from soil C and soil N products  
258 from SoilGrids (Poggio et al., 2021), which provides globally gridded datasets of soil organic C  
259 and total soil N at a 250m x 250m resolution for six layers up to a depth of 200 cm. These  
260 estimates are derived using machine learning methods and soil observations from 240 000  
261 locations across the globe and over 400 environmental covariates. We summed soil C over all  
262 layers and soil N over all layers (using the bulk density and depth of each layer) then obtained  
263 the soil C:N ratio.

### 264 2.3.4 C cycling variables

265 In addition to evaluating N cycling variables, we also evaluated the primary C cycling  
266 variables: gross primary productivity (GPP), net biome productivity (NBP), vegetation C  
267 (CVEG), soil C (CSOIL), and leaf area index (LAI). These variables have been previously  
268 evaluated in detail for the terrestrial biosphere models in the TRENDY ensemble (GCP 2021) in  
269 Seiler et al. (2022). Seiler et al. (2022) gives further details on the observation-based datasets  
270 used to evaluate the primary C cycling variables. Briefly, we evaluated GPP against MODIS  
271 (Zhang et al., 2017), GOSIF (Li and Xiao, 2019), and FLUXCOM (Jung et al., 2020) products.  
272 We evaluated NBP against the CAMS (Agustí-Panareda et al., 2019), CarboScope (Rödenbeck  
273 et al., 2018), and CT2019 (Jacobson et al., 2020) products. We evaluated CVEG against the  
274 GEOCARBON (Avitabile et al., 2016; Santoro et al., 2015), Zhang and Liang (2020), and Huang  
275 et al. (2021) products. We evaluated LAI against AVHRR (Claverie et al., 2016), Copernicus  
276 (Verger et al., 2014), and MODIS (Myneni et al., 2002) products. We evaluated CSOIL against  
277 HWSO (Todd-Brown et al., 2013; Wieder, 2014) and SoilGrids (Hengl et al., 2017) products.  
278 These observation-based products are globally gridded.

## 279 **2.4 Model evaluation with the Automated Model Benchmarking R Package (AMBER)**

280 The Automated Model Benchmarking R (AMBER) package developed by Seiler et al.  
281 (2021) quantifies model performance in reproducing observation-based datasets using a skill  
282 score system that is based on ILAMB (Collier et al., 2018). Five scores assess the simulated  
283 time-mean bias ( $S_{bias}$ ), monthly centralised root-mean-square-error ( $S_{rmse}$ ), seasonality ( $S_{phase}$ ),  
284 inter-annual variability ( $S_{iav}$ ), and spatial distribution ( $S_{dist}$ ) in comparison to the observation-  
285 based dataset. Scores are dimensionless and range from 0 to 1, where higher values indicate  
286 better model performance. The overall score for each variable ( $S_{overall}$ ) is

$$287 \quad S_{overall} = \text{mean}(S_{bias}, S_{rmse}, S_{phase}, S_{iav}, S_{dist})$$

288 We calculated the overall score for each C and N cycling variable. Because biological N fixation,  
289 vegetation C:N ratio, and soil C:N ratio datasets are representative of the present-day (as a single  
290 time point),  $S_{rmse}$ ,  $S_{phase}$ , and  $S_{iav}$  are not defined and thus do not contribute to  $S_{overall}$ . This also  
291 holds for vegetation C and soil C. The calculation of each score is described in detail in Seiler et  
292 al. (2022).

## 293 **2.5 Statistics**

294 We used a Mann-Kendall trend test to assess the existence of a statistically significant  
295 trend in the time series over the historical period for simulated C and N cycling variables (Hipel  
296 and McLeod, 1994). **We conducted two analyses to compare model performance in**  
297 **simulating C cycling vs. N cycling. First, we** calculated Spearman's rank correlation coefficient  
298 to assess the existence of statistically significant correlations between overall scores, present-day  
299 global values, and Kendall's tau. **We** **Second, we** used a t-test or ANOVA (p-value < 0.05) to  
300 assess the existence of statistically significant differences between overall scores, present-day  
301 global values, and Kendall's tau for models with different representations of N limitation of  
302 vegetation growth, biological N fixation, vegetation response to N limitation, and N limitation of  
303 decomposition (Table 1).

304

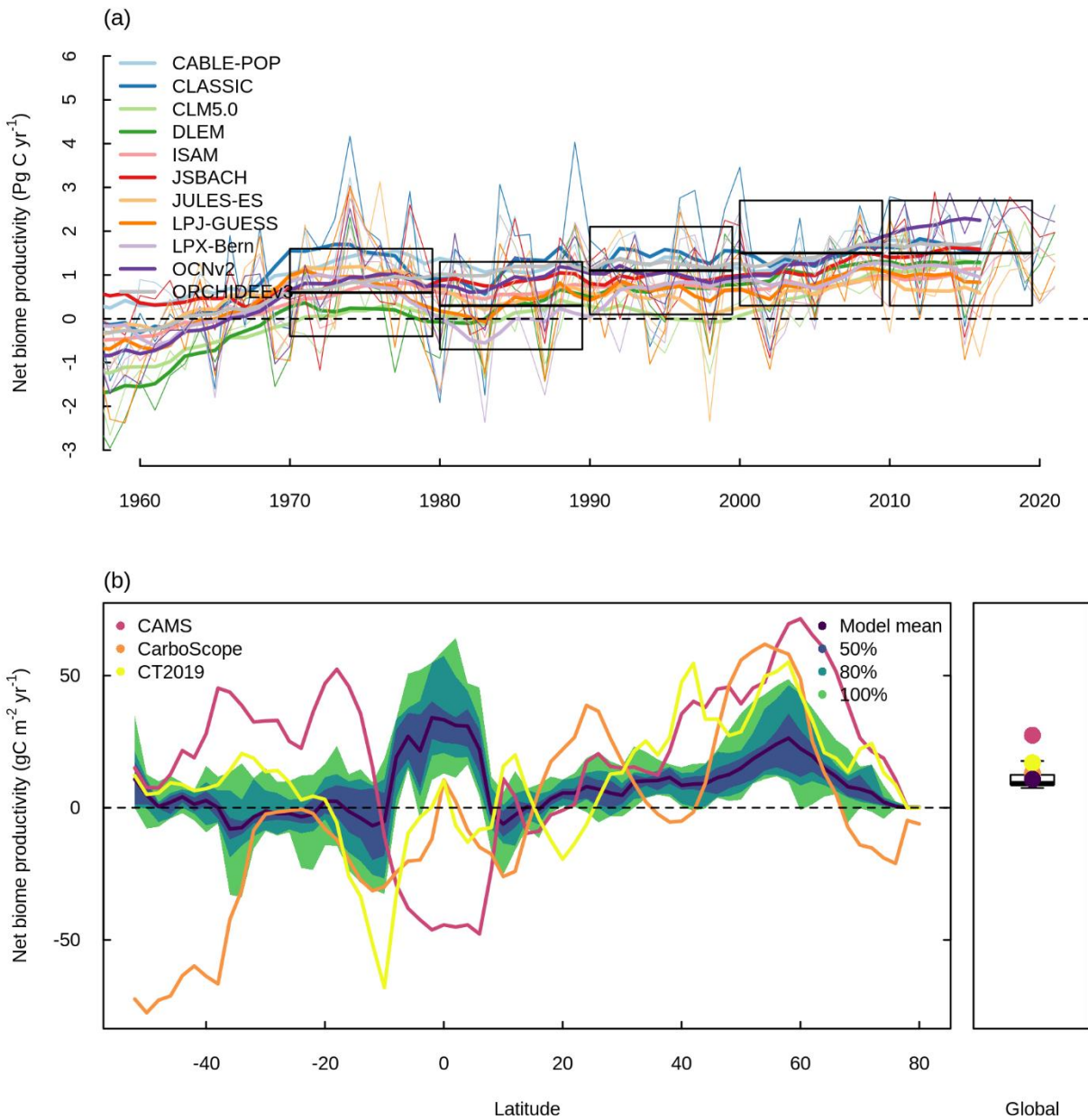
## 305 **3 Results**

### 306 **3.1 Net biome productivity**

307 Figure 2 shows NBP simulated by the TRENDY ensemble models with coupled C-N  
308 cycling (hereafter referred to as the TRENDY-N ensemble). NBP is the difference between the  
309 net natural atmosphere-land flux of CO<sub>2</sub> and land use change CO<sub>2</sub> emissions. Positive values of  
310 NBP indicate a terrestrial C sink whereas negative values of NBP indicate a terrestrial C source.  
311 All TRENDY-N ensemble models suggest a terrestrial C sink for the present-day, agreeing with  
312 the global C budget constraint from the 2022 Global C Budget with most models within two  
313 standard deviations of the mean ( $1.5 \pm 0.6$  Pg C for 2012–2021) (Figure 2a). The TRENDY-N  
314 ensemble agrees reasonably well with observations globally, agreeing somewhat better with  
315 CarboScope and CT2019 than with CAMS (Figure 2b). However, the latitudinal distributions of  
316 the observation-based datasets display weak agreement among themselves, with opposing signs

317 in multiple regions, especially due to differences in the inversion models and atmospheric CO<sub>2</sub>  
318 measurements used in each dataset (Figure 2b). The largest differences occur at southern  
319 latitudes and at high northern latitudes (Figure 2b). This and is in part due to the smaller land area  
320 at these latitudes. The region showing the strongest agreement is mid to high northern latitudes,  
321 in which both the TRENDY-N ensemble and observations suggest a terrestrial C sink (Figure  
322 2b).

323 Figure 2: Net biome productivity (NBP) simulated by the TRENDY-N ensemble. a. Global NBP  
 324 from 1960 to 2021. The boxes indicate the global C budget constraint (difference between fossil  
 325 fuel CO<sub>2</sub> emissions and the growth rate of atmospheric CO<sub>2</sub> and the uptake of CO<sub>2</sub> by oceans;  
 326 mean ± 2 standard deviation) from the 2022 Global C Budget (Friedlingstein et al., 2022). Thick  
 327 lines indicate the moving average over 10 years and thin lines indicate the annual time series. b.  
 328 Latitudinal distribution and global mean of NBP (averaged over 1980–2021) in comparison to  
 329 three datasets (CAMS (Agustí-Panareda et al., 2019), CarboScope (Rödenbeck et al., 2018), and  
 330 CT2019 (Jacobson et al., 2020)). The boxplot shows the median, interquartile range (box), and  
 331 80% percentiles (whiskers) of the global mean of NBP.



332

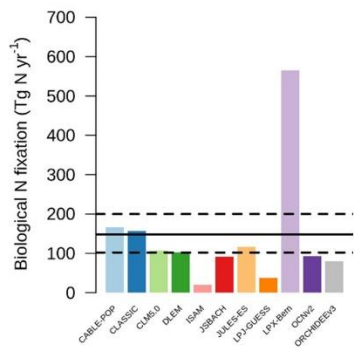


### 333 3.2 Overview of N cycling

334 Figure 3 shows a schematic of the N cycle alongside the primary N fluxes and C:N ratios  
335 of the primary pools simulated by the TRENDY-N ensemble for the present-day (averaged over  
336 1980–2021) as well as observation-based estimates for these variables that have previously been  
337 used for model evaluation (Davies-Barnard et al., 2020). Simulated biological N fixation ranged  
338 between 20 and 566 Tg N yr<sup>-1</sup> (Table 2) in comparison to the observation-based estimate of ~~148~~  
339 ~~Tg N yr<sup>-1</sup>, which includes both natural biological N fixation (88 Tg N yr<sup>-1</sup> (52 – 130 Tg N yr<sup>-1</sup>))~~  
340 ~~and agricultural biological N fixation (50–70 Tg N yr<sup>-1</sup>).~~ Simulated N<sub>2</sub>O emissions ranged  
341 between 0.9 and 11.0 Tg N yr<sup>-1</sup> (Table 2) in comparison to the observation-based estimate of  
342 10.8 Tg N yr<sup>-1</sup> (7.1 – 16.0 Tg N yr<sup>-1</sup>) (Tian et al., 2020). Simulated N losses (which include  
343 emissions of NH<sub>3</sub>, N<sub>2</sub>O, NO<sub>x</sub> and N<sub>2</sub> as well as NO<sub>3</sub><sup>-</sup> and NH<sub>4</sub><sup>+</sup> leaching) ranged between 87 and  
344 603 Tg N yr<sup>-1</sup> (Table 2) in comparison to the observation-based estimate of 293 Tg N yr<sup>-1</sup>  
345 (Fowler et al., 2013). The simulated vegetation C:N ratio ranged between 103 and 222 (Table 2)  
346 in comparison to the observation-based estimate of 133 (Zechmeister-Boltenstern et al., 2015).  
347 The simulated combined litter-soil C:N ratio ranged between 10 and 64 (Table 2) in comparison  
348 to the observation-based estimate of 15 (Zechmeister-Boltenstern et al., 2015). Biological N  
349 fixation has the largest inter-model spread with a coefficient of variation of 1.06 (Table 2).  
350 Figure 4 shows the geographical distribution of the primary N pools and fluxes simulated by the  
351 TRENDY-N ensemble for the present-day (averaged over 1980–2021) ~~and variation across~~  
352 ~~models is shown in Figure A1.~~

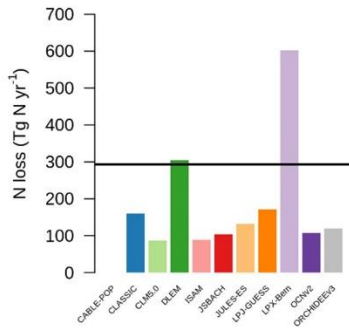
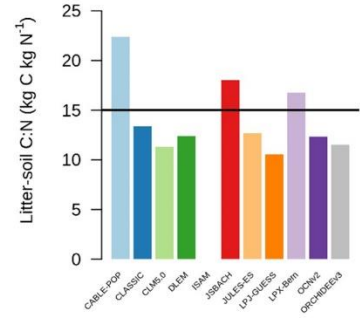
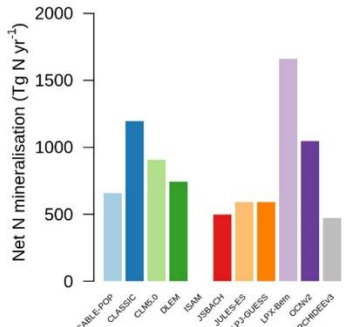
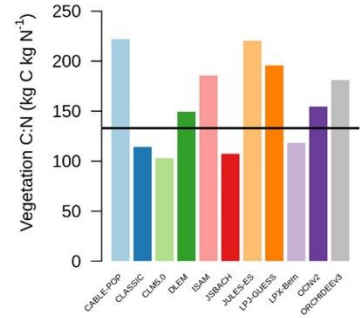
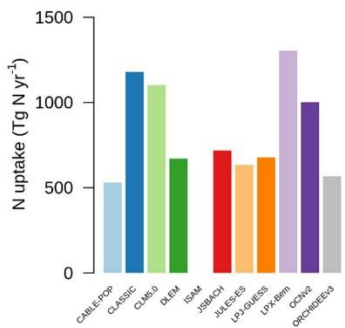
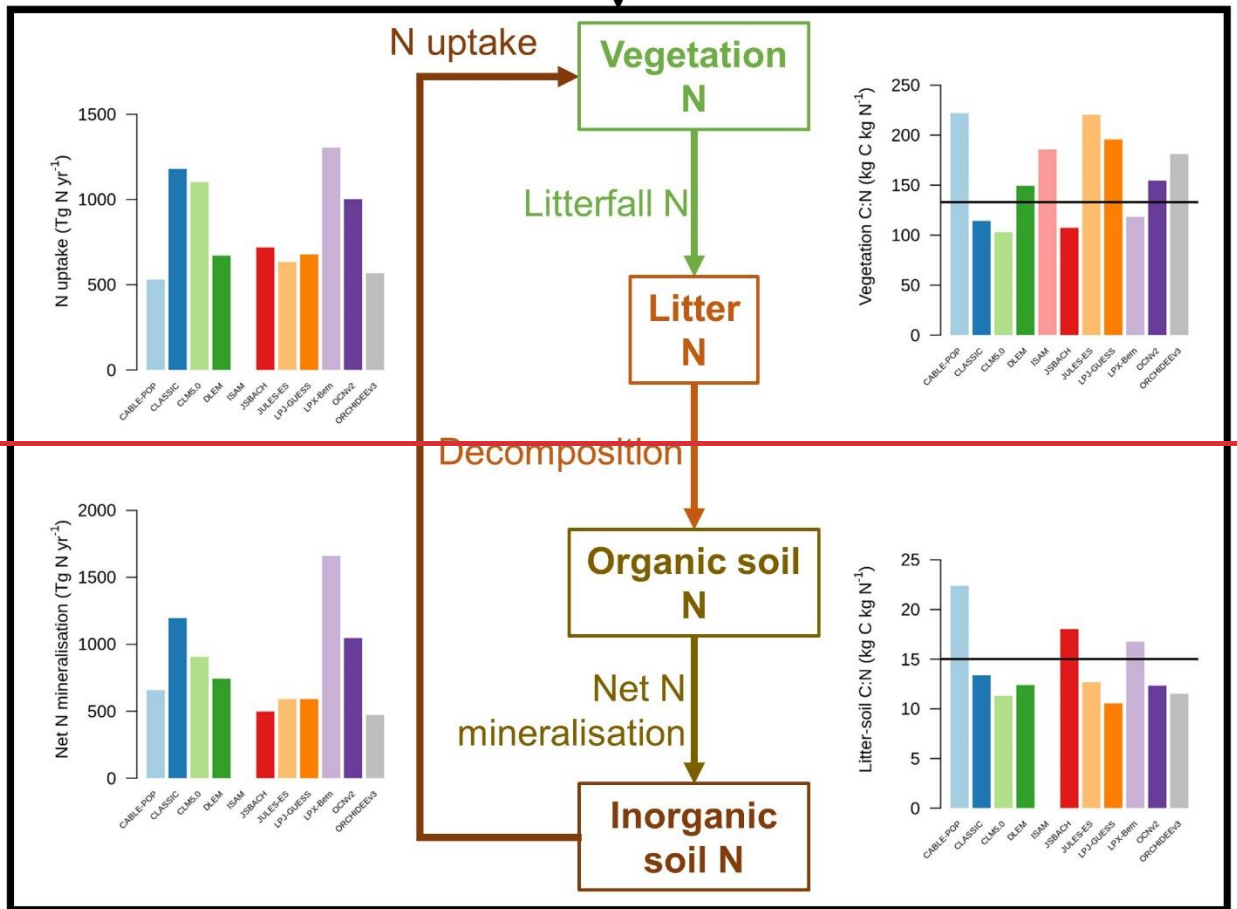
353 Figure 3: The N cycle and the primary N pools and fluxes simulated by the TRENDY-N  
354 ensemble (averaged over 1980–2021). Horizontal black lines indicate observation-based  
355 estimates that have previously been used for model evaluation (biological N fixation from  
356 Davies-Barnard and Friedlingstein (2020)~~and~~, vegetation and combined litter-soil C:N ratios  
357 from Zechmeister-Boltenstern et al. (2015), N<sub>2</sub>O emissions from Tian et al. (2020), and N losses  
358 from Fowler et al. (2013)). The black box indicates the terrestrial biosphere. N enters the  
359 terrestrial biosphere via biological N fixation, N deposition, and N fertilisation (entering the  
360 organic soil N pool, the inorganic soil N pool (ammonium (NH<sub>4</sub><sup>+</sup>) or nitrate (NO<sub>3</sub><sup>-</sup>)), or the  
361 vegetation N pool). N is transferred from the inorganic soil N pool to the vegetation N pool via N  
362 uptake. N is transferred from the vegetation N pool to the litter N pool via N litterfall. N is  
363 transferred from the litter N pool to the organic soil N pool via decomposition. N is transferred  
364 from the organic soil N pool to the inorganic soil N pool via net N mineralisation. N exits the  
365 terrestrial biosphere via N loss (which includes N leaching from soils and N<sub>2</sub>O, NO<sub>x</sub>, NH<sub>3</sub>, and  
366 N<sub>2</sub> emissions from both soils and land use change). Not all models provide output for each N  
367 pool or flux. Note that biological N fixation simulated by LPX-Bern implicitly includes rock N  
368 sources.



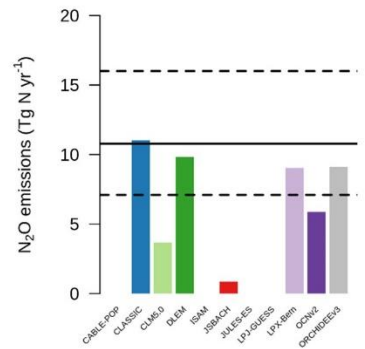


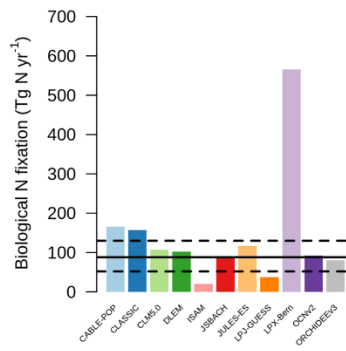
Biological N fixation  
N deposition  
N fertilisation

- CABLE-POP
- CLASSIC
- CLM5.0
- DLEM
- ISAM
- JSBACH
- JULES-ES
- LPJ-GUESS
- LPX-Bern
- OCNv2
- ORCHIDEEv3



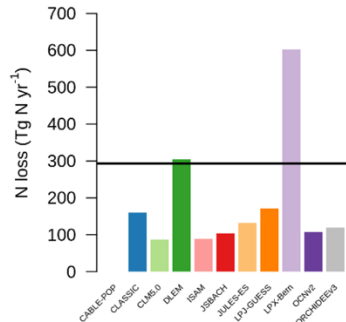
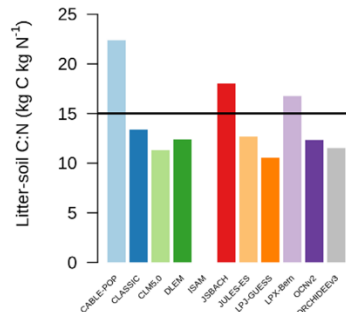
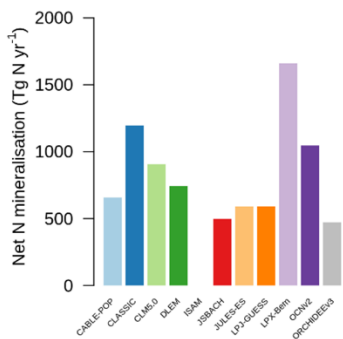
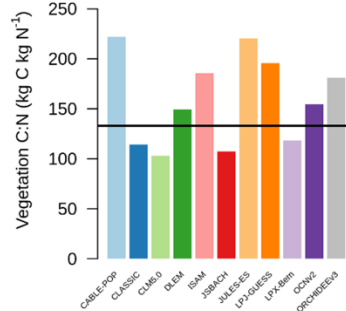
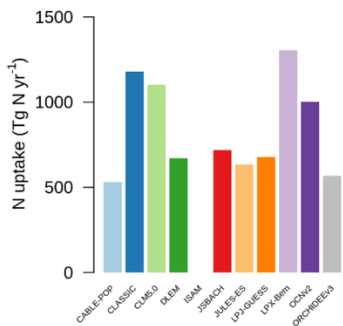
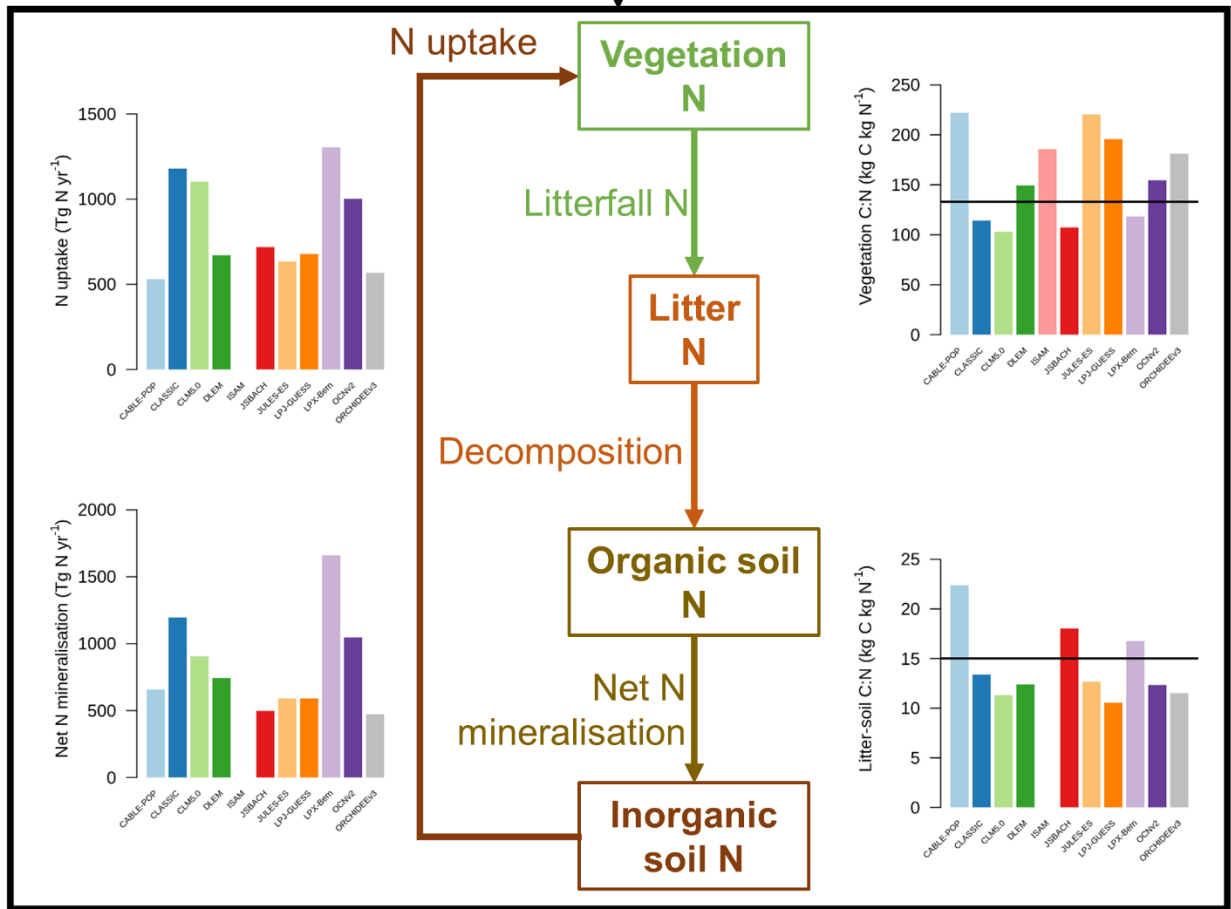
N loss



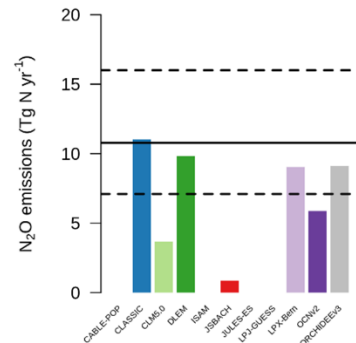


Biological N fixation  
N deposition  
N fertilisation

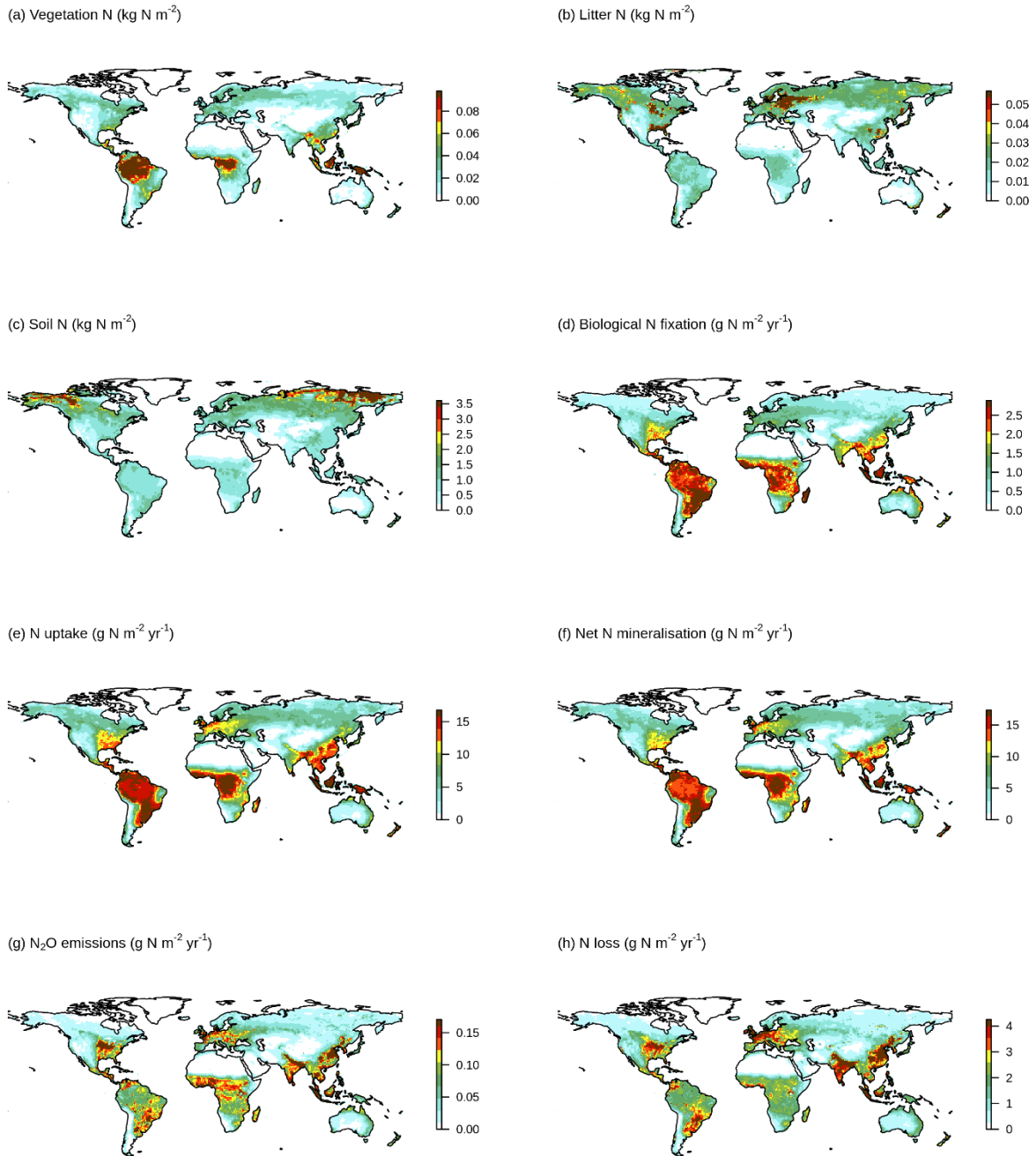
- CABLE-POP
- CLASSIC
- CLM5.0
- DLEM
- ISAM
- JSBACH
- JULES-ES
- LPJ-GUESS
- LPX-Bern
- OCNv2
- ORCHIDEEv3



N loss



371 Figure 4: Geographical distributions of a. vegetation N, b. litter N, c. soil N, d. biological N  
372 fixation, e. N uptake, f. net N mineralisation, g. N<sub>2</sub>O emissions, and h. N loss simulated by the  
373 TRENDY-N ensemble (averaged across models over 1980–2021). Variation across models is  
374 shown in Figure A1.



375

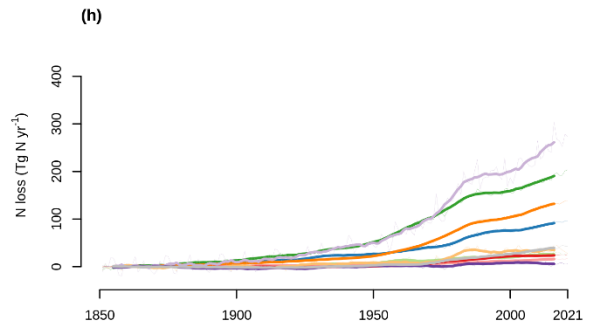
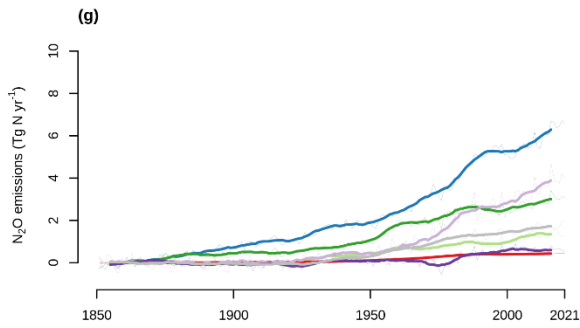
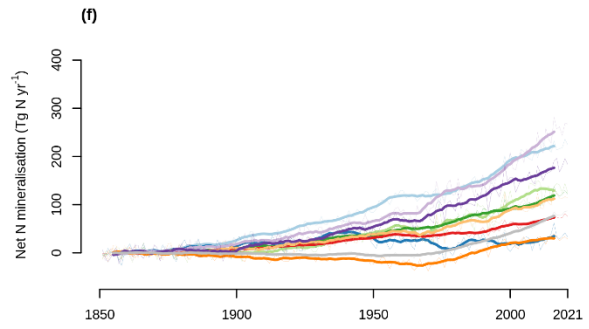
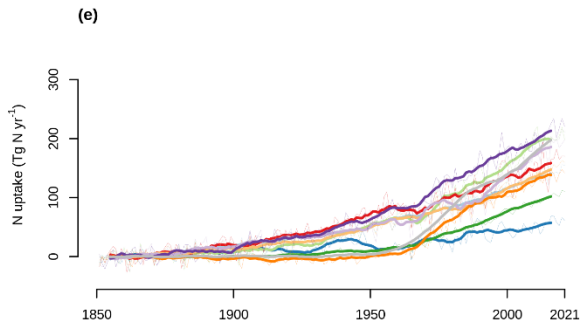
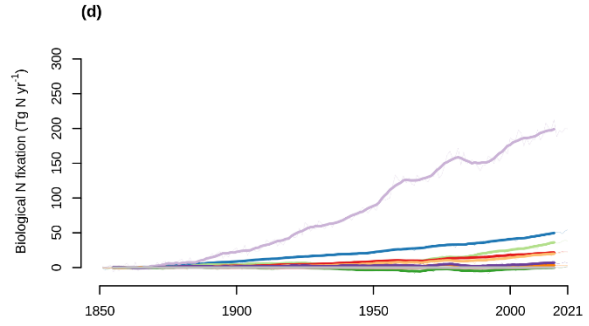
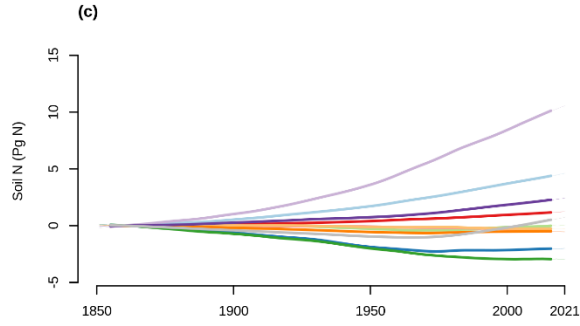
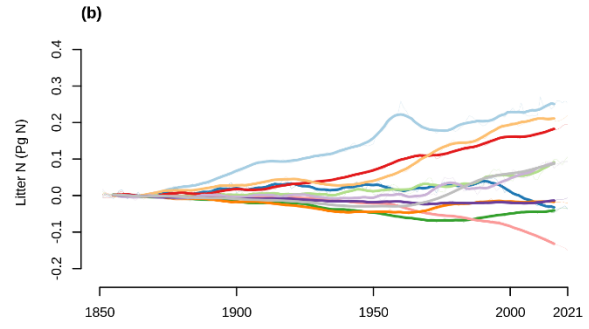
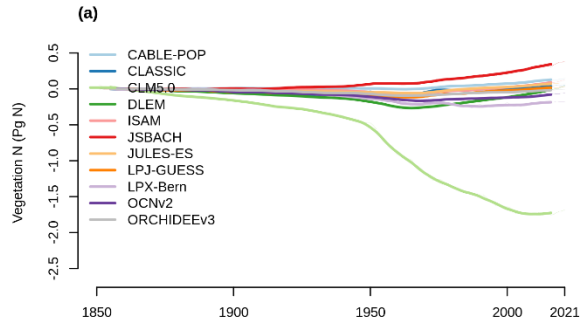
376 Table 2: Global ~~mean and coefficient of variation of each N pool~~ pools, N fluxes, and ~~flux~~ C:N  
 377 ratios simulated by the TRENDY-N ensemble (mean and coefficient of variation across models  
 378 over 1980–2021).

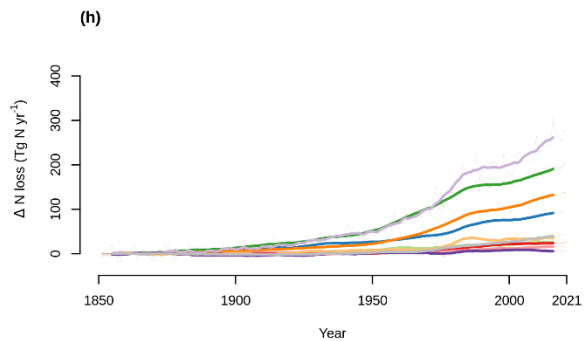
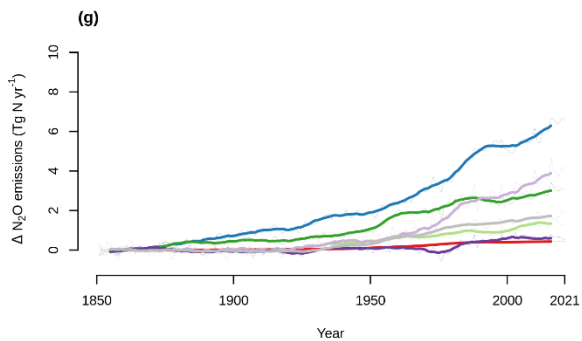
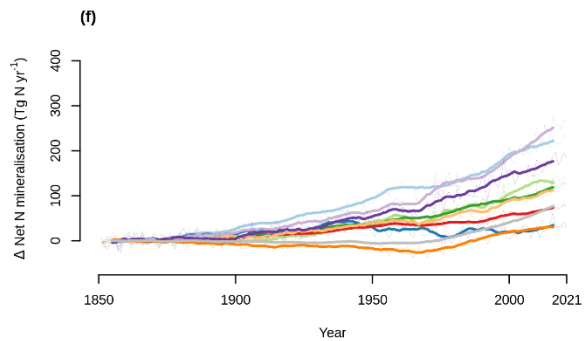
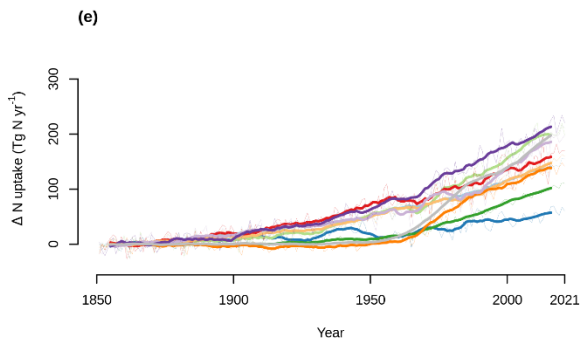
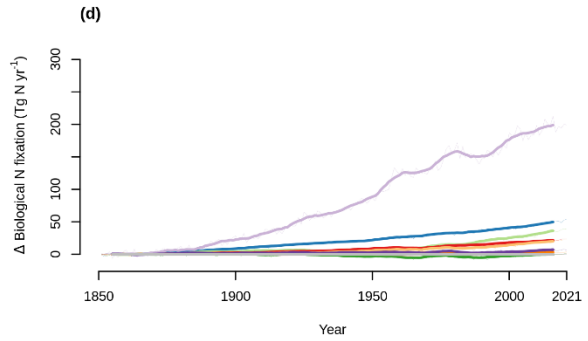
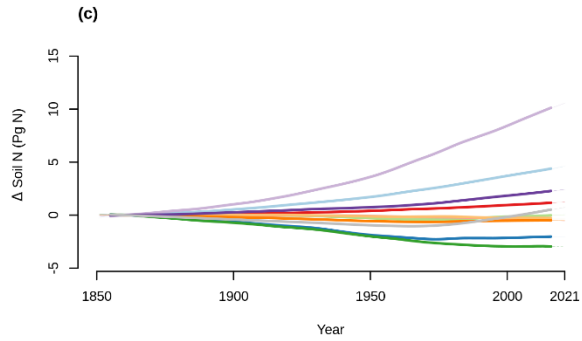
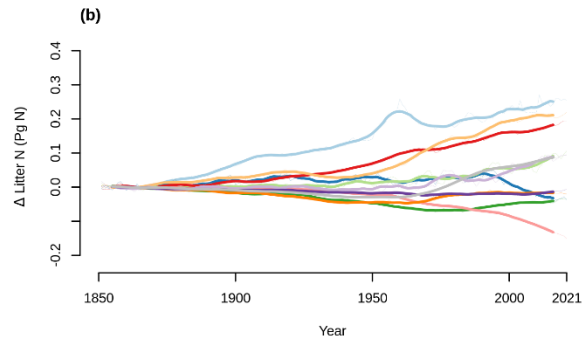
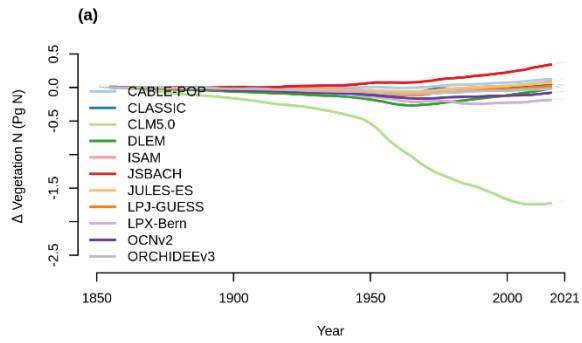
	Coefficient of variation	Global mean	Global median	Global minimum	Global maximum
Vegetation N (Tg N)	0.41	2.94	2.94	1.50	5.58
Litter N (Tg N)	0.81	1.94	1.08	0.73	5.61
Soil N (Tg N)	0.67	101.43	81.21	32.10	277.41
Biological N fixation (Tg N yr <sup>-1</sup> )	1.06	139.63	101.83	19.92	565.53
N uptake (Tg N yr <sup>-1</sup> )	0.33	838.78	698.11	529.53	1304.87
Net N mineralisation (Tg N yr <sup>-1</sup> )	0.45	836.00	700.28	471.39	1661.53
N <sub>2</sub> O emissions (Tg N yr <sup>-1</sup> )	0.53	7.06	9.04	0.86	11.01
N loss (Tg N yr <sup>-1</sup> )	0.85	187.62	125.96	87.02	602.77
Vegetation C:N ratio	0.28	159.28	154.50	102.84	222.22
Soil C:N ratio	0.90	17.32	11.13	10.00	63.57

379

380 Figure 5 shows the time series of the change from pre-industrial levels of the primary N  
381 pools and fluxes from 1850 to 2021 simulated by the TRENDY-N ensemble. Figure 6 shows the  
382 corresponding Kendall's tau which identifies the existence of a statistically significant trend  
383 (Table A2). ~~Some~~Over the historical period, some models suggest decreasing vegetation N (6/11  
384 models), whereas other models suggest increasing vegetation N (2/11 models) or no trend in  
385 vegetation N (3/11 models). Some models suggest decreasing soil N (7/11 models), whereas  
386 other models suggest increasing soil N (4/11 models). Some models suggest increasing  
387 biological N fixation (7/11 models), whereas other models suggest decreasing biological N  
388 fixation (2/11 models) or no trend in biological N fixation (2/11 models). All models suggest  
389 increasing N uptake (10/10 models). Most models suggest increasing net N mineralisation rate  
390 (9/10 models) or no trend in N mineralisation rate (1/10 models). All models suggest increasing  
391 N<sub>2</sub>O emissions (7/7 models) and increasing N loss (10/10 models).

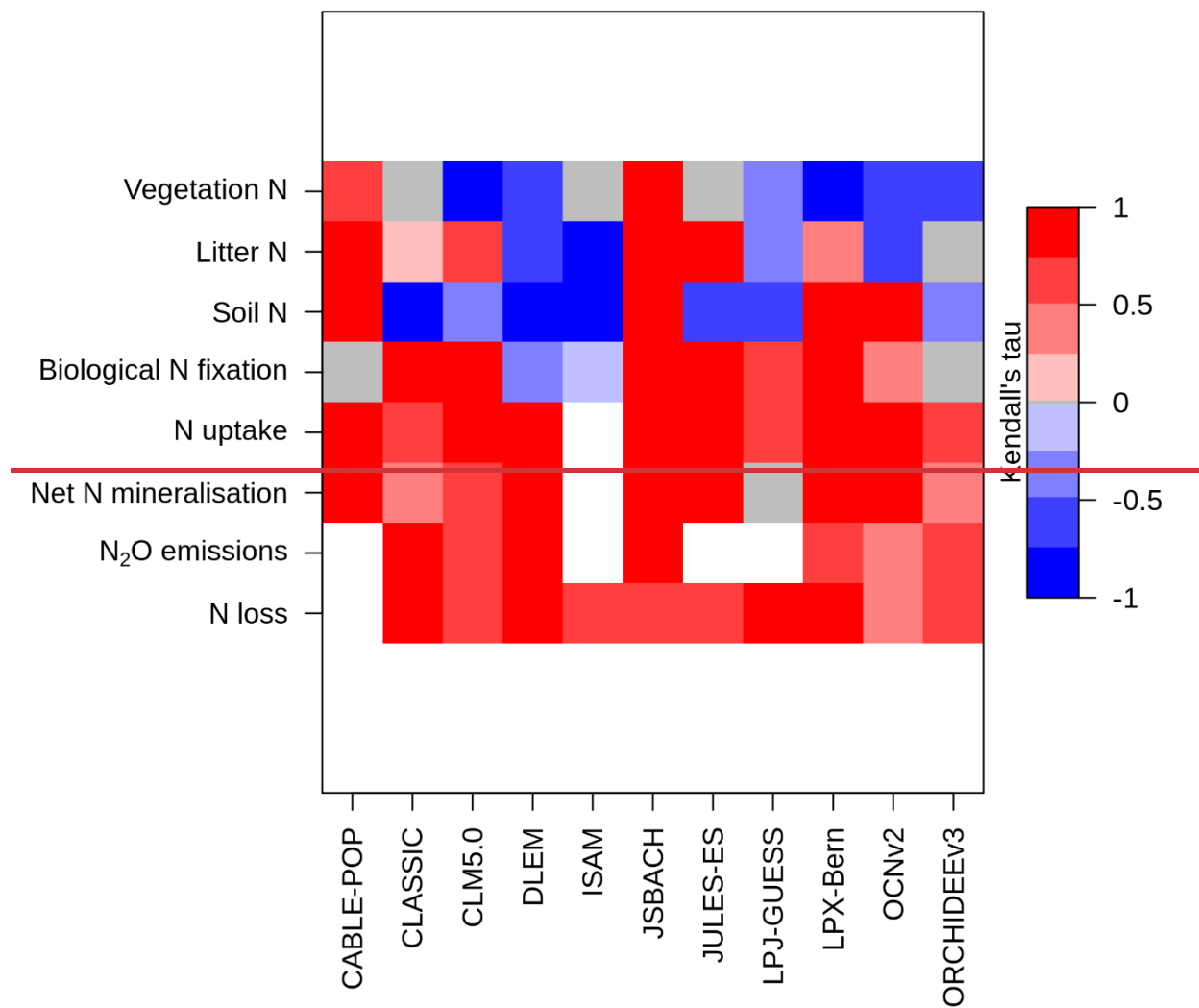
392 Figure 5: Time series of the change from the pre-industrial level (averaged over 1850–1870) of a.  
393 vegetation N, b. litter N, c. soil N, d. biological N fixation, e. N uptake, f. net N mineralisation,  
394 g. N<sub>2</sub>O emissions, and h. N loss simulated by the TRENDY-N ensemble from 1850 to 2021.  
395 Figure [A4A5](#) shows the time series for each N pool and N flux simulated by the TRENDY-N  
396 ensemble from 1850 to 2021.

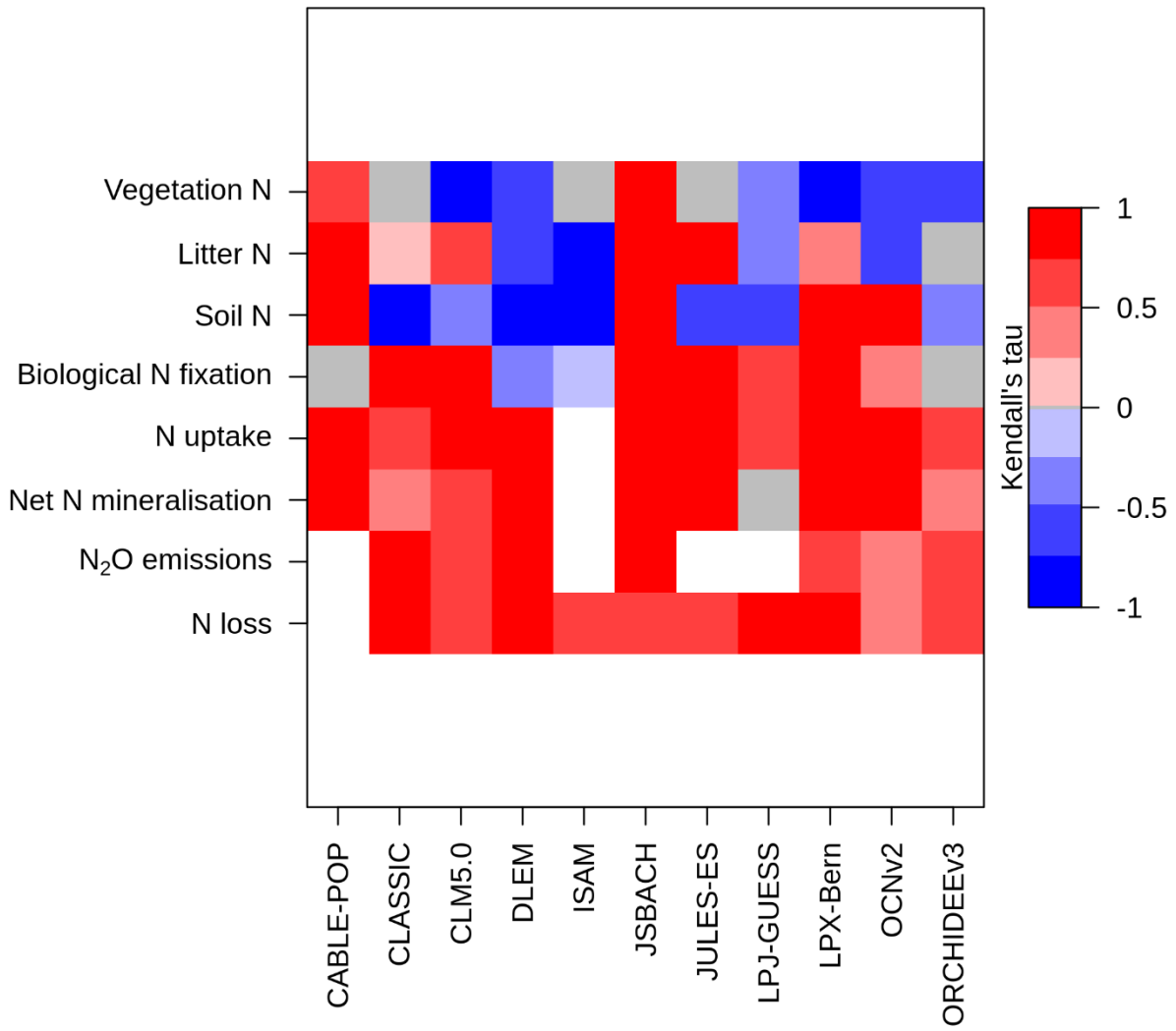






399 Figure 6: Kendall's tau from the Mann-Kendall test ( $p$ -value  $< 0.05$ ) for each N pool and N flux  
400 time series simulated by the TRENDY-N ensemble from 1850 to 2021 (Table A2). A positive  
401 value (red) indicates an increasing trend and a negative value (blue) indicates a decreasing trend  
402 Gray indicates a statistically insignificant value and white indicates a missing value.

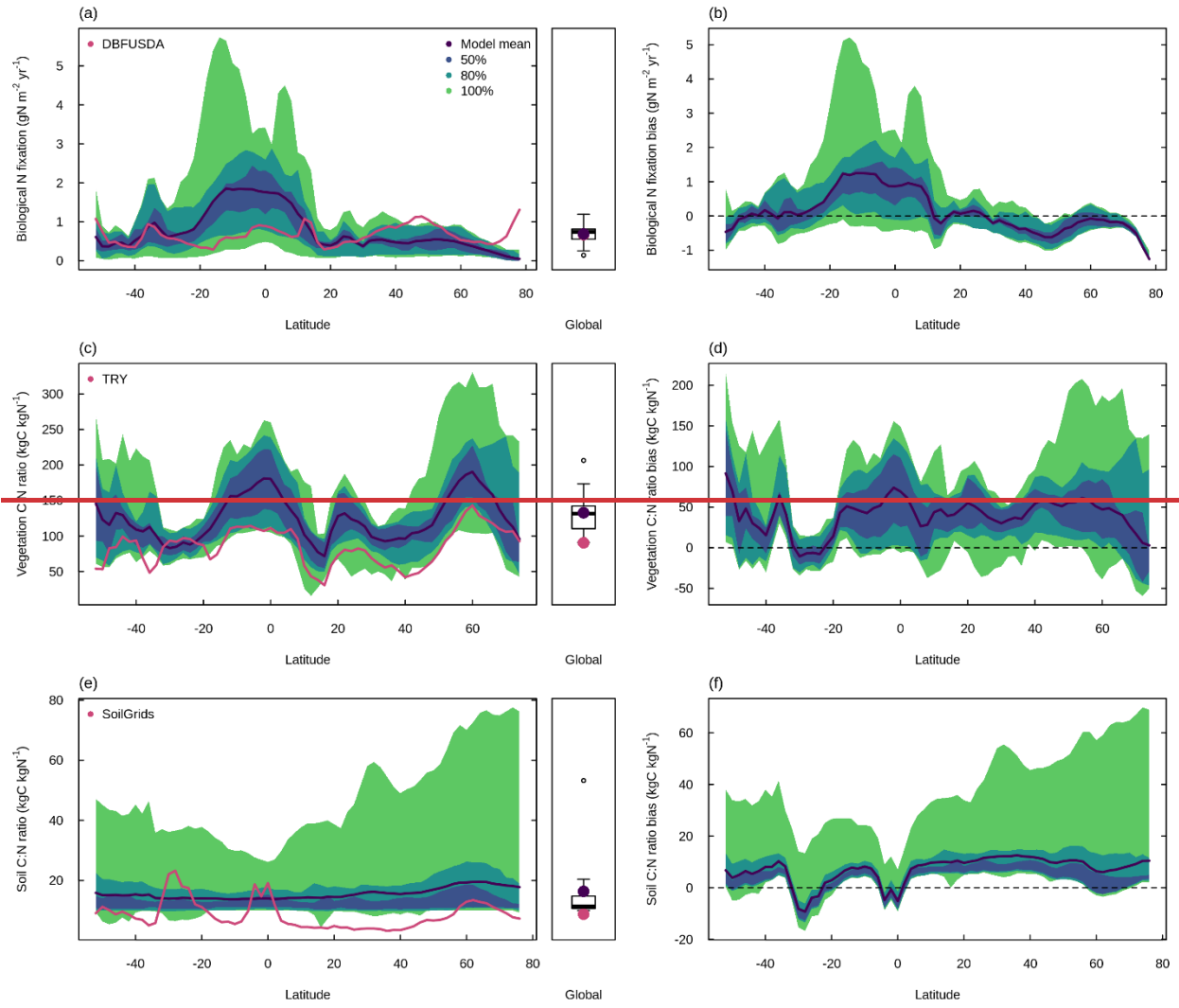


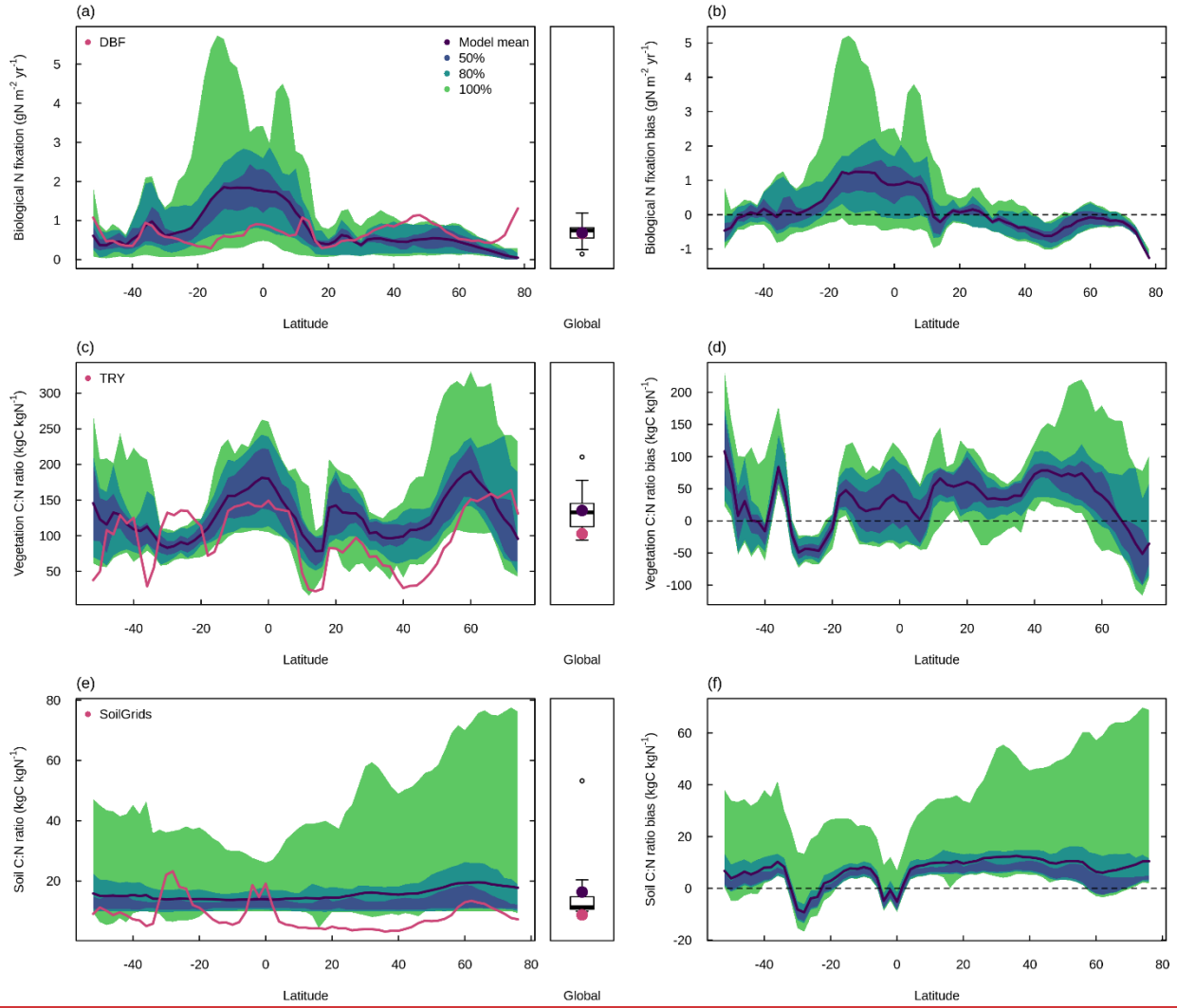


### 405 3.3 Evaluation of biological N fixation, vegetation C:N ratio, and soil C:N ratio

406 In comparison to the observation-based dataset from Davies-Barnard and Friedlingstein  
407 (~~2020) and the U.S. Department of Agriculture (USDA)~~), the TRENDY-N ensemble reproduced  
408 global biological N fixation (101.8 Tg N yr<sup>-1</sup> vs. ~~108.088~~ Tg N yr<sup>-1</sup>; Figure 7a and Table 2) but  
409 overestimated low-latitude biological N fixation and underestimated high-latitude biological N  
410 fixation in the Northern hemisphere (Figure 7b). In comparison to the observation-based dataset  
411 from the TRY plant trait database, the TRENDY-N ensemble overestimated the global  
412 vegetation C:N ratio (154.5 vs. ~~90.5~~102.8; Figure 7c and Table 2) and overestimated the  
413 vegetation C:N ratio across latitudes while capturing its latitudinal pattern (Figure 7d). In  
414 comparison to the observation-based dataset from SoilGrids, the TRENDY-N ensemble  
415 overestimated the global soil C:N ratio, simulating a relatively constant soil C:N ratio across  
416 latitudes (11.1 vs. 8.8; Figure 7e and Table 2). The TRENDY-N ensemble was thus unable to  
417 capture the latitudinal pattern of the soil C:N ratio (Figure 7f).

418 Figure 7: Latitudinal distributions and global means of biological N fixation, vegetation C:N  
419 ratio, and soil C:N ratio simulated by the TRENDY-N ensemble (averaged across models over  
420 1980–2021) in comparison to observations. ace. show the latitudinal distribution of the mean and  
421 boxplots show the global mean. bdf. show the latitudinal distribution of the bias. Latitudinal  
422 distributions show the mean (black line) and the 50%, 80%, and 100% percentiles across models.  
423 Boxplots show the median, interquartile range (box), and 80% percentiles (whiskers) across  
424 models. Observation-based datasets are from Davies-Barnard and Friedlingstein (2020) ~~and the~~  
425 ~~U.S. Department of Agriculture (USDA)~~ for biological N fixation, the TRY plant trait database  
426 for vegetation C:N ratio, and SoilGrids for soil C:N ratio. LPX-Bern simulations are not shown  
427 in ab. Latitudinal distributions and global means of individual models in the TRENDY-N  
428 ensemble are shown in Figure [A5A6](#).

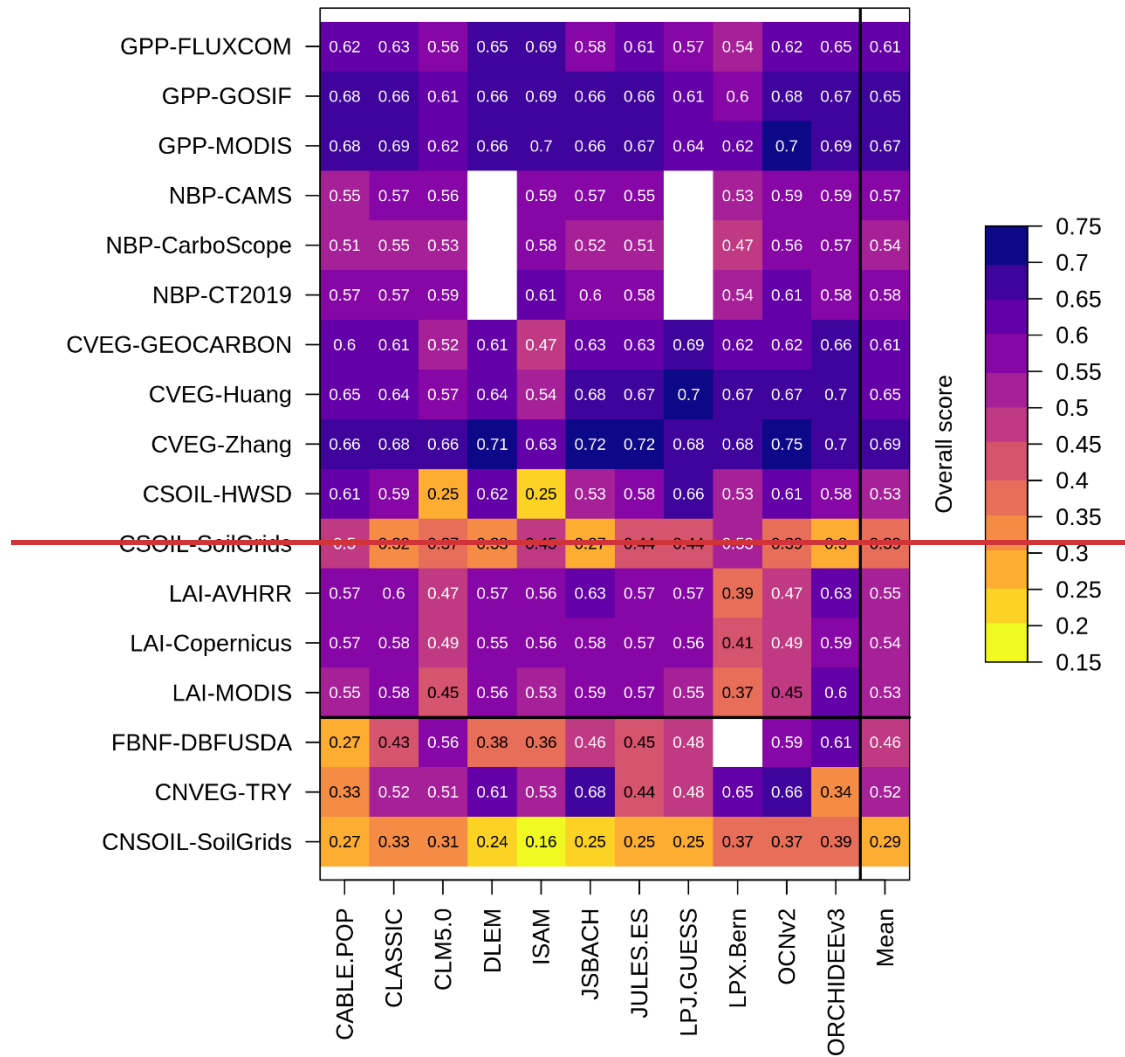


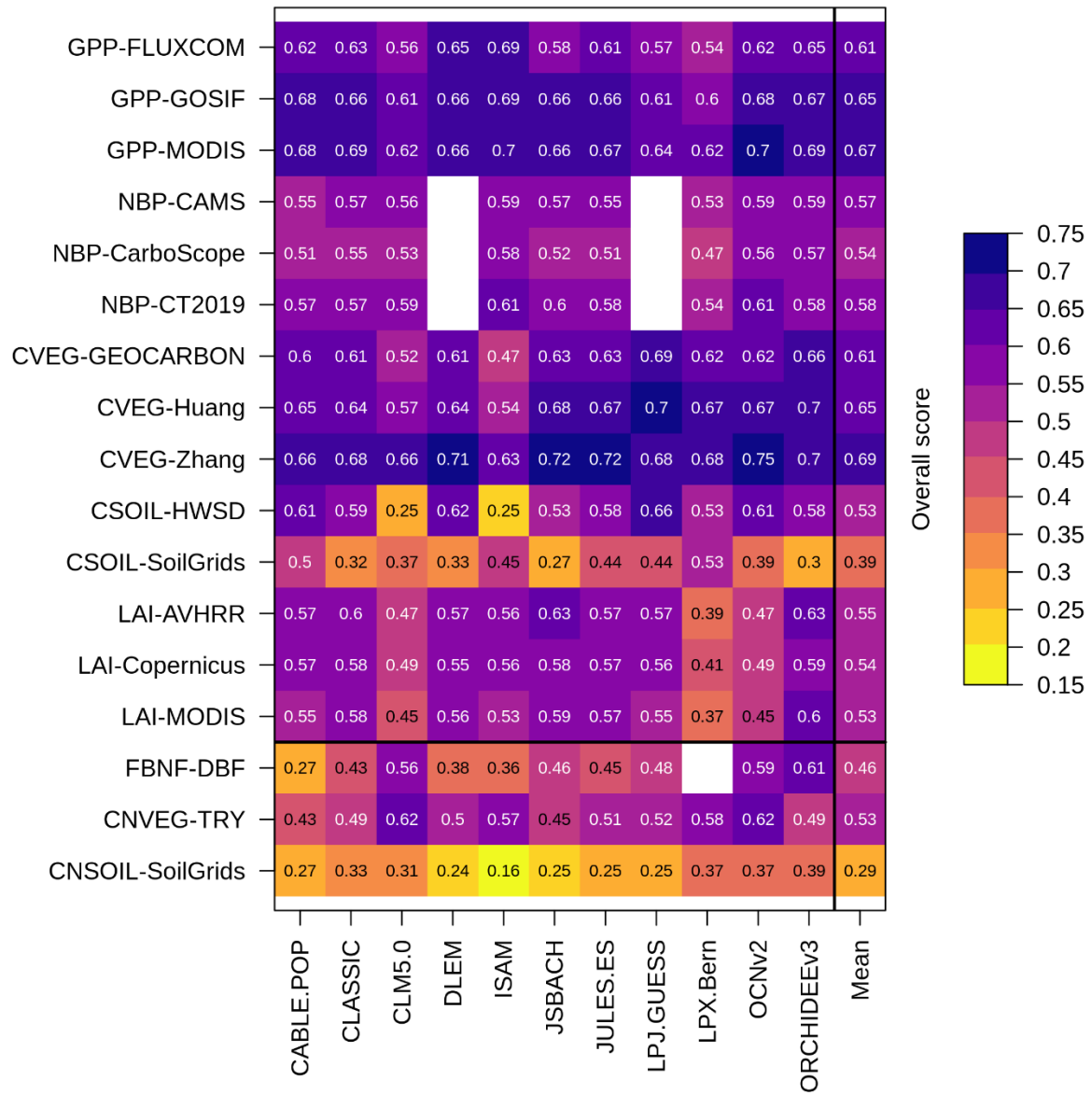


431 The overall score is a metric of model performance in reproducing an observation-based  
432 dataset. Overall scores for biological N fixation, vegetation C:N ratio, and soil C:N ratio (0.46,  
433 ~~0.5253~~, and 0.29 averaged across models, respectively) were lower than those for C cycling  
434 variables (0.58 averaged across all C cycling variables and across models) (Figure 8). The mean  
435 overall score for vegetation C:N ratio across models (~~0.5253~~) was lower than the mean overall  
436 scores for vegetation C across models (which ranged from 0.61 to 0.69 depending on the  
437 observation-based dataset used to derive the score). Similarly, the mean overall score for soil  
438 C:N ratio across models (~~0.2029~~) was lower than the mean overall scores for soil C across  
439 models (which ranged from 0.39 to 0.53 depending on the observation-based dataset used to  
440 derive the score). ~~Overall scores varied between 0.27 and 0.61 for biological N fixation, between~~  
441 ~~0.33 and 0.68 for vegetation C:N ratio, and between 0.16 and 0.39 for soil C:N ratio.~~



442 Figure 8: Overall scores of the TRENDY-N ensemble in simulating C and N cycling variables:  
443 gross primary productivity (GPP), net biome productivity (NBP), vegetation C (CVEG), soil C  
444 (CSOIL), leaf area index (LAI), biological N fixation (FBNF), vegetation C:N ratio (CNVEG),  
445 and soil C:N ratio (CNSOIL). Abbreviations of the observation-based datasets are described in  
446 the Methods and in Seiler et al. (2022).





449 For N cycling variables, the overall score is composed of the time-mean bias score  
450 (which assesses the difference between the time-mean of model simulations and the time-mean  
451 of the observation-based dataset) and the spatial distribution score (which assesses the ability of  
452 the model to reproduce the spatial pattern of the observation-based dataset) (Collier et al., 2018;  
453 Seiler et al., 2022). For biological N fixation, the time-mean bias score averaged across models  
454 was 0.50 and the mean spatial distribution score across models was 0.41 (Table A3). For the  
455 vegetation C:N ratio, the time-mean bias averaged score across models was 0.4746 and the mean  
456 spatial distribution score across models was 0.5859 (Table A3). For the soil C:N ratio, the time-  
457 mean bias score averaged across models was 0.39 and the mean spatial distribution score across  
458 models was 0.19 (Table A3).

459 Note that, for C fluxes, the overall score is composed of not only the time-mean bias  
460 score and the spatial distribution score, but also the monthly centralised root-mean-square-error  
461 score (which assesses the ability of the model to reproduce the time series of the observation-  
462 based dataset), the seasonality score (which assess the ability of the model to reproduce the  
463 seasonality of the observation-based dataset), and the inter-annual variability score (which  
464 assesses the ability of the model to reproduce the inter-annual variability of the observation-  
465 based dataset) because observation-based datasets of C fluxes are available over time (whereas  
466 observation-based datasets of C pools and all N cycling variables are representative of the  
467 present-day (as a single time point)).

### 468 **3.4 Representation Model performance for C cycling vs. N cycling**

469 There were no statistically significant correlations between the overall score of NBP (as  
470 well as other primary C variables) and the overall scores of the primary N variables across the  
471 TRENDY-N ensemble (Figure A2). Furthermore, there were no statistically significant  
472 correlations between the present-day global value of NBP and the present-day global values of  
473 the primary N variables across the TRENDY-N ensemble (Figure A3). Finally, there were no  
474 statistically significant correlations between Kendall's tau of NBP and Kendall's tau of the  
475 primary N variables across the TRENDY-N ensemble (Figure A4).

### 476 **3.5 Model performance for different representations of N cycling processes**

477 There were no statistically significant differences in overall scores between models with  
478 different representations of N limitation of vegetation growth (decreasing  $V_{\text{cmax}}$  and flexible C:N  
479 stoichiometry vs. decreasing NPP), different representations of biological N fixation (function of  
480 N limitation of vegetation growth vs. function of NPP or ET vs. time-invariant), different  
481 representations of the response of vegetation to N limitation (dynamic vs. static), or different  
482 representations of N limitation of decomposition (function of soil N vs. N-invariant) (Table A4).  
483 However, models that represented decomposition as a function of soil N had a significantly  
484 higher NBP score (~~corresponding to~~for CT2019) than models that represented decomposition as  
485 N-invariant. Similarly, there were no statistically significant differences between present-day  
486 global values or Kendall's tau of primary C and N pools and fluxes between models with  
487 different representations of N limitation of vegetation growth, biological N fixation, vegetation  
488 response to N limitation, and N limitation of decomposition (Table A5 and A6). **Figure A1**

489 shows correlations between present-day global values of the primary C and N pools and fluxes  
490 across the TRENDY N ensemble. Figure A2 shows correlations between Kendall's tau of the  
491 primary C and N pools and fluxes across the TRENDY N ensemble. Figure A3 shows  
492 correlations between overall scores of the primary C and N pools and fluxes across the  
493 TRENDY N ensemble. This is likely in part due to the low number of models and the  
494 confounding influence of other process representations.

## 495 496 **4 Discussion**

### 497 **4.1 Evaluation of N cycling in terrestrial biosphere models**

498 Despite the pivotal importance of N in constraining terrestrial C cycling and ultimately  
499 the ability of all TRENDY-N models to simulate the historical terrestrial C sink, in line with  
500 observations (Figure 2), there is substantial variation in simulated N cycling processes by the  
501 terrestrial biosphere models in the TRENDY N ensemble models. The magnitude of N pools and  
502 fluxes differ considerably between models, between 19.9 and 565.5 Tg N yr<sup>-1</sup> for biological N  
503 fixation (CV = 1.1), between 1.5 and 5.6 Tg N for vegetation N (CV = 0.4), between 32.1 and  
504 277.4 Tg N for soil N (CV = 0.7), and between 87.0 and 602.8 Tg N yr<sup>-1</sup> for N loss (CV = 0.9).  
505 The spread across the TRENDY N ensemble suggests that approaches to represent N cycling  
506 processes vary among terrestrial biosphere models and that there is no clear consensus yet on  
507 what the best approaches are, supporting the use of an ensemble approach to capture the  
508 uncertainties in our understanding of the N cycle, similarly to the C cycle.

509 (Figures 3 and A1). Additionally, the historical trajectories of these N pools and  
510 fluxes differ between models: some models simulate increasing vegetation N and soil N whereas  
511 others simulate decreasing vegetation N and soil N between 1850 and 2021 (Figures 5 and 6).  
512 These trajectories are the result of a host of interacting global change drivers (CO<sub>2</sub> fertilisation,  
513 intensifying N deposition, rising temperature and varying precipitation, land use change and  
514 associated N fertilisation regimes) whose effects are challenging to disentangle without  
515 additional simulations. For example, while intensifying N deposition and N fertiliser use could  
516 drive increasing soil N and N uptake, land use change could increase N losses from both  
517 vegetation N and soil N. Despite these large differences across models in the historical  
518 trajectories of vegetation N and soil N, all models simulate the historical terrestrial C sink in line  
519 with observations. This suggests that the underlying N cycling processes that regulate terrestrial  
520 C sequestration operate differently across models and may not be fully captured. Modelled  
521 experimental manipulations (such as CO<sub>2</sub> fertilisation or N fertilisation experiments) are  
522 imperative to evaluate model formulations of the underlying mechanisms of C-N cycling  
523 interactions given that it is these processes that dictate the response of terrestrial C sequestration  
524 to global change.

525 Most models suggest increasing biological N fixation between 1850 and 2021. This  
526 occurs either as a result of increasing vegetation biomass or the up-regulation of biological N  
527 fixation due to N limitation imposed by CO<sub>2</sub> fertilisation or a combination thereof, depending on  
528 the representation of biological N fixation in a given model (Table 1). This follows observations

529 that suggest that biological N fixation is stimulated by CO<sub>2</sub> fertilisation (Zheng et al., 2020;  
530 Liang et al., 2016), although its mechanism (i.e., up-regulated biological N fixation in N-limited  
531 conditions) may not be captured. Similarly, most models also suggest increasing N uptake  
532 between 1850 and 2021. This also occurs as a result of increasing vegetation biomass, increasing  
533 soil N from intensifying N deposition and N fertiliser use, or increasing biological N fixation,  
534 mycorrhizae and root allocation due to N limitation imposed by CO<sub>2</sub> fertilisation, again  
535 dependent on the representation of the vegetation response to N limitation in a given model  
536 (Table 1). Most models suggest increasing net N mineralisation rate between 1850 and 2021  
537 likely due to rising temperature following observations (Liu et al., 2017). Most models suggest  
538 increasing N<sub>2</sub>O emissions (and N losses) between 1850 and 2021 likely due to rising temperature  
539 and intensifying N deposition and N fertiliser use following observations (Tian et al., 2020).

540 We focused on three key N cycling processes for evaluation: biological N fixation,  
541 vegetation C:N ratio, and soil C:N ratio. These three key N cycling processes have important  
542 implications for projecting the future terrestrial C sink. Biological N fixation is the dominant  
543 natural N supply to terrestrial ecosystems and allows vegetation to increase N uptake in N-  
544 limited conditions, reduce N limitation, and thus sustain terrestrial C sequestration, such as in  
545 response to N limitation imposed by CO<sub>2</sub> fertilisation (Zheng et al., 2020; Liang et al., 2016).  
546 Vegetation and soil C:N ratios reflect assimilated C per unit N and thus terrestrial C  
547 sequestration. They can potentially vary, such as in response to high photosynthesis rates relative  
548 to N uptake rates driven by CO<sub>2</sub> fertilisation (Elser et al., 2010). Overall scores of N cycling  
549 variables, which quantify model performance in reproducing an observation-based dataset, are  
550 lower than overall scores of corresponding C cycling variables, suggesting that models could be  
551 less capable of capturing N cycling processes than C cycling processes- (Figure 8). However, this  
552 could also be due to the significant uncertainty associated with measurements of N cycling  
553 processes as discussed below. ~~Besides models that represent N limitation of decomposition  
554 yielding a higher overall NBP score, there were no statistically significant differences between  
555 models with different representations of N limitation of vegetation growth, biological N fixation,  
556 the response of vegetation to N limitation, and N limitation of decomposition for the overall  
557 score, present day global value, or Kendall's tau. This is likely due to the low number of models  
558 in the TRENDY-N ensemble and the confounding influence of other process representations.  
559 Studies have explored the validity of different representations of N cycling processes within a  
560 single model, suggesting that alternative representations of a biological N fixation, ecosystem  
561 C:N stoichiometry, and ecosystem N losses lead to substantial differences in simulated C cycling~~  
562 :

563 The TRENDY-N ensemble reproduced global observation-based biological N fixation  
564 but tended to overestimate low-latitude biological N fixation and underestimate high-latitude  
565 biological N fixation- (Figure 7ab). This is likely because most models represented biological N  
566 fixation phenomenologically as a function of a measure of vegetation activity (either NPP or  
567 ET). Since there is higher vegetation activity at low latitudes than at high latitudes these models  
568 thus represent higher biological N fixation at low latitudes than at high latitudes. However,  
569 because biological N fixation is down-regulated in non-N-limited conditions, it is often down-  
570 regulated at low latitudes, which are generally not (or at least less) N-limited (Barron et al.,

571 2011; Batterman et al., 2013; Sullivan et al., 2014). While CLASSIC, CLM5.0, and OCNv2 can  
572 represent the down-regulation of biological N fixation in non-N-limited conditions, they still  
573 simulate high low-latitude biological N fixation. This suggests that the strength of regulation of  
574 biological N fixation could be insufficient and/or that there could be unaccounted N sources at  
575 low latitudes. For example, rock N weathering could be a significant N source to terrestrial  
576 ecosystems. Some estimates have suggested that rock N weathering could be as high as 11 – 18  
577 Tg N yr<sup>-1</sup> globally (Houlton et al., 2018) but is not explicitly represented in the TRENDY-N  
578 ensemble (with the exception of LPX-Bern which calculates all external N sources post hoc to  
579 simulate a closed N cycle thereby implicitly including rock N sources). The discrepancy between  
580 modelled and observed biological N fixation could also be due to uncertainty in the observation-  
581 based dataset given the difficulties associated with measuring biological N fixation (Soper et al.,  
582 2021). Ecological theory (Hedin et al., 2009) has suggested that natural biological N fixation  
583 should be higher at low latitudes given large N losses, in contrast to the observation-based  
584 dataset from Davies-Barnard and Friedlingstein (2020). Furthermore, the observation-based  
585 dataset from Davies-Barnard and Friedlingstein (2020) did not explicitly account for agricultural  
586 biological N fixation but rather assumed that crop biological N fixation rates are equivalent to  
587 those of grasses although they are likely to be much greater (Peoples et al., 2021; Herridge et al.,  
588 2022)~~Observational uncertainty is discussed further below.~~

589 The TRENDY-N ensemble overestimated global observation-based vegetation C:N ratio  
590 but reproduced its latitudinal pattern (as also indicated by its higher spatial distribution score)  
591 (Figure 7cd). This is because most models represent different plant functional types (e.g.,  
592 evergreen needleleaf trees, deciduous broadleaf trees, evergreen broadleaf trees, etc.) with  
593 different tissue C:N ratios (which can either be flexible within a constrained range or time-  
594 invariant). These plant functional types are geographically distributed according to similar land  
595 cover products. The TRENDY-N ensemble overestimated global observation-based soil C:N  
596 ratio and failed to reproduce its latitudinal pattern (as also indicated by its lower spatial  
597 distribution score) (Figure 7ef). In particular, models failed to reproduce the peak at the equator  
598 and the peak at approximately -30°S, corresponding to tropical forests and deserts respectively.  
599 This is because most models represent a constant soil C:N ratio (both temporally and spatially)  
600 and are thus unable to capture the spatial variability in the soil C:N ratio. Improving the  
601 representation of soil N is an important future direction for terrestrial biosphere model  
602 development given the essential feedbacks between soil N and soil C.

#### 603 4.2 Disconnect between C and N cycling in terrestrial biosphere models

604 The importance of N limitation of terrestrial C sequestration is empirically established.  
605 (Elser et al., 2007; LeBauer and Treseder, 2008; Wright et al., 2018). It has already influenced  
606 the historical terrestrial C sink (Wang et al., 2020a) and it is expected to be especially important  
607 under future CO<sub>2</sub> fertilisation and global change (Terrer et al., 2019). While all TRENDY-N  
608 models simulate the historical terrestrial C sink in line with observations (and are no different  
609 from TRENDY models without a representation N cycling (Seiler et al., 2022)), our results  
610 suggest a disconnect between C and N cycling in these models. First, the models exhibit a wide  
611 spread across simulated N pools and fluxes. Second, there are no significant correlations between



612 model performance in simulating N cycling and model performance in simulating C cycling.  
613 Third, there are no statistically significant differences between models with different  
614 representations of fundamental N cycling processes (N limitation of vegetation growth,  
615 biological N fixation, the response of vegetation to N limitation, and N limitation of  
616 decomposition).

617 Overall, our results suggest that the underlying N cycling processes that regulate  
618 terrestrial C sequestration operate differently across models and may not be fully captured given  
619 that models are calibrated to C cycling. The spread across models suggests that approaches to  
620 represent N cycling processes vary among models and that there is no clear consensus yet on  
621 what the best approaches are. Studies have explored the validity of different representations of N  
622 cycling processes within a single model, suggesting that alternative representations of a  
623 biological N fixation, ecosystem C:N stoichiometry, and ecosystem N losses lead to substantial  
624 differences in simulated C cycling (Kou-Giesbrecht and Arora, 2022; Meyerholt et al., 2020;  
625 Peng et al., 2020; Wieder et al., 2015a). This disconnect between C and N cycling will become  
626 particularly consequential for projecting the terrestrial C sink under future global change, which  
627 is likely to modify the C-N balance through N limitation of CO<sub>2</sub> fertilisation and intensifying N  
628 deposition among other effects of global change.

### 629 4.3 Future directions

630 Evaluating N cycling in terrestrial biosphere models is severely restricted by the lack of  
631 available observations of N cycling. N cycling processes are notoriously difficult to measure,  
632 such as biological N fixation (Soper et al., 2021) and gaseous N losses (Barton et al., 2015). In  
633 the past, N cycling has been commonly evaluated by comparison to estimates of global N pools  
634 and fluxes derived from a small number of observations that have been scaled up or averaged to  
635 yield a value with wide confidence intervals (Davies-Barnard et al., 2020). Not only are these  
636 global totals highly uncertain, but they also do not allow for the analysis of spatial patterns. Here,  
637 we present an improved framework to evaluate three key N cycling processes – biological N  
638 fixation, vegetation C:N ratio, and soil C:N ratio – in terrestrial biosphere models. However,  
639 these globally-gridded observation-based datasets are also uncertain, given uncertainty in the  
640 estimates of tissue C:N ratios for different plant functional types and tissue fraction of total  
641 biomass (especially those of roots and wood which had a lower number of measurements in  
642 comparison to that of leaves), as well as in the measurements and models used to derive soil N  
643 (Batjes et al., 2020). ~~Importantly, more~~ More observations of ~~additional~~ these N cycling processes  
644 are necessary to ~~fully evaluate N cycling in terrestrial biosphere models. Multiple observation-~~  
645 ~~based datasets from different sources of a given N cycling process are necessary to evaluate~~  
646 ~~observational~~ reduce uncertainty. ~~Observation-based datasets of N cycling processes at,~~  
647 Temporally explicit measurements are important for assessing intra-annual and inter-annual ~~time~~  
648 ~~scales are necessary to assess temporal patterns. Paleoclimatic observations could also be utilised~~  
649 ~~for evaluation~~ variability. Leveraging advances in remote sensing (Knyazikhin et al., 2013;  
650 Townsend et al., 2013; Cawse-Nicholson et al., 2021) as well as incorporating N cycling process  
651 measurements into research networks such as FLUXNET (Vicca et al., 2018) is essential.  
652 Multiple observation-based datasets from different sources and derived via different



653 methodologies of a given N cycling process are necessary to evaluate observational uncertainty  
654 (Seiler et al., 2021). Global observations of other important N cycling processes (such as N  
655 mineralisation and N losses) are necessary to fully evaluate N cycling in terrestrial biosphere  
656 models. Additionally, hindcast simulations of the transition from the Last Glacial Maximum to  
657 the preindustrial period can be used in combination with proxy-based reconstructions of past  
658 N<sub>2</sub>O emissions (Fischer et al., 2019) as well as C stocks (Jeltsch-Thömmes et al., 2019) for  
659 model evaluation and can serve as a constraint for terrestrial biosphere models (Joos et al., 2020).

660 Modelled experimental manipulations (such as CO<sub>2</sub> fertilisation or N fertilisation  
661 experiments) are imperative to evaluate model formulations of the underlying mechanisms of C-  
662 N cycling interactions (Medlyn et al., 2015; Wieder et al., 2019; Zaehle et al., 2014). Derived  
663 nutrient limitation products (Fisher et al., 2012) can also be applied to evaluate present-day  
664 nutrient cycling when phosphorus (P) is accounted for (Braghiere et al., 2022). Evaluating the  
665 ability of models to simulate present-day N cycling processes, as we did here, is only one method  
666 of assessing their ability to simulate N limitation of terrestrial C sequestration. A robust test of  
667 the simulated response to CO<sub>2</sub> fertilisation and N fertilisation across models would be ideal for  
668 evaluating the ability of models to represent the regulation of C cycling by N cycling under  
669 global change and thus their ability to realistically simulate the future terrestrial C sink.

670 While some of the models in the TRENDY-N ensemble have the capability of  
671 representing coupled C, N, and ~~phosphorus (P)~~P cycling (Goll et al., 2012; Nakhavali et al.,  
672 2022; Sun et al., 2021; Wang et al., 2010, 2020b; Yang et al., 2014), P cycling was not active in  
673 the model simulations in the GCP 2022. P limitation could be important for limiting terrestrial C  
674 sequestration, especially in low-latitude forests (Elser et al., 2007; Terrer et al., 2019; Wieder et  
675 al., 2015b). As more models incorporate coupled C-N-P cycling (Reed et al., 2015; Braghiere et  
676 al., 2022), observation-based datasets of P will also be necessary for model evaluation.

677

## 678 **5 Conclusions**

679 Because the TRENDY-N ensemble overestimated both vegetation and soil C:N ratios, it  
680 is possible that models could overestimate assimilated C per unit N and thus future terrestrial C  
681 sequestration under CO<sub>2</sub> fertilisation. Alongside discrepancies in biological N fixation, this could  
682 lead to biases in projections of the future terrestrial C sink by the TRENDY-N ensemble ~~(not,~~  
683 Not to mention ~~the~~there are several other terrestrial biosphere models in the TRENDY ensemble  
684 that do not represent coupled C-N cycling). While ~~terrestrial biosphere~~the models are capable of  
685 reproducing the current terrestrial C sink, the ~~results presented here suggest that underlying~~  
686 mechanisms of C spread across the models in simulating N cycling suggests that C-N  
687 interactions operate differently across models and may not be fully captured. These given that  
688 models are calibrated to C cycling. However, these C-N interactions are critical for projections  
689 of projecting the future terrestrial C sink as the C/N balance is expected to shift in the future  
690 under interacting global change drivers in the future.

691 **Code availability**

692 AMBER is available at <https://gitlab.com/cseiler/AMBER>.

693

694 **Data availability**

695 Biological N fixation, vegetation C:N ratio, and soil C:N ratio are available at  
696 <https://gitlab.com/sian.kougiesbrecht/trendy-nitrogen>.

697

698 **Author contribution**

699 SKG designed and conducted the study and prepared the initial manuscript. VA and CS provided  
700 feedback on the initial manuscript and its subsequent revisions. The other co-authors conducted  
701 TRENDY simulations and provided feedback on the manuscript.

702

703 **Competing interests**

704 The authors declare that they have no conflict of interest.

705

706 **Acknowledgements**

707 The authors would like to thank T Davies-Barnard for compiling the observations used to  
708 evaluate biological N fixation. ORCHIDEEv3 simulations were granted access to the HPC  
709 resources of GENCI-TGCC under the allocation A0130106328.

710 **Appendix A**

711  
 712 Table A1: IGBP land cover type, corresponding TRY plant trait database PFT, tissue C:N ratios  
 713 (from the TRY plant trait database (Kattge et al., 2020)), tissue fractions (Poorter et al., 2012),  
 714 and calculated total C:N ratio.

IGBP land cover type	TRY plant trait database PFT	Leaf C:N	Leaf fraction	Root C:N	Root fraction	Stem C:N	Stem fraction	Total C:N
0 bare	-							
1 Evergreen needleleaf forest	<del>Boreal evergreen needleleaf</del> <del>Tree evergreen needleleaf</del> Temperate evergreen needleleaf <del>Evergreen needleleaf</del> <del>Tree evergreen needleleaf</del> <del>Boreal evergreen needleleaf</del> Gymnosperm evergreen needleleaf tree Temperate conifer Boreal conifer Evergreen gymnosperm	<del>40.15</del>	0.04	<del>51.943.1</del>	0.21	<del>305.4236</del> .0	0.75	<del>241.5187.</del> 7
2 Evergreen broadleaf forest	<del>Boreal evergreen broadleaf</del> <del>Tree evergreen broadleaf</del> Temperate evergreen broadleaf Tropical evergreen broadleaf <del>Evergreen broadleaf</del> <del>Tree evergreen broadleaf</del> <del>Boreal evergreen broadleaf</del> Angiosperm evergreen broadleaf tree Gymnosperm evergreen broadleaf tree Temperate evergreen Rainforest Evergreen angiosperm	<del>26.831.</del> 3	0.02	<del>26.435.1</del>	0.16	<del>139.3180</del> .7	0.82	<del>119.0154.</del> 4

3 Deciduous needleleaf forest	<del>Tree deciduous needleleaf Boreal deciduous needleleaf Gymnosperm deciduous needleleaf tree Deciduous gymnosperm</del>							<del>241.5<sup>a</sup>187. 7<sup>a</sup></del>
4 Deciduous broadleaf forest	<del>Boreal deciduous broadleaf Tree deciduous broadleaf Temperate deciduous broadleaf Tropical deciduous broadleaf Deciduous broadleaf Tree deciduous broadleaf Boreal deciduous broadleaf Angiosperm deciduous broadleaf tree Gymnosperm deciduous broadleaf tree Temperate deciduous Deciduous angiosperm</del>	21.56	0.03	39.637.4	0.21	102.172. 3	0.76	86.663.5
5 Mixed forest								149. 0 <sup>b</sup> 135.2 <sup>b</sup>
6 Closed shrubland	<del>Evergreen shrub Shrub evergreen broadleaf Evergreen shrub</del>	34.536. 1	0.09	24.938.2	0.4742	216.7234 .2	0.49	121.0134. 1
7 Open shrubland	<del>Deciduous shrub Shrub Angiosperm evergreen broadleaf shrub</del>	34.5	0.09	24.9	0.47	216.7	0.49	121.0
8 Woody savannas	<del>Angiosperm deciduous broadleaf shrub</del>	34.5	0.09	24.9	0.36	216.7	0.57	134.5
9 Savannas	<del>Gymnosperm evergreen broadleaf shrub Desert shrub Savanna evergreen Savanna deciduous</del>	34.5	0.09	24.9	0.36	216.7	0.57	134.5

10 Grasslands	Grass C3 Grass C4 Temperate herbaceous Tropical herbaceous Herbaceous C3 Herbaceous C4 Angiosperm herbaceous C3 Angiosperm herbaceous C4	<del>18.6</del> <u>19.1</u>	0.17	<del>30.9</del> <u>29.3</u>	<del>0.77</del> <u>0.56</u>	<del>29.3</del> <u>27.2</u>	0.27	<del>34.9</del> <u>27.0</u>
11 Permanent wetlands								<del>34.9</del> <u>27.0</u> <sup>c</sup>
12 Croplands	Crop C3	<del>41.7</del> <u>10.5</u>	0.17	<del>29.3</del> <u>30.9</u> <sup>e</sup>	<del>0.77</del> <u>0.56</u> <sup>c</sup>	<del>27.2</del> <u>29.3</u> <sup>e</sup>	<del>0.27</del> <u>0.27</u> <sup>c</sup>	<del>28.9</del> <u>25.5</u>
13 Urban and built-up	-							
14 Cropland / natural vegetation mosaic								<del>28.9</del> <u>25.5</u> <sup>d</sup>
15 Snow and ice	-							
16 Barren or sparsely vegetated	-							

715 <sup>a</sup> Value from evergreen needleleaf forest.

716 <sup>b</sup> Average of evergreen needleleaf forest, evergreen broadleaf forest, and deciduous broadleaf forest.

717 <sup>c</sup> Value from grasslands.

718 <sup>d</sup> Value from croplands.

719 Table A2: Kendall's tau from the Mann-Kendall test ( $p$ -value  $< 0.05$ ) for each N pool and N flux  
 720 time series simulated by the TRENDY-N ensemble from 1850 to 2021. NS indicates that  
 721 Kendall's tau is not significant. NA indicates that the variable was not reported by the model.

	CABLE-POP	CLASSIC	CLM5.0	DLEM	ISAM	JSBACH	JULES-ES	LPJ-GUESS	LPX-Bern	OCNv2	ORCHIDEEv3
Vegetation N	0.58	NS	-0.97	-0.51	NS	0.83	NS	-0.25	-0.75	-0.67	-0.51
Litter N	0.88	0.15	0.65	-0.7	-0.87	0.92	0.86	-0.35	0.44	-0.69	NS
Soil N	1	-0.8	-0.47	-0.97	-0.91	0.99	-0.67	-0.68	1	1	-0.3
Biological N fixation	NS	0.95	0.84	-0.33	-0.11	0.89	0.79	0.62	0.92	0.45	NS
N uptake	0.89	0.64	0.81	0.78	NA	0.81	0.85	0.54	0.82	0.85	0.71
Net N mineralisation	0.91	0.33	0.73	0.87	NA	0.85	0.76	NS	0.86	0.82	0.31
N <sub>2</sub> O emissions	NA	0.92	0.7	0.87	NA	0.95	NA	NA	0.7	0.42	0.69
N loss	NA	0.94	0.67	0.94	0.73	0.59	0.63	0.94	0.81	0.42	0.65

722

723 Table A3: Time-mean bias score ( $S_{\text{bias}}$ ), spatial distribution score ( $S_{\text{dist}}$ ), and overall score  
 724 ( $S_{\text{overall}}$ ) of the TRENDY-N ensemble in simulating biological N fixation, vegetation C:N ratio,  
 725 and soil C:N ratio.

	Biological N fixation			Vegetation C:N ratio			Soil C:N ratio		
	$S_{\text{bias}}$	$S_{\text{dist}}$	$S_{\text{overall}}$	$S_{\text{bias}}$	$S_{\text{dist}}$	$S_{\text{overall}}$	$S_{\text{bias}}$	$S_{\text{dist}}$	$S_{\text{overall}}$
CABLE-POP	0.46	0.08	0.27	<u>0.3436</u>	<u>0.3350</u>	<u>0.3343</u>	0.2	0.34	0.27
CLASSIC	0.46	<u>0.440</u>	0.43	<u>0.4547</u>	<u>0.5952</u>	<u>0.5249</u>	0.43	0.22	0.33
CLM5.0	0.55	0.56	0.56	<u>0.5756</u>	<u>0.4668</u>	<u>0.5162</u>	0.45	0.16	0.31
DLEM	0.46	0.29	0.38	<u>0.4750</u>	<u>0.7550</u>	<u>0.6150</u>	0.48	0.01	0.24
ISAM	0.47	0.24	0.36	<u>0.4945</u>	<u>0.5770</u>	<u>0.5357</u>	0.05	0.28	0.16
JSBACH	0.48	0.44	0.46	<u>0.6353</u>	<u>0.7437</u>	<u>0.6845</u>	0.38	0.11	0.25
JULES-ES	0.47	0.43	0.45	<u>0.440</u>	<u>0.4962</u>	<u>0.4451</u>	0.51	0	0.25
LPJ-GUESS	0.51	0.45	0.48	<u>0.4541</u>	<u>0.5263</u>	<u>0.4852</u>	0.49	0.01	0.25
LPX-Bern	NA	NA	NA	<u>0.5451</u>	<u>0.7664</u>	<u>0.6558</u>	0.33	0.4	0.37
OCNv2	0.56	0.62	0.59	<u>0.5654</u>	<u>0.7671</u>	<u>0.6662</u>	0.47	0.26	0.37
ORCHIDEEv3	<u>0.660</u>	0.63	0.61	<u>0.2735</u>	<u>0.4163</u>	<u>0.3449</u>	0.48	0.31	0.39
<u>Mean</u>	<u>0.50</u>	<u>0.41</u>	<u>0.46</u>	<u>0.46</u>	<u>0.59</u>	<u>0.53</u>	<u>0.39</u>	<u>0.19</u>	<u>0.29</u>

726

727 Table A4: Overall scores of biological N fixation, vegetation C:N ratio, soil C:N ratio, and NBP  
 728 ~~of~~averaged across TRENDY-N ensemble models with different representations of key N cycling  
 729 processes (N limitation of vegetation growth, biological N fixation, vegetation response to N  
 730 limitation, and N limitation of decomposition, see Table 1). p-values are from t-tests and  
 731 ANOVAs assessing differences between these representations of key N cycling processes.

		BNF- DBFUSDA DBF	CNVEG- TRY	CNSOIL- SoilGrids	NBP- CAMS	NBP- Carboscope	NBP- CT2019
N limitation of vegetation growth	V <sub>max</sub> / flexible C:N stoichiometry	0.49	<u>0.4753</u>	0.32	0.57	0.54	0.58
	NPP	0.41	<u>0.5852</u>	0.26	0.56	0.52	0.58
	p-value	0.21	<u>0.1488</u>	0.15	0.59	0.44	<u>0.990</u>
Biological N fixation	f(N limitation of vegetation growth)	0.44	<u>0.3446</u>	0.33	0.57	0.54	0.57
	f(NPP) or f(ET)	0.44	<u>0.5351</u>	0.23	0.57	0.54	<u>0.660</u>
	Time-invariant	0.53	<u>0.5658</u>	0.33	0.57	0.55	0.59
	p-value	0.59	<u>0.0715</u>	0.06	0.92	0.91	0.28
Vegetation response to N limitation	Dynamic	0.49	<u>0.5655</u>	<u>0.330</u>	0.57	0.55	0.59
	Static	0.43	<u>0.551</u>	0.28	0.56	0.53	0.58
	p-value	0.44	<u>0.4125</u>	0.71	0.48	<u>0.330</u>	0.67
N limitation of decomposition	f(soil N)	0.47	<u>0.5755</u>	0.26	0.57	0.54	<u>0.660</u>
	N-invariant	0.45	<u>0.4650</u>	0.32	0.56	0.52	0.56
	p-value	0.86	<u>0.1726</u>	0.16	0.26	0.44	<u>0.02</u>

732



733 Table A5: Present-day global values of biological N fixation, vegetation C:N ratio, and soil C:N  
 734 ratio simulated by averaged across TRENDY-N ensemble models with different representations  
 735 of key N cycling processes (N limitation of vegetation growth, biological N fixation, vegetation  
 736 response to N limitation, and N limitation of decomposition, see Table 1). p-values are from t-  
 737 tests and ANOVAs assessing differences between these representations of key N cycling  
 738 processes.

		Biological N fixation	Vegetation C:N ratio	Soil C:N ratio
N limitation of vegetation growth	V <sub>cmax</sub> / flexible C:N stoichiometry	106.78	161.8	12.75
	NPP	179.06	156.26	22.79
	p-value	0.51	0.85	0.39
Biological N fixation	f(N limitation of vegetation growth)	123.14	201.68	15.71
	f(NPP) or f(ET)	66.37	177.37	24.31
	Time-invariant	118.95	123.89	11.64
	p-value	0.27	0.15	0.68
Vegetation response to N limitation	Dynamic	99.25	143.32	11.22
	Static	173.29	172.58	22.4
	p-value	0.41	0.29	0.24
N limitation of decomposition	f(soil N)	88.21	153.36	20.04
	N-invariant	201.34	166.38	14.04
	p-value	0.3	0.66	0.53

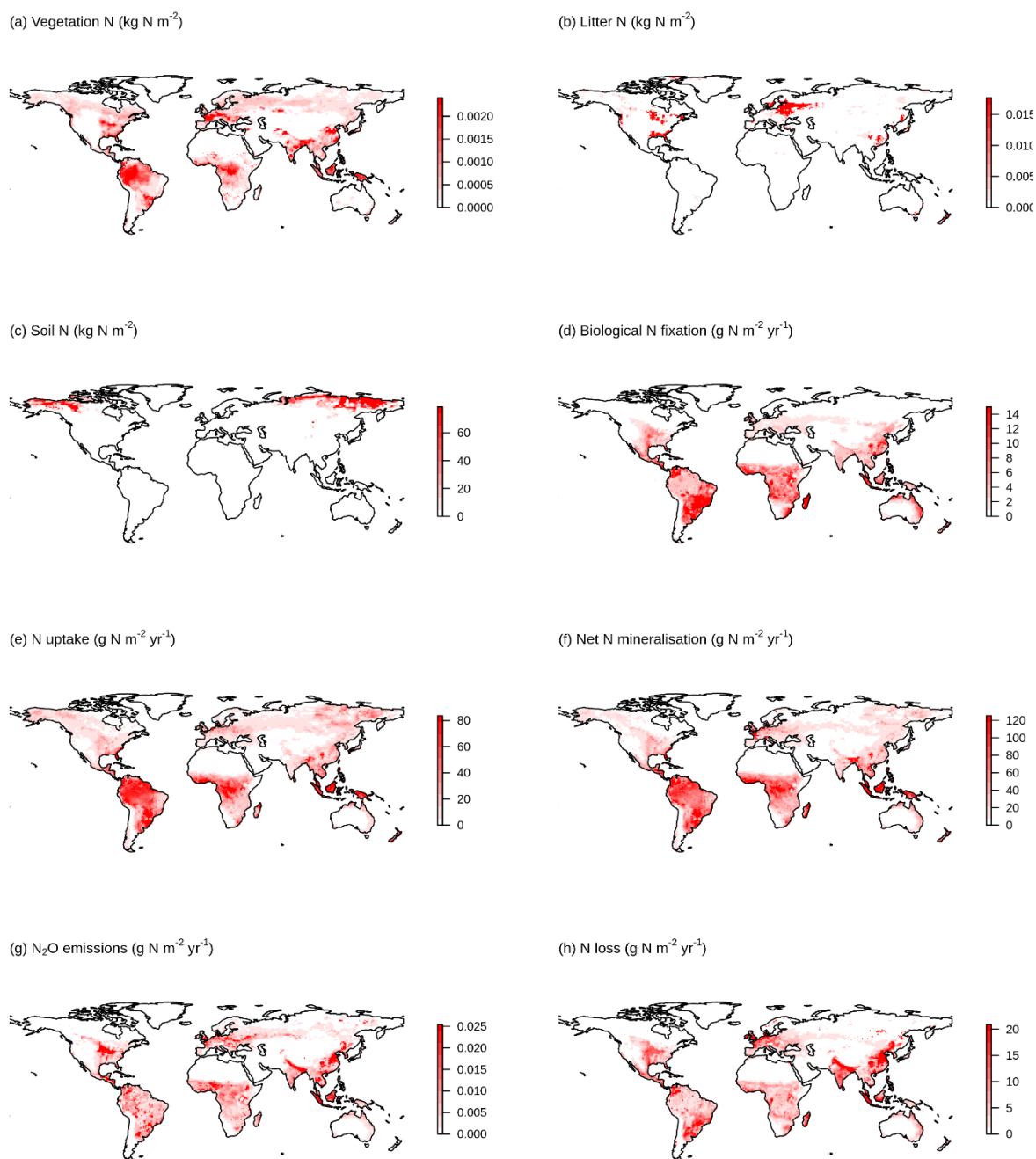
739

740 Table A6: Kendall's tau from the Mann-Kendall test ( $p$ -value  $< 0.05$ ) for biological N fixation,  
 741 vegetation C:N ratio, and soil C:N ratio simulated by averaged across TRENDY-N ensemble  
 742 models with different representations of key N cycling processes (N limitation of vegetation  
 743 growth, biological N fixation, vegetation response to N limitation, and N limitation of  
 744 decomposition, see Table 1). p-values are from t-tests and ANOVAs assessing differences  
 745 between these representations of key N cycling processes.

		Biological N fixation	Vegetation C:N ratio	Soil C:N ratio
N limitation of vegetation growth	$V_{\text{cmax}}$ / flexible C:N stoichiometry	0.48	-0.01	-0.04
	NPP	0.43	-0.74	0
	p-value	0.89	0.06	0.94
Biological N fixation	f(N limitation of vegetation growth)	0	-0.31	0.02
	f(NPP) or f(ET)	0.55	-0.6	0.14
	Time-invariant	0.74	0.39	-0.03
	p-value	0.15	0.15	0.97
Vegetation response to N limitation	Dynamic	0.5	-0.08	0.01
	Static	0.41	-0.56	-0.04
	p-value	0.77	0.3	0.93
N limitation of decomposition	f(soil N)	0.42	-0.42	0.31
	N-invariant	0.5	-0.25	-0.42
	p-value	0.8	0.7	0.14

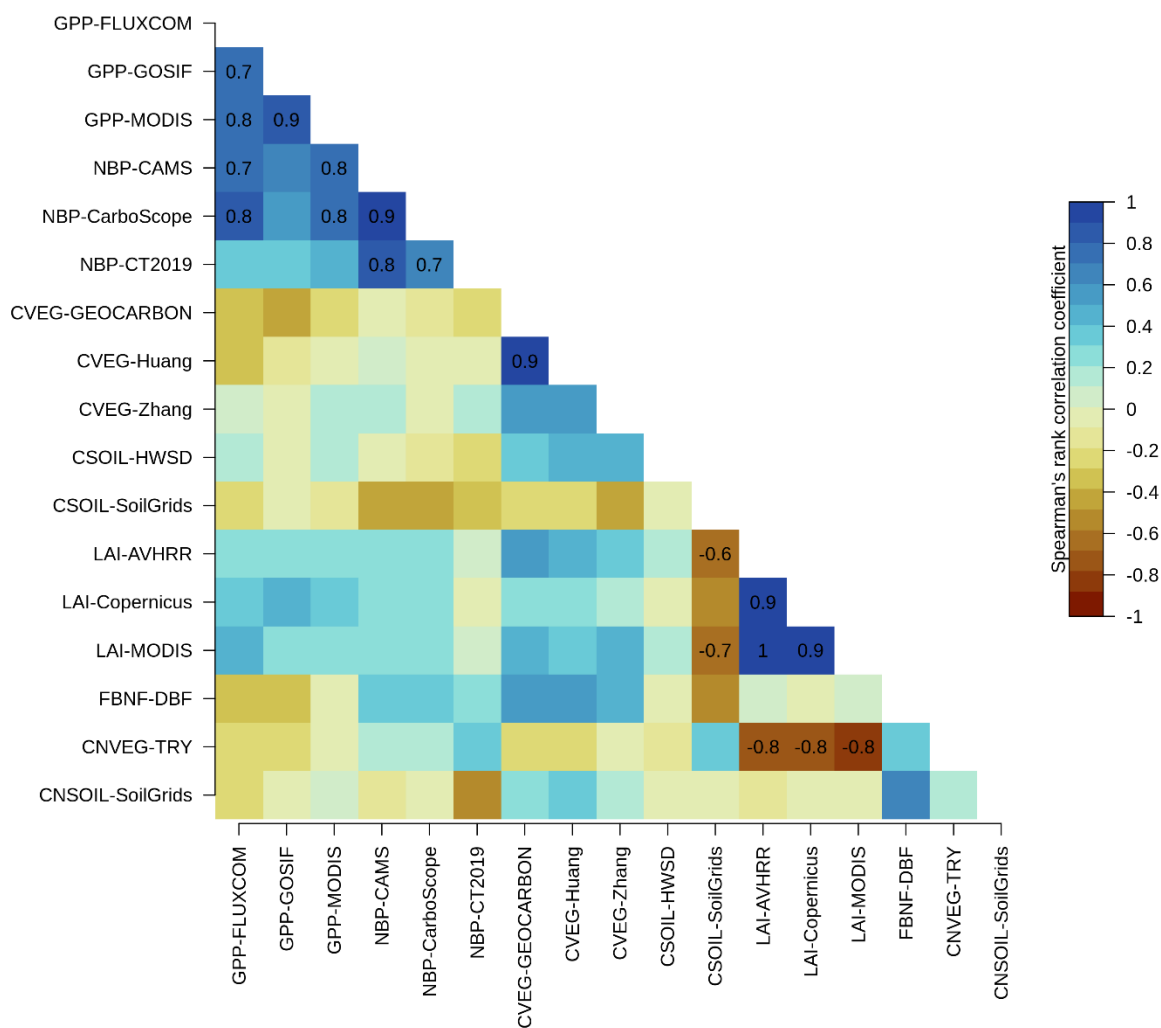
746

747 **Figure A1** **Figure A1: Geographical distributions of variation in a. vegetation N, b. litter N, c. soil N,**  
748 **N, d. biological N fixation, e. N uptake, f. net N mineralisation, g. N<sub>2</sub>O emissions, and h. N loss**  
749 **simulated by the TRENDY-N ensemble (across models over 1980–2021).**



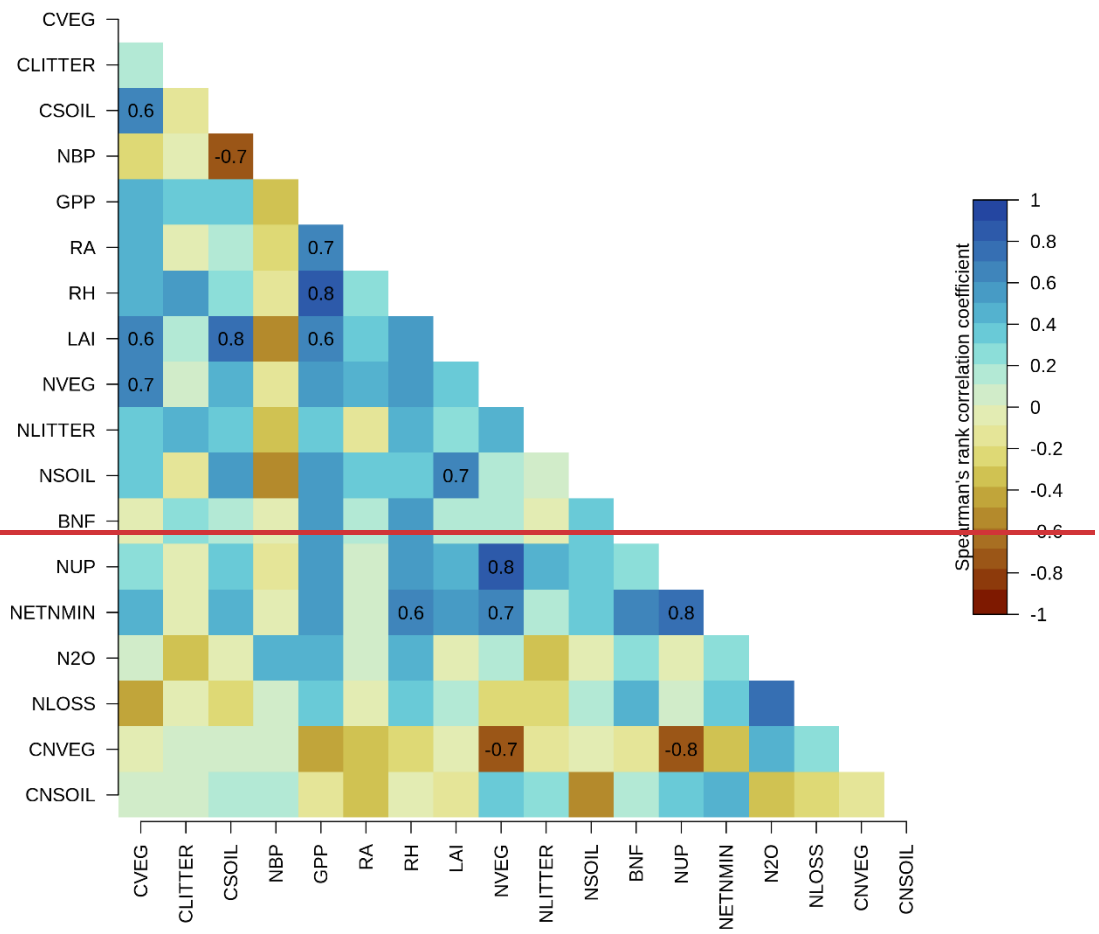
750  
751

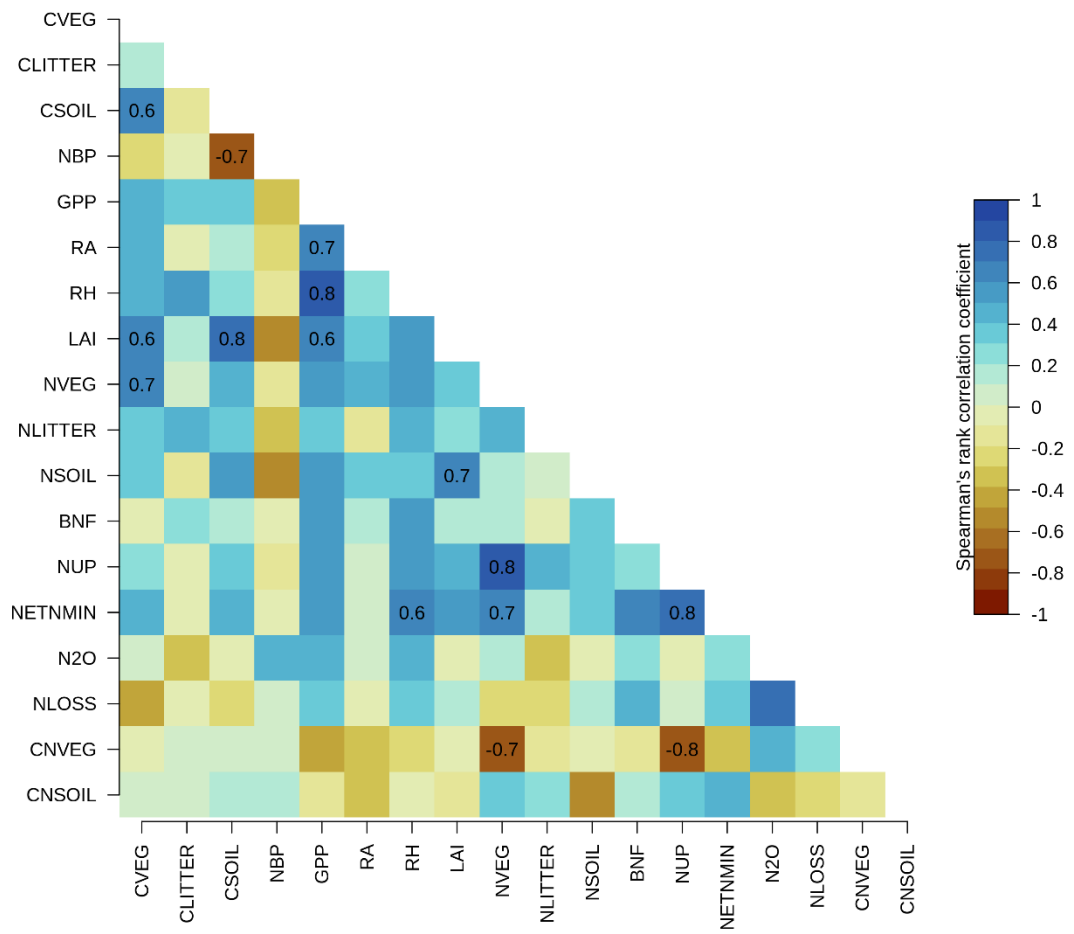
752 Figure A2: Correlations between overall scores of primary C and N pools and fluxes across  
 753 TRENDY-N ensemble models: gross primary productivity (GPP), net biome productivity (NBP),  
 754 vegetation C (CVEG), soil C (CSOIL), leaf area index (LAI), biological N fixation (FBNF),  
 755 vegetation C:N ratio (CNVEG), and soil C:N ratio (CNSOIL). Abbreviations of the observation-  
 756 based datasets are described in the Methods and in (Seiler et al., 2022). Spearman's rank  
 757 correlation coefficient is shown for statistically significant correlations (p-value < 0.05).



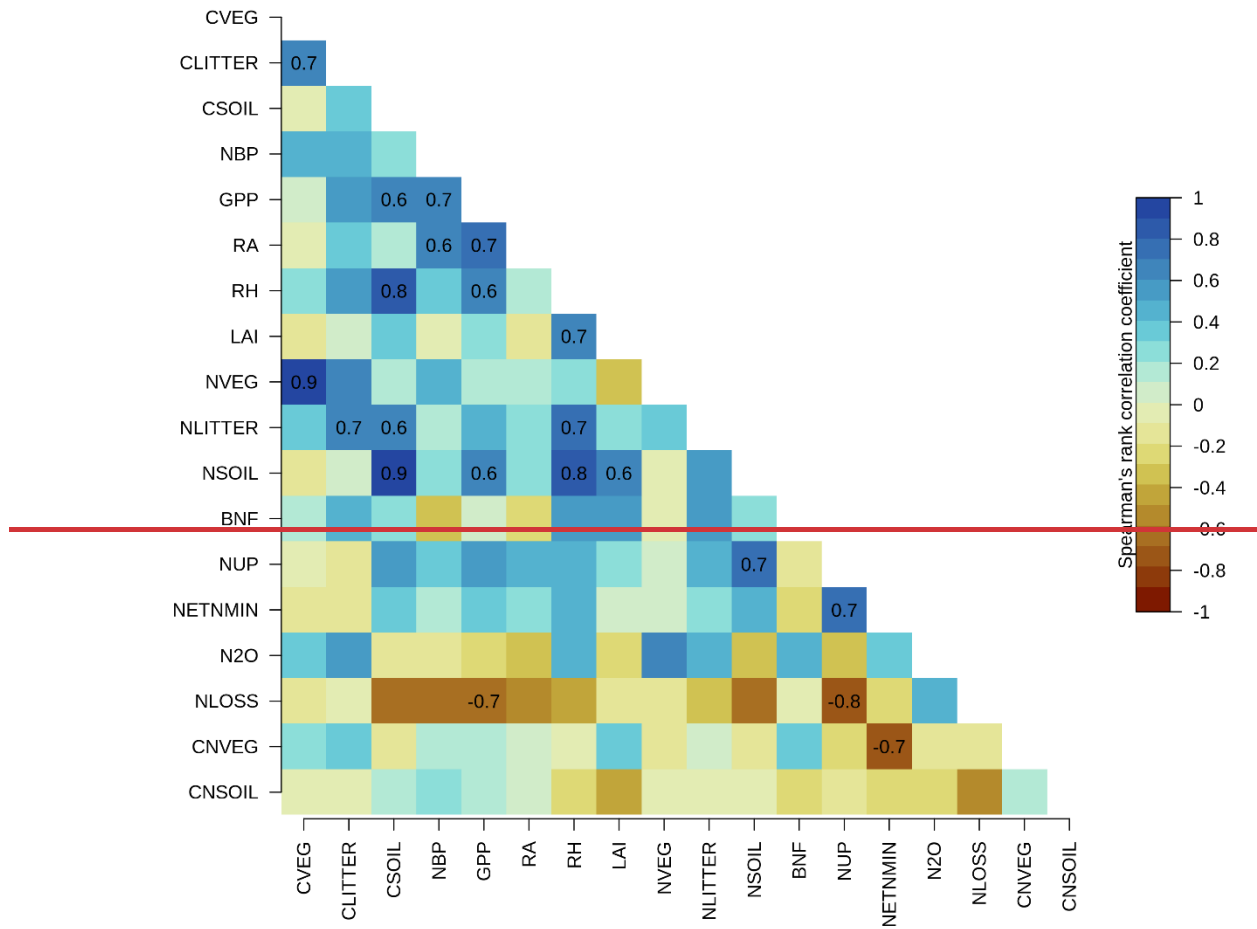
758

759 **Figure A3:** Correlations between present-day global values (averaged over 1980–2021) of  
760 primary C and N pools and fluxes across TRENDY-N ensemble models: vegetation C (CVEG),  
761 litter C (CLITTER), soil C (CSOIL) ), net biome productivity (NBP), gross primary productivity  
762 (GPP), autotrophic respiration (RA), heterotrophic respiration (RH), leaf area index (LAI),  
763 vegetation N (NVEG), litter N (NLITTER), soil N (NSOIL), biological N fixation (FBNF), N  
764 uptake (NUP), net N mineralisation (NETNMIN), N<sub>2</sub>O emissions (N<sub>2</sub>O), N loss (NLOSS),  
765 vegetation C:N ratio (CNVEG), and soil C:N ratio (CNSOIL). Spearman’s rank correlation  
766 coefficient is shown for statistically significant correlations (p-value < 0.05).





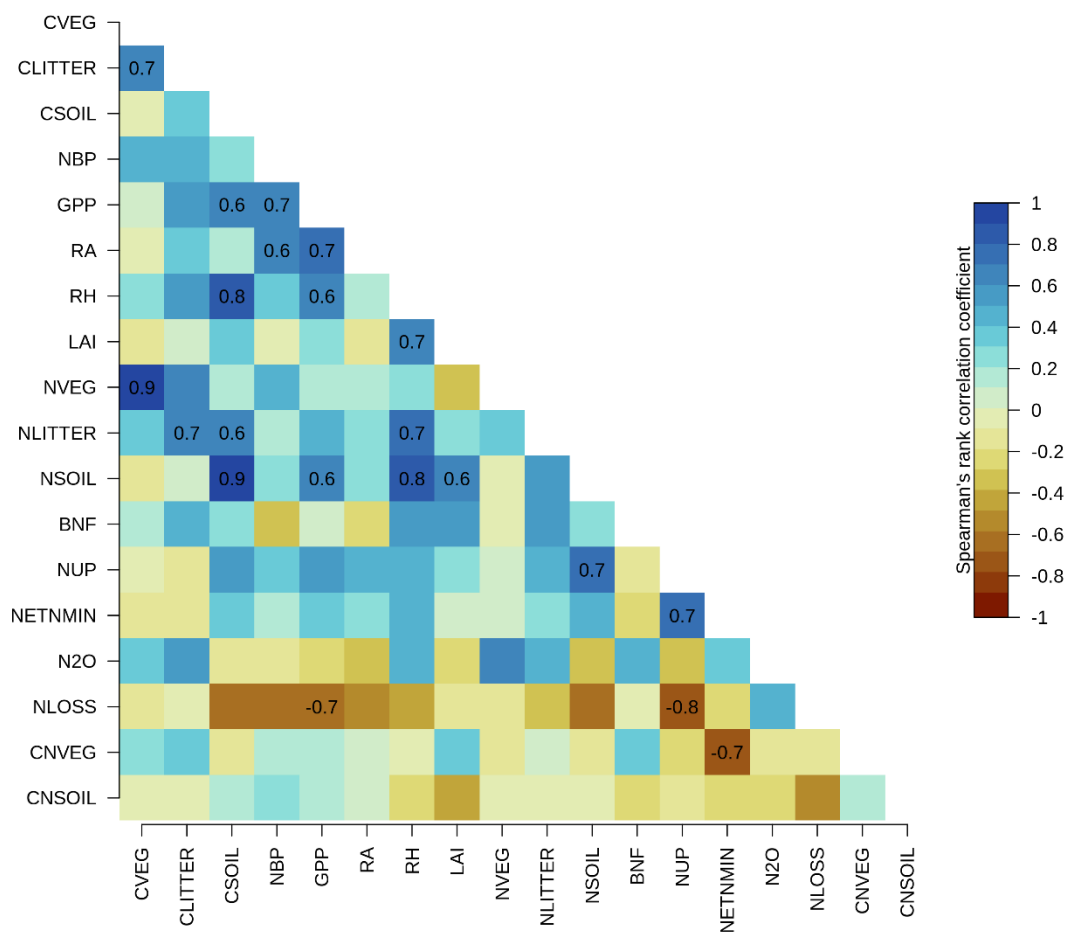
769 Figure [A2A4](#): Correlations between Kendall's tau of primary C and N pools and fluxes across  
 770 TRENDY-N ensemble models: vegetation C (CVEG), litter C (CLITTER), soil C (CSOIL), net  
 771 biome productivity (NBP), gross primary productivity (GPP), autotrophic respiration (RA),  
 772 heterotrophic respiration (RH), leaf area index (LAI), vegetation N (NVEG), litter N  
 773 (NLITTER), soil N (NSOIL), biological N fixation (BNF), N uptake (NUP), net N  
 774 mineralisation (NETNMIN), N<sub>2</sub>O emissions (N2O), N loss (NLOSS), vegetation C:N ratio  
 775 (CNVEG), and soil C:N ratio (CNSOIL). Spearman's rank correlation coefficient is shown for  
 776 statistically significant correlations (p-value < 0.05).



777

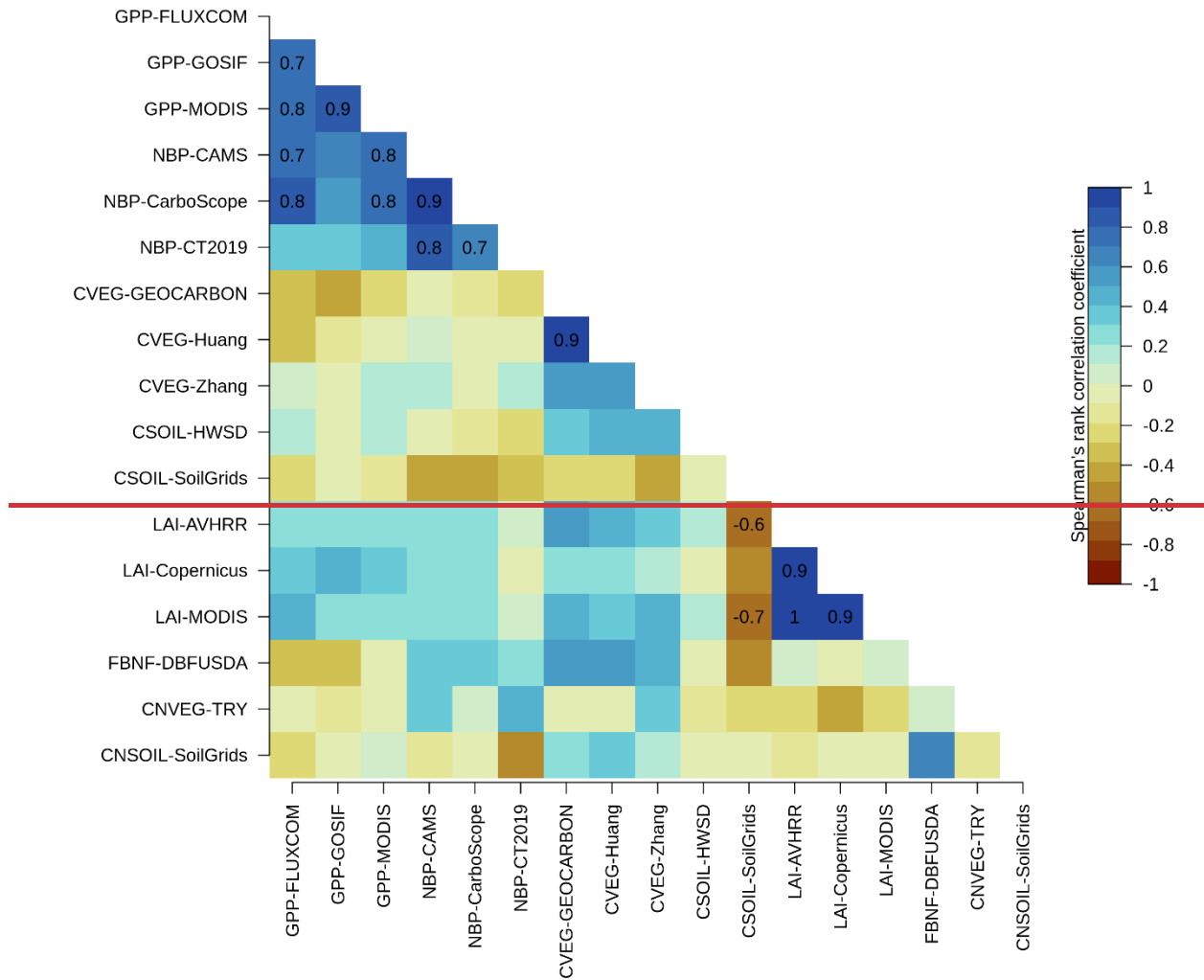


778 **Figure A3: Correlations between overall scores of primary C and N pools and fluxes across**  
 779 **TRENDY N ensemble models: gross primary productivity (GPP), net biome productivity (NBP),**  
 780 **vegetation C (CVEG), soil C (CSOIL), leaf area index (LAI), biological N fixation (BNF),**  
 781 **vegetation C:N ratio (CNVEG), and soil C:N ratio (CNSOIL). Abbreviations of the observation-**  
 782 **based datasets are described in the Methods and in**



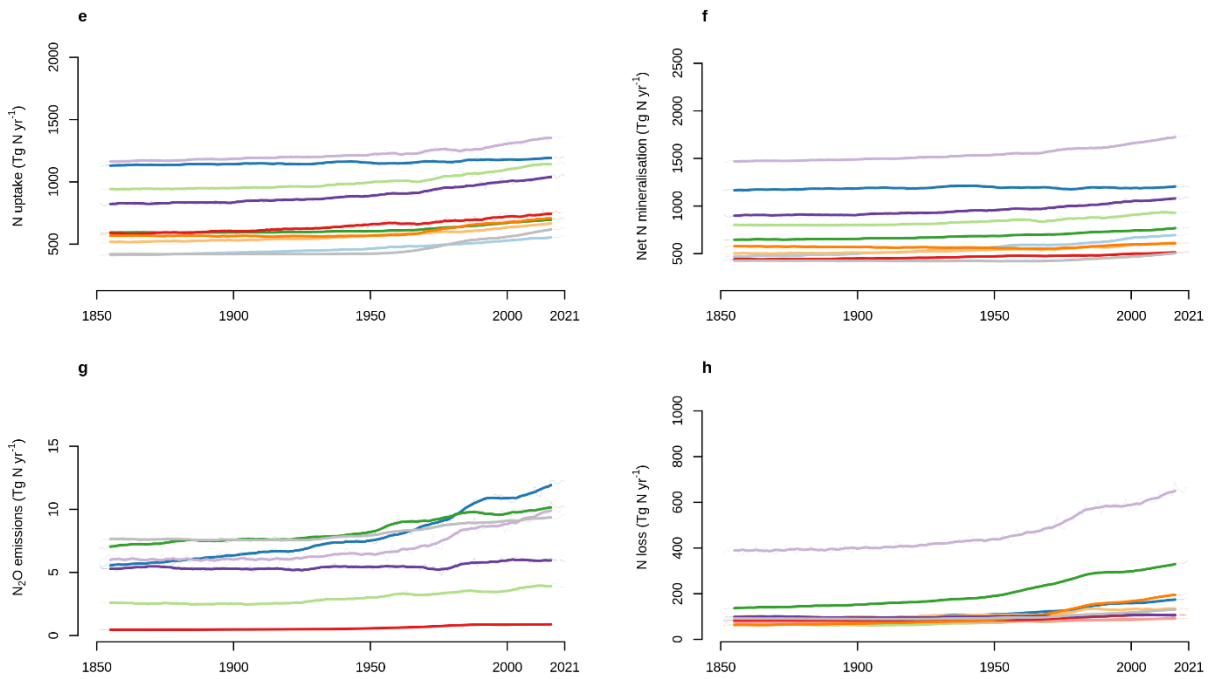
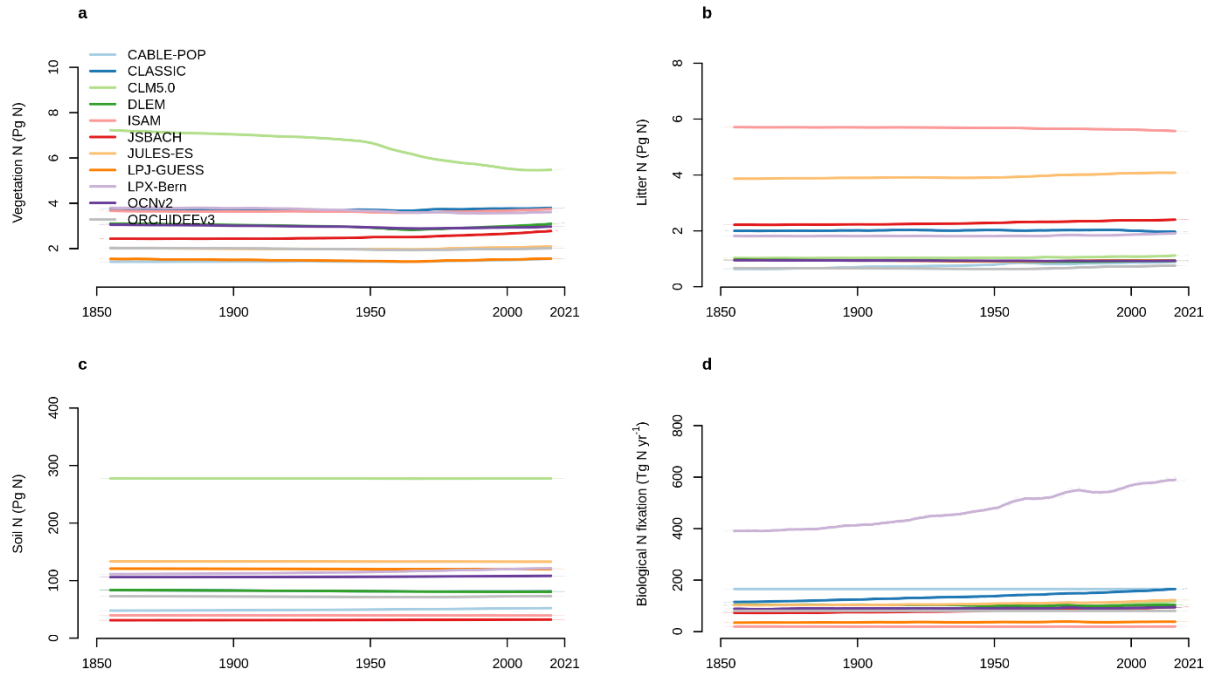
783

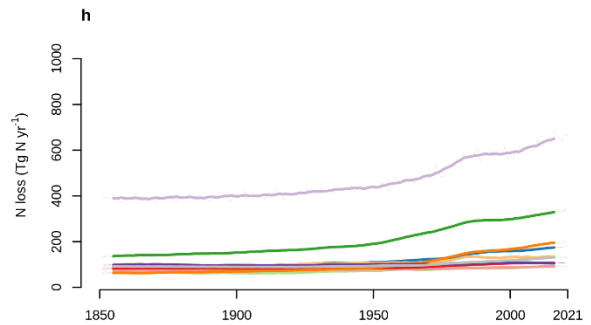
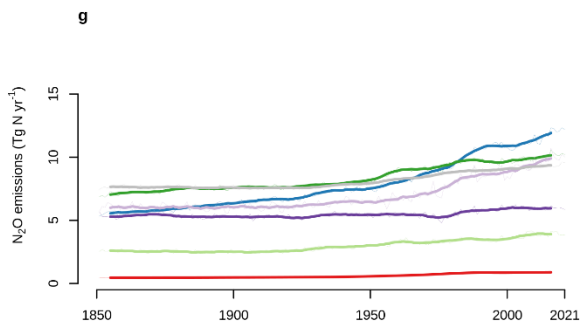
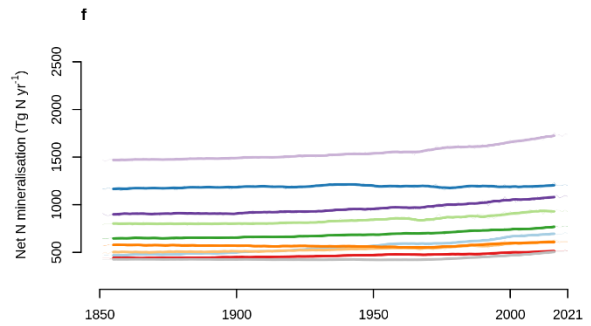
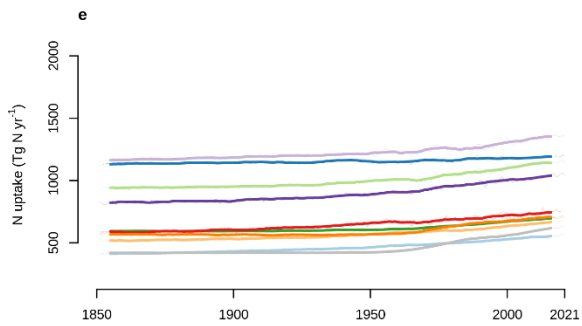
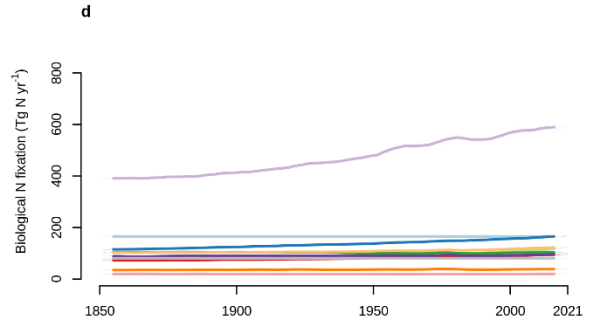
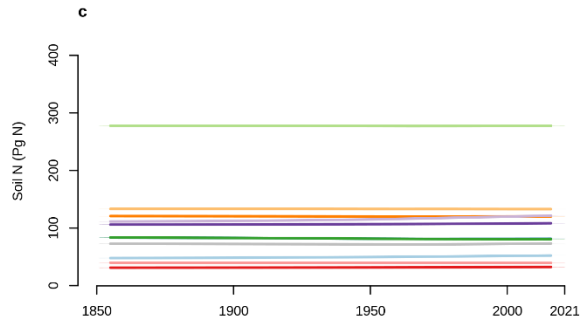
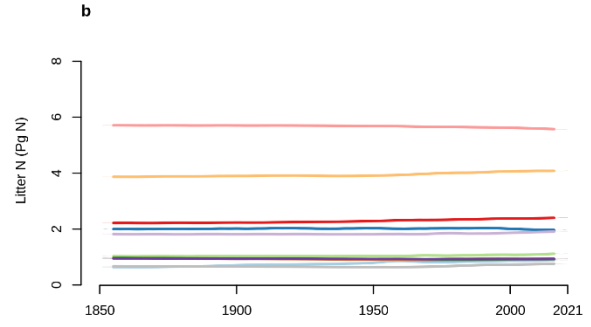
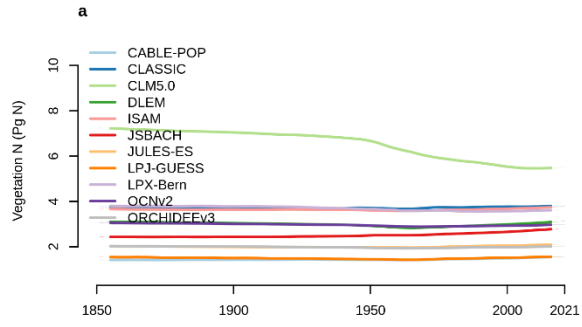
784 **Figure A5** Spearman's rank correlation coefficient is shown for statistically significant  
 785 correlations (p-value < 0.05).



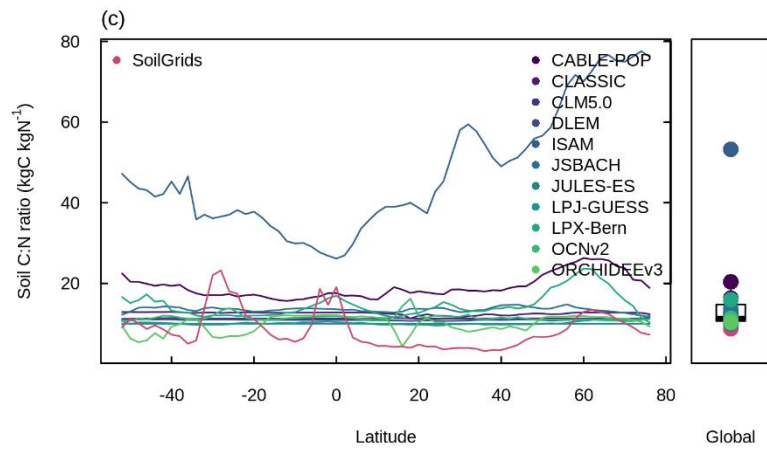
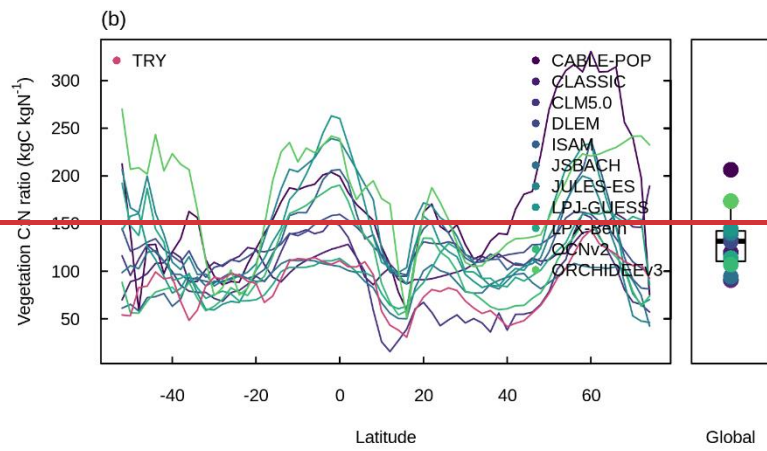
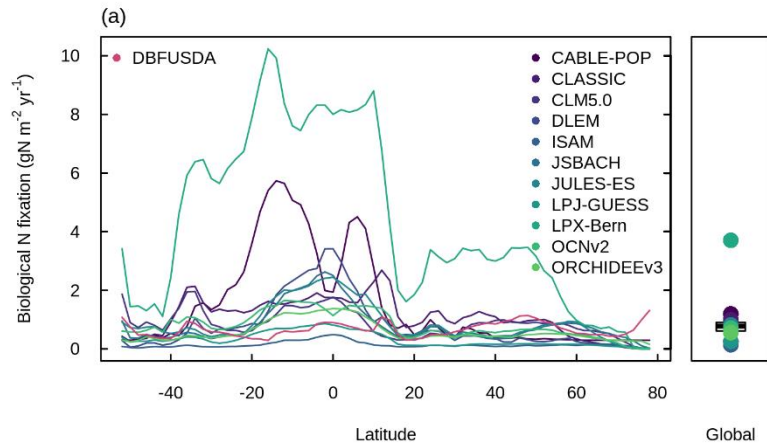
786

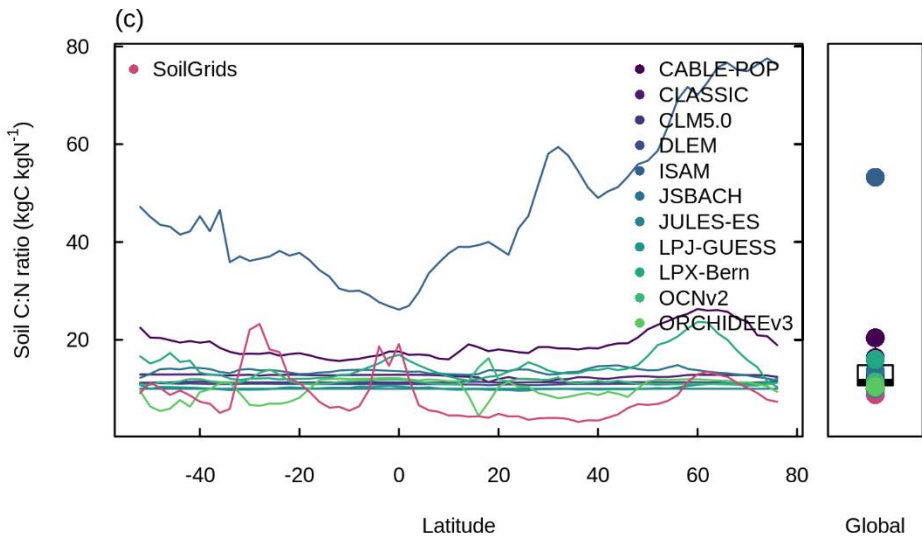
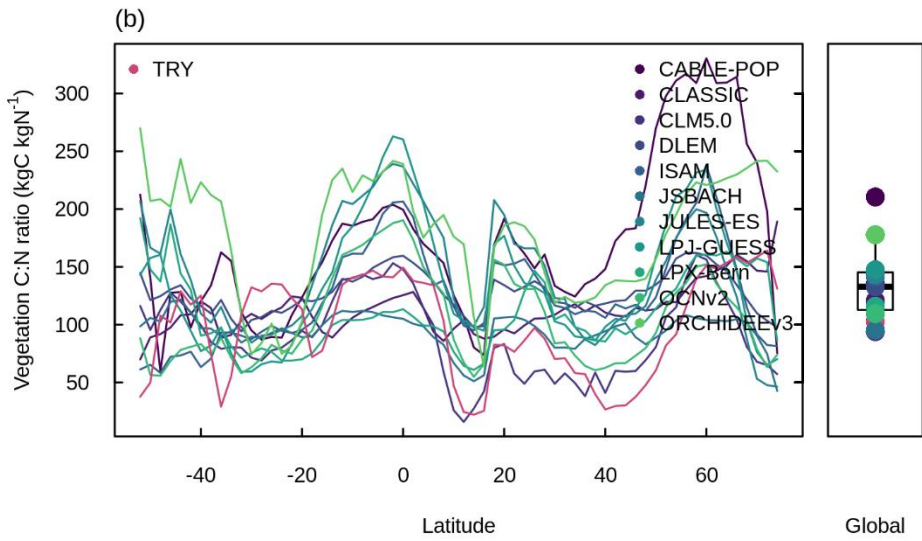
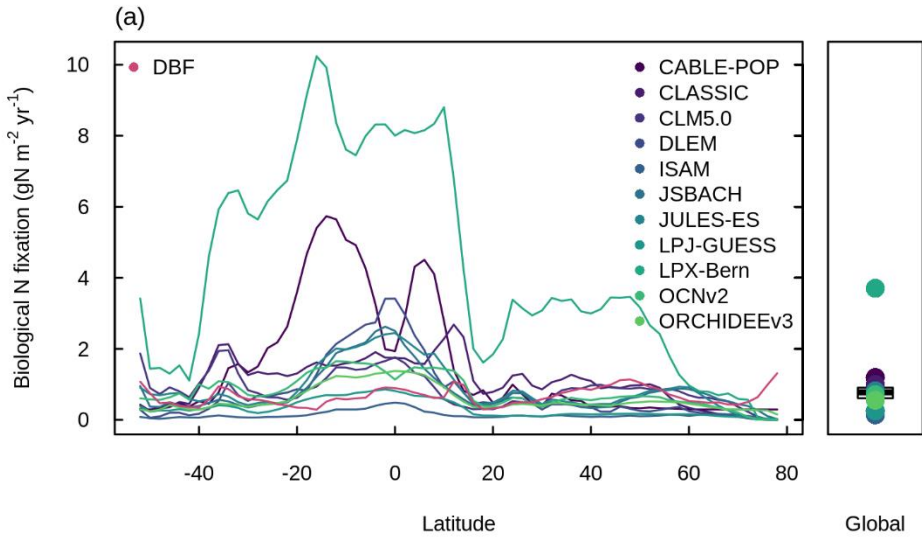
787 ~~Figure A4~~: Time series of a. vegetation N, b. litter N, c. soil N, d. biological N fixation, e. N  
788 uptake, f. net N mineralisation, g. N<sub>2</sub>O emissions, and h. N loss simulated by the TRENDY-N  
789 ensemble from 1850 to 2021.





793 Figure [A5A6](#): Latitudinal distributions and global means of ab. biological N fixation, cd.  
794 vegetation C:N ratio, and ef. soil C:N ratio simulated by the TRENDY-N ensemble (averaged  
795 across models over 1980–2021) in comparison to observation-based datasets from (Davies-  
796 Barnard and Friedlingstein, 2020) for biological N fixation, the TRY plant trait database for  
797 vegetation C:N ratio, and SoilGrids for soil C:N ratio. Boxplots show the median, interquartile  
798 range (box), and 80% percentiles (whiskers) of the global mean.







801 **References**

- 802 Agustí-Panareda, A., Diamantakis, M., Massart, S., Chevallier, F., Muñoz-Sabater, J., Barré, J., Curcoll, R.,  
803 Engelen, R., Langerock, B., Law, R. M., Loh, Z., Morguí, J. A., Parrington, M., Peuch, V.-H., Ramonet, M.,  
804 Roehl, C., Vermeulen, A. T., Warneke, T., and Wunch, D.: Modelling CO<sub>2</sub> weather – why horizontal  
805 resolution matters, *Atmospheric Chem. Phys.*, 19, 7347–7376, [https://doi.org/10.5194/acp-19-7347-](https://doi.org/10.5194/acp-19-7347-2019)  
806 2019, 2019.
- 807 Avitabile, V., Herold, M., Heuvelink, G. B. M., Lewis, S. L., Phillips, O. L., Asner, G. P., Armston, J., Ashton,  
808 P. S., Banin, L., Bayol, N., Berry, N. J., Boeckx, P., de Jong, B. H. J., DeVries, B., Girardin, C. A. J., Kearsley,  
809 E., Lindsell, J. A., Lopez-Gonzalez, G., Lucas, R., Malhi, Y., Morel, A., Mitchard, E. T. A., Nagy, L., Qie, L.,  
810 Quinones, M. J., Ryan, C. M., Ferry, S. J. W., Sunderland, T., Laurin, G. V., Gatti, R. C., Valentini, R.,  
811 Verbeeck, H., Wijaya, A., and Willcock, S.: An integrated pan-tropical biomass map using multiple  
812 reference datasets, *Glob. Change Biol.*, 22, 1406–1420, <https://doi.org/10.1111/gcb.13139>, 2016.
- 813 Barron, A. R., Purves, D. W., and Hedin, L. O.: Facultative nitrogen fixation by canopy legumes in a  
814 lowland tropical forest, *Oecologia*, 165, 511–520, <https://doi.org/10.1007/s00442-010-1838-3>, 2011.
- 815 Barton, L., Wolf, B., Rowlings, D., Scheer, C., Kiese, R., Grace, P., Stefanova, K., and Butterbach-Bahl, K.:  
816 Sampling frequency affects estimates of annual nitrous oxide fluxes, *Sci. Rep.*, 5, 1–9,  
817 <https://doi.org/10.1038/srep15912>, 2015.
- 818 Batjes, N. H., Ribeiro, E., and van Oostrum, A.: Standardised soil profile data to support global mapping  
819 and modelling (WoSIS snapshot 2019), *Earth Syst. Sci. Data*, 12, 299–320, [https://doi.org/10.5194/essd-](https://doi.org/10.5194/essd-12-299-2020)  
820 12-299-2020, 2020.
- 821 Batterman, S. A., Hedin, L. O., Breugel, M. van, Ransijn, J., Craven, D. J., and Hall, J. S.: Key role of  
822 symbiotic dinitrogen fixation in tropical forest secondary succession, *Nature*, 502, 224–227,  
823 <https://doi.org/10.1038/nature12525>, 2013.
- 824 Braghiere, R. K., Fisher, J. B., Allen, K., Brzostek, E., Shi, M., Yang, X., Ricciuto, D. M., Fisher, R. A., Zhu, Q.,  
825 and Phillips, R. P.: Modeling Global Carbon Costs of Plant Nitrogen and Phosphorus Acquisition, *J. Adv.*  
826 *Model. Earth Syst.*, 14, e2022MS003204, <https://doi.org/10.1029/2022MS003204>, 2022.
- 827 Cawse-Nicholson, K., Townsend, P. A., Schimel, D., Assiri, A. M., Blake, P. L., Buongiorno, M. F.,  
828 Campbell, P., Carmon, N., Casey, K. A., Correa-Pabón, R. E., Dahlin, K. M., Dashti, H., Dennison, P. E.,  
829 Dierssen, H., Erickson, A., Fisher, J. B., Frouin, R., Gatebe, C. K., Gholizadeh, H., Gierach, M., Glenn, N. F.,  
830 Goodman, J. A., Griffith, D. M., Guild, L., Hakkenberg, C. R., Hochberg, E. J., Holmes, T. R. H., Hu, C.,  
831 Hulley, G., Huemmrich, K. F., Kudela, R. M., Kokaly, R. F., Lee, C. M., Martin, R., Miller, C. E., Moses, W. J.,  
832 Muller-Karger, F. E., Ortiz, J. D., Otis, D. B., Pahlevan, N., Painter, T. H., Pavlick, R., Poulter, B., Qi, Y.,  
833 Realmuto, V. J., Roberts, D., Schaepman, M. E., Schneider, F. D., Schwandner, F. M., Serbin, S. P.,  
834 Shiklomanov, A. N., Stavros, E. N., Thompson, D. R., Torres-Perez, J. L., Turpie, K. R., Tzortziou, M., Ustin,  
835 S., Yu, Q., Yusup, Y., and Zhang, Q.: NASA’s surface biology and geology designated observable: A  
836 perspective on surface imaging algorithms, *Remote Sens. Environ.*, 257, 112349,  
837 <https://doi.org/10.1016/j.rse.2021.112349>, 2021.
- 838 Chini, L., Hurtt, G., Sahajpal, R., Frohling, S., Goldewijk, K. K., Sitch, S., Ganzenmüller, R., Ma, L., Ott, L.,  
839 Pongratz, J., and Poulter, B.: Land-use harmonization datasets for annual global carbon budgets, *Earth*  
840 *Syst. Sci. Data*, 13, 4175–4189, <https://doi.org/10.5194/essd-13-4175-2021>, 2021.

841 Claverie, M., Matthews, J. L., Vermote, E. F., and Justice, C. O.: A 30+ Year AVHRR LAI and FAPAR Climate  
842 Data Record: Algorithm Description and Validation, *Remote Sens.*, 8,  
843 <https://doi.org/10.3390/rs8030263>, 2016.

844 Cleveland, C. C., Townsend, A. R., Schimel, D. S., Fisher, H., Hedin, L. O., Perakis, S., Latty, E. F., Fischer, C.  
845 V., Elseroad, A., and Wasson, M. F.: Global patterns of terrestrial biological nitrogen (N<sub>2</sub>) fixation in  
846 natural ecosystems, *Glob. Biochem. Cycles*, 13, 623–645, <https://doi.org/10.1029/1999GB900014>, 1999.

847 Collier, N., Hoffman, F. M., Lawrence, D. M., Keppel-Aleks, G., Koven, C. D., Riley, W. J., Mu, M., and  
848 Randerson, J. T.: The International Land Model Benchmarking (ILAMB) System: Design, Theory, and  
849 Implementation, *J. Adv. Model. Earth Syst.*, 10, 2731–2754, <https://doi.org/10.1029/2018MS001354>,  
850 2018.

851 Cotrufo, M. F., Wallenstein, M. D., Boot, C. M., Deneff, K., and Paul, E.: The Microbial Efficiency-Matrix  
852 Stabilization (MEMS) framework integrates plant litter decomposition with soil organic matter  
853 stabilization: Do labile plant inputs form stable soil organic matter?, *Glob. Change Biol.*, 19, 988–995,  
854 <https://doi.org/10.1111/gcb.12113>, 2013.

855 Davies-Barnard, T. and Friedlingstein, P.: The Global Distribution of Biological Nitrogen Fixation in  
856 Terrestrial Natural Ecosystems, *Glob. Biogeochem. Cycles*, 34, 1–17,  
857 <https://doi.org/10.1029/2019GB006387>, 2020.

858 Davies-Barnard, T., Meyerholt, J., Zaehle, S., Friedlingstein, P., Brovkin, V., Fan, Y., Fisher, R. A., Jones, C.  
859 D., Lee, H., Peano, D., Smith, B., Wärlind, D., and Wiltshire, A. J.: Nitrogen cycling in CMIP6 land surface  
860 models: Progress and limitations, *Biogeosciences*, 17, 5129–5148, [https://doi.org/10.5194/bg-17-5129-](https://doi.org/10.5194/bg-17-5129-2020)  
861 2020, 2020.

862 Dlugokencky, E. and Tans, P.: Trends in atmospheric carbon dioxide, National Oceanic and Atmospheric  
863 Administration, Global Monitoring Laboratory (NOAA/GML), 2022.

864 Du, E., Terrer, C., Pellegrini, A. F. A., Ahlstrom, A., Lissa, C. J. van, Zhao, X., Xia, N., Wu, X., and Jackson, R.  
865 B.: Global patterns of terrestrial nitrogen and phosphorus limitation, *Nat. Geosci.*, 13, 221–226,  
866 <https://doi.org/10.1038/s41561-019-0530-4>, 2020.

867 Elser, J. J., Bracken, M. E. S., Cleland, E. E., Gruner, D. S., Harpole, W. S., Hillebrand, H., Ngai, J. T.,  
868 Seabloom, E. W., Shurin, J. B., and Smith, J. E.: Global analysis of nitrogen and phosphorus limitation of  
869 primary producers in freshwater, marine and terrestrial ecosystems, *Ecol. Lett.*, 10, 1135–1142,  
870 <https://doi.org/10.1111/j.1461-0248.2007.01113.x>, 2007.

871 Elser, J. J., Fagan, W. F., Kerkhoff, A. J., Swenson, N. G., and Enquist, B. J.: Biological stoichiometry of  
872 plant production: Metabolism, scaling and ecological response to global change, *New Phytol.*, 186, 593–  
873 608, <https://doi.org/10.1111/j.1469-8137.2010.03214.x>, 2010.

874 Fischer, H., Schmitt, J., Bock, M., Seth, B., Joos, F., Spahni, R., Lienert, S., Battaglia, G., Stocker, B. D.,  
875 Schilt, A., and Brook, E. J.: N<sub>2</sub>O changes from the Last Glacial Maximum to the preindustrial – Part 1:  
876 Quantitative reconstruction of terrestrial and marine emissions using N<sub>2</sub>O stable isotopes in ice cores,  
877 *Biogeosciences*, 16, 3997–4021, <https://doi.org/10.5194/bg-16-3997-2019>, 2019.

878 Fisher, J. B., Sitch, S., Malhi, Y., Fisher, R. A., Huntingford, C., and Tan, S.-Y.: Carbon cost of plant nitrogen  
879 acquisition: A mechanistic, globally applicable model of plant nitrogen uptake, retranslocation, and  
880 fixation, *Glob. Biogeochem. Cycles*, 24, 1–17, <https://doi.org/10.1029/2009gb003621>, 2010.

881 Fisher, J. B., Badgley, G., and Blyth, E.: Global nutrient limitation in terrestrial vegetation, *Glob.*  
882 *Biogeochem. Cycles*, 26, 1–9, <https://doi.org/10.1029/2011GB004252>, 2012.

883 Fisher, R. A. and Koven, C. D.: Perspectives on the Future of Land Surface Models and the Challenges of  
884 Representing Complex Terrestrial Systems, *J. Adv. Model. Earth Syst.*, 12,  
885 <https://doi.org/10.1029/2018MS001453>, 2020.

886 Fowler, D., Coyle, M., Skiba, U., Sutton, M. A., Cape, J. N., Reis, S., Sheppard, L. J., Jenkins, A., Grizzetti,  
887 B., Galloway, J. N., Vitousek, P., Leach, A., Bouwman, A. F., Butterbach-Bahl, K., Dentener, F., Stevenson,  
888 D., Amann, M., and Voss, M.: The global nitrogen cycle in the twenty-first century, *Philos. Trans. R. Soc.*  
889 *B Biol. Sci.*, 368, 20130164, <https://doi.org/10.1098/rstb.2013.0164>, 2013.

890 Friedl, M. A., Sulla-Menashe, D., Tan, B., Schneider, A., Ramankutty, N., Sibley, A., and Huang, X.: MODIS  
891 Collection 5 global land cover: Algorithm refinements and characterization of new datasets, *Remote*  
892 *Sens. Environ.*, 114, 168–182, <https://doi.org/10.1016/j.rse.2009.08.016>, 2010.

893 Friedlingstein, P., O’Sullivan, M., Jones, M. W., Andrew, R. M., Gregor, L., Hauck, J., Le Quéré, C., Luijckx, I.  
894 T., Olsen, A., Peters, G. P., Peters, W., Pongratz, J., Schwingshackl, C., Sitch, S., Canadell, J. G., Ciais, P.,  
895 Jackson, R. B., Alin, S. R., Alkama, R., Arneeth, A., Arora, V. K., Bates, N. R., Becker, M., Bellouin, N., Bittig,  
896 H. C., Bopp, L., Chevallier, F., Chini, L. P., Cronin, M., Evans, W., Falk, S., Feely, R. A., Gasser, T., Gehlen,  
897 M., Gkritzalis, T., Gloege, L., Grassi, G., Gruber, N., Gürses, Ö., Harris, I., Hefner, M., Houghton, R. A.,  
898 Hurtt, G. C., Iida, Y., Ilyina, T., Jain, A. K., Jersild, A., Kadono, K., Kato, E., Kennedy, D., Klein Goldewijk, K.,  
899 Knauer, J., Korsbakken, J. I., Landschützer, P., Lefèvre, N., Lindsay, K., Liu, J., Liu, Z., Marland, G., Mayot,  
900 N., McGrath, M. J., Metz, N., Monacci, N. M., Munro, D. R., Nakaoka, S.-I., Niwa, Y., O’Brien, K., Ono, T.,  
901 Palmer, P. I., Pan, N., Pierrot, D., Pocock, K., Poulter, B., Resplandy, L., Robertson, E., Rödenbeck, C.,  
902 Rodriguez, C., Rosan, T. M., Schwinger, J., Séférian, R., Shutler, J. D., Skjelvan, I., Steinhoff, T., Sun, Q.,  
903 Sutton, A. J., Sweeney, C., Takao, S., Tanhua, T., Tans, P. P., Tian, X., Tian, H., Tilbrook, B., Tsujino, H.,  
904 Tubiello, F., van der Werf, G. R., Walker, A. P., Wanninkhof, R., Whitehead, C., Willstrand Wranne, A., et  
905 al.: Global Carbon Budget 2022, *Earth Syst. Sci. Data*, 14, 4811–4900, [https://doi.org/10.5194/essd-14-](https://doi.org/10.5194/essd-14-4811-2022)  
906 [4811-2022](https://doi.org/10.5194/essd-14-4811-2022), 2022.

907 Goll, D. S., Brovkin, V., Parida, B. R., Reick, C. H., Kattge, J., Reich, P. B., Bodegom, P. M. V., and  
908 Niinemets, Ü.: Nutrient limitation reduces land carbon uptake in simulations with a model of combined  
909 carbon, nitrogen and phosphorus cycling, *Biogeosciences*, 9, 3547–3569, [https://doi.org/10.5194/bg-9-](https://doi.org/10.5194/bg-9-3547-2012)  
910 [3547-2012](https://doi.org/10.5194/bg-9-3547-2012), 2012.

911 Han, W., Tang, L., Chen, Y., and Fang, J.: Relationship between the relative limitation and resorption  
912 efficiency of nitrogen vs phosphorus in woody plants, *PLoS ONE*, 8, e83366,  
913 <https://doi.org/10.1371/journal.pone.0083366>, 2013.

914 Harris, I., Osborn, T. J., Jones, P., and Lister, D.: Version 4 of the CRU TS monthly high-resolution gridded  
915 multivariate climate dataset, *Sci. Data*, 7, 1–18, <https://doi.org/10.1038/s41597-020-0453-3>, 2020.

916 Haverd, V., Smith, B., Nieradzic, L., Briggs, P. R., Woodgate, W., Trudinger, C. M., Canadell, J. G., and  
917 Cuntz, M.: A new version of the CABLE land surface model (Subversion revision r4601) incorporating

918 land use and land cover change, woody vegetation demography, and a novel optimisation-based  
919 approach to plant coordination of photosynthesis, *Geosci. Model Dev.*, 11, 2995–3026,  
920 <https://doi.org/10.5194/gmd-11-2995-2018>, 2018.

921 Hedin, L. O., Brookshire, E. N. J., Menge, D. N. L., and Barron, A. R.: The Nitrogen Paradox in Tropical  
922 Forest Ecosystems, *Annu. Rev. Ecol. Evol. Syst.*, 40, 613–635,  
923 <https://doi.org/10.1146/annurev.ecolsys.37.091305.110246>, 2009.

924 Hegglin, M., Kinnison, D., and Lamarque, J.-F.: CCMI nitrogen surface fluxes in support of CMIP6 - version  
925 2.0, Earth System Grid Federation, <https://doi.org/10.22033/ESGF/input4MIPs.1125>, 2016.

926 Hengl, T., Jesus, J. M. D., Heuvelink, G. B. M., Gonzalez, M. R., Kilibarda, M., Blagotić, A., Shangguan, W.,  
927 Wright, M. N., Geng, X., Bauer-Marschallinger, B., Guevara, M. A., Vargas, R., MacMillan, R. A., Batjes, N.  
928 H., Leenaars, J. G. B., Ribeiro, E., Wheeler, I., Mantel, S., and Kempen, B.: SoilGrids250m: Global gridded  
929 soil information based on machine learning, *PLoS ONE*, 12, e0169748,  
930 <https://doi.org/10.1371/journal.pone.0169748>, 2017.

931 Herridge, D. F., Giller, K. E., Jensen, E. S., and Peoples, M. B.: Quantifying country-to-global scale  
932 nitrogen fixation for grain legumes II. Coefficients, templates and estimates for soybean, groundnut and  
933 pulses, *Plant Soil*, 474, 1–15, <https://doi.org/10.1007/s11104-021-05166-7>, 2022.

934 Hipel, K. W. and McLeod, A. I.: Time series modelling of water resources and environmental systems,  
935 Elsevier, 1994.

936 Houlton, B. Z., Morford, S. L., and Dahlgren, R. A.: Convergent evidence for widespread rock nitrogen  
937 sources in Earth’s surface environment, *Science*, 360, 58–62, <https://doi.org/10.1126/science.aan4399>,  
938 2018.

939 Huang, Y., Ciais, P., Santoro, M., Makowski, D., Chave, J., Schepaschenko, D., Abramoff, R. Z., Goll, D. S.,  
940 Yang, H., Chen, Y., Wei, W., and Piao, S.: A global map of root biomass across the world’s forests, *Earth  
941 Syst. Sci. Data*, 13, 4263–4274, <https://doi.org/10.5194/essd-13-4263-2021>, 2021.

942 Hungate, B. A., Dukes, J. S., Shaw, M. R., Luo, Y., and Field, C. B.: Nitrogen and Climate Change, *Science*,  
943 302, 1512–1513, 2003.

944 Huntzinger, D. N., Michalak, A. M., Schwalm, C., Ciais, P., King, A. W., Fang, Y., Schaefer, K., Wei, Y., Cook,  
945 R. B., Fisher, J. B., Hayes, D., Huang, M., Ito, A., Jain, A. K., Lei, H., Lu, C., Maignan, F., Mao, J., Parazoo,  
946 N., Peng, S., Poulter, B., Ricciuto, D., Shi, X., Tian, H., Wang, W., Zeng, N., and Zhao, F.: Uncertainty in the  
947 response of terrestrial carbon sink to environmental drivers undermines carbon-climate feedback  
948 predictions, *Sci. Rep.*, 7, 1–8, <https://doi.org/10.1038/s41598-017-03818-2>, 2017.

949 Hurtt, G. C., Chini, L., Sahajpal, R., Froking, S., Boudirsky, B. L., Calvin, K., Doelman, J. C., Fisk, J., Fujimori,  
950 S., Klein Goldewijk, K., Hasegawa, T., Havlik, P., Heinemann, A., Humpenöder, F., Jungclaus, J., Kaplan, J.  
951 O., Kennedy, J., Krisztin, T., Lawrence, D., Lawrence, P., Ma, L., Mertz, O., Pongratz, J., Popp, A., Poulter,  
952 B., Riahi, K., Shevliakova, E., Stehfest, E., Thornton, P., Tubiello, F. N., van Vuuren, D. P., and Zhang, X.:  
953 Harmonization of global land use change and management for the period 850–2100 (LUH2) for CMIP6,  
954 *Geosci. Model Dev.*, 13, 5425–5464, <https://doi.org/10.5194/gmd-13-5425-2020>, 2020.

955 Jacobson, A. R., Schuldt, K. N., Miller, J. B., Oda, T., Tans, P., Andrews, A., Mund, J., Ott, L., Collatz, G. J.,  
956 and Aalto, T.: CarbonTracker CT2019, NOAA Earth Syst. Res. Lab. Glob. Monit. Div., 10, 2020.

957 Jeltsch-Thömmes, A., Battaglia, G., Cartapanis, O., Jaccard, S. L., and Joos, F.: Low terrestrial carbon  
958 storage at the Last Glacial Maximum: constraints from multi-proxy data, *Clim Past*, 15, 849–879,  
959 <https://doi.org/10.5194/cp-15-849-2019>, 2019.

960 Joos, F., Spahni, R., Stocker, B. D., Lienert, S., Müller, J., Fischer, H., Schmitt, J., Prentice, I. C., Otto-  
961 Bliesner, B., and Liu, Z.: N<sub>2</sub>O changes from the Last Glacial Maximum to the preindustrial – Part 2:  
962 terrestrial N<sub>2</sub>O emissions and carbon–nitrogen cycle interactions, *Biogeosciences*, 17, 3511–3543,  
963 <https://doi.org/10.5194/bg-17-3511-2020>, 2020.

964 Jung, M., Schwalm, C., Migliavacca, M., Walther, S., Camps-Valls, G., Koirala, S., Anthoni, P., Besnard, S.,  
965 Bodesheim, P., Carvalhais, N., Chevallier, F., Gans, F., Goll, D. S., Haverd, V., Köhler, P., Ichii, K., Jain, A.  
966 K., Liu, J., Lombardozzi, D., Nabel, J. E. M. S., Nelson, J. A., O’Sullivan, M., Pallandt, M., Papale, D., Peters,  
967 W., Pongratz, J., Rödenbeck, C., Sitch, S., Tramontana, G., Walker, A., Weber, U., and Reichstein, M.:  
968 Scaling carbon fluxes from eddy covariance sites to globe: synthesis and evaluation of the FLUXCOM  
969 approach, *Biogeosciences*, 17, 1343–1365, <https://doi.org/10.5194/bg-17-1343-2020>, 2020.

970 Kattge, J., Bönisch, G., Díaz, S., Lavorel, S., Prentice, I. C., Leadley, P., Tautenhahn, S., Werner, G. D. A.,  
971 Aakala, T., Abedi, M., Acosta, A. T. R., Adamidis, G. C., Adamson, K., Aiba, M., Albert, C. H., Alcántara, J.  
972 M., C. C. A., Aleixo, I., Ali, H., Amiaud, B., Ammer, C., Amoroso, M. M., Anand, M., Anderson, C., Anten,  
973 N., Antos, J., Apgaua, D. M. G., Ashman, T. L., Asmara, D. H., Asner, G. P., Aspinwall, M., Atkin, O., Aubin,  
974 I., Bastrup-Spohr, L., Bahalkeh, K., Bahn, M., Baker, T., Baker, W. J., Bakker, J. P., Baldocchi, D., Baltzer,  
975 J., Banerjee, A., Baranger, A., Barlow, J., Barneche, D. R., Baruch, Z., Bastianelli, D., Battles, J., Bauerle,  
976 W., Bauters, M., Bazzato, E., Beckmann, M., Beeckman, H., Beierkuhnlein, C., Bekker, R., Belfry, G.,  
977 Belluau, M., Beloiu, M., Benavides, R., Benomar, L., Berdugo-Lattke, M. L., Berenguer, E., Bergamin, R.,  
978 Bergmann, J., Carlucci, M. B., Berner, L., Bernhardt-Römermann, M., Bigler, C., Bjorkman, A. D.,  
979 Blackman, C., Blanco, C., Blonder, B., Blumenthal, D., Bocanegra-González, K. T., Boeckx, P., Bohlman, S.,  
980 Böhning-Gaese, K., Boisvert-Marsh, L., Bond, W., Bond-Lamberty, B., Boom, A., Boonman, C. C. F.,  
981 Bordin, K., Boughton, E. H., Boukili, V., Bowman, D. M. J. S., Bravo, S., Brendel, M. R., Broadley, M. R.,  
982 Brown, K. A., Bruelheide, H., Brumnich, F., Bruun, H. H., Bruy, D., Buchanan, S. W., Bucher, S. F.,  
983 Buchmann, N., Buitenwerf, R., Bunker, D. E., et al.: TRY plant trait database – enhanced coverage and  
984 open access, *Glob. Change Biol.*, 26, 119–188, <https://doi.org/10.1111/gcb.14904>, 2020.

985 Klein Goldewijk, K., Beusen, A., Doelman, J., and Stehfest, E.: Anthropogenic land use estimates for the  
986 Holocene – HYDE 3.2, *Earth Syst. Sci. Data*, 9, 927–953, <https://doi.org/10.5194/essd-9-927-2017>,  
987 2017a.

988 Klein Goldewijk, K., Dekker, S. C., and Zanden, J. L. van: Per-capita estimations of long-term historical  
989 land use and the consequences for global change research, *J. Land Use Sci.*, 12, 313–337,  
990 <https://doi.org/10.1080/1747423X.2017.1354938>, 2017b.

991 Knyazikhin, Y., Schull, M. A., Stenberg, P., Möttus, M., Rautiainen, M., Yang, Y., Marshak, A., Latorre  
992 Carmona, P., Kaufmann, R. K., Lewis, P., Disney, M. I., Vanderbilt, V., Davis, A. B., Baret, F., Jacquemoud,  
993 S., Lyapustin, A., and Myneni, R. B.: Hyperspectral remote sensing of foliar nitrogen content, *Proc. Natl.  
994 Acad. Sci.*, 110, E185–E192, <https://doi.org/10.1073/pnas.1210196109>, 2013.

- 995 Kobe, R. K., Lepczyk, C. A., and Iyer, M.: Resorption efficiency decreases with increasing green leaf  
996 nutrients in a global data set, *Ecology*, 86, 2780–2792, 2005.
- 997 Kou-Giesbrecht, S. and Arora, V. K.: Representing the Dynamic Response of Vegetation to Nitrogen  
998 Limitation via Biological Nitrogen Fixation in the CLASSIC Land Model, *Glob. Biogeochem. Cycles*, 36,  
999 e2022GB007341, <https://doi.org/10.1029/2022GB007341>, 2022.
- 1000 Lawrence, D. M., Fisher, R. A., Koven, C. D., Oleson, K. W., Swenson, S. C., Bonan, G., Collier, N., Ghimire,  
1001 B., Kampenhout, L. van, Kennedy, D., Kluzek, E., Lawrence, P. J., Li, F., Li, H., Lombardozzi, D., Riley, W. J.,  
1002 Sacks, W. J., Shi, M., Vertenstein, M., Wieder, W. R., Xu, C., Ali, A. A., Badger, A. M., Bisht, G., Broeke, M.  
1003 van den, Brunke, M. A., Burns, S. P., Buzan, J., Clark, M., Craig, A., Dahlin, K., Drewniak, B., Fisher, J. B.,  
1004 Flanner, M., Fox, A. M., Gentine, P., Hoffman, F., Keppel-Aleks, G., Knox, R., Kumar, S., Lenaerts, J.,  
1005 Leung, L. R., Lipscomb, W. H., Lu, Y., Pandey, A., Pelletier, J. D., Perket, J., Randerson, J. T., Ricciuto, D.  
1006 M., Sanderson, B. M., Slater, A., Subin, Z. M., Tang, J., Thomas, R. Q., Martin, M. V., and Zeng, X.: The  
1007 Community Land Model Version 5: Description of New Features, Benchmarking, and Impact of Forcing  
1008 Uncertainty, *J. Adv. Model. Earth Syst.*, 11, 4245–4287, <https://doi.org/10.1029/2018MS001583>, 2019.
- 1009 LeBauer, D. S. and Treseder, K. K.: Nitrogen Limitation of Net Primary Productivity in Terrestrial  
1010 Ecosystems is Globally Distributed, *Ecology*, 89, 371–379, <https://doi.org/10.1016/j.agee.2013.04.020>,  
1011 2008.
- 1012 Li, X. and Xiao, J.: Mapping Photosynthesis Solely from Solar-Induced Chlorophyll Fluorescence: A Global,  
1013 Fine-Resolution Dataset of Gross Primary Production Derived from OCO-2, *Remote Sens.*, 11,  
1014 <https://doi.org/10.3390/rs11212563>, 2019.
- 1015 Liang, J., Qi, X., Souza, L., and Luo, Y.: Processes regulating progressive nitrogen limitation under  
1016 elevated carbon dioxide: A meta-analysis, *Biogeosciences*, 13, 2689–2699, [https://doi.org/10.5194/bg-  
1017 13-2689-2016](https://doi.org/10.5194/bg-13-2689-2016), 2016.
- 1018 Lienert, S. and Joos, F.: A Bayesian ensemble data assimilation to constrain model parameters and land-  
1019 use carbon emissions, *Biogeosciences*, 15, 2909–2930, <https://doi.org/10.5194/bg-15-2909-2018>, 2018.
- 1020 Liu, Y., Wang, C., He, N., Wen, X., Gao, Y., Li, S., Niu, S., Butterbach-Bahl, K., Luo, Y., and Yu, G.: A global  
1021 synthesis of the rate and temperature sensitivity of soil nitrogen mineralization: latitudinal patterns and  
1022 mechanisms, *Glob. Change Biol.*, 23, 455–464, <https://doi.org/10.1111/gcb.13372>, 2017.
- 1023 Medlyn, B. E., Zaehle, S., Kauwe, M. G. D., Walker, A. P., Dietze, M. C., Hanson, P. J., Hickler, T., Jain, A.  
1024 K., Luo, Y., Parton, W., Prentice, I. C., Thornton, P. E., Wang, S., Wang, Y. P., Weng, E., Iversen, C. M.,  
1025 McCarthy, H. R., Warren, J. M., Oren, R., and Norby, R. J.: Using ecosystem experiments to improve  
1026 vegetation models, *Nat. Clim. Change*, 5, 528–534, <https://doi.org/10.1038/nclimate2621>, 2015.
- 1027 Melton, J. R., Arora, V. K., Wisernig-Cojoc, E., Seiler, C., Fortier, M., Chan, E., and Teckentrup, L.: CLASSIC  
1028 v1.0: The open-source community successor to the Canadian Land Surface Scheme (CLASS) and the  
1029 Canadian Terrestrial Ecosystem Model (CTEM)-Part 1: Model framework and site-level performance,  
1030 *Geosci. Model Dev.*, 13, 2825–2850, <https://doi.org/10.5194/gmd-13-2825-2020>, 2020.
- 1031 Menge, D. N. L., Wolf, A. A., and Funk, J. L.: Diversity of nitrogen fixation strategies in Mediterranean  
1032 legumes, *Nat. Plants*, 1, 1–5, <https://doi.org/10.1038/nplants.2015.64>, 2015.

- 1033 Meyerholt, J., Zaehle, S., and Smith, M. J.: Variability of projected terrestrial biosphere responses to  
1034 elevated levels of atmospheric CO<sub>2</sub> due to uncertainty in biological nitrogen fixation, *Biogeosciences*, 13,  
1035 1491–1518, <https://doi.org/10.5194/bg-13-1491-2016>, 2016.
- 1036 Meyerholt, J., Sickel, K., and Zaehle, S.: Ensemble projections elucidate effects of uncertainty in  
1037 terrestrial nitrogen limitation on future carbon uptake, *Glob. Change Biol.*, 26, 3978–3996,  
1038 <https://doi.org/10.1111/gcb.15114>, 2020.
- 1039 Moreno-Martínez, Á., Camps-Valls, G., Kattge, J., Robinson, N., Reichstein, M., van Bodegom, P., Kramer,  
1040 K., Cornelissen, J. H. C., Reich, P., Bahn, M., Niinemets, Ü., Peñuelas, J., Craine, J. M., Cerabolini, B. E. L.,  
1041 Minden, V., Laughlin, D. C., Sack, L., Allred, B., Baraloto, C., Byun, C., Soudzilovskaia, N. A., and Running,  
1042 S. W.: A methodology to derive global maps of leaf traits using remote sensing and climate data, *Remote*  
1043 *Sens. Environ.*, 218, 69–88, <https://doi.org/10.1016/j.rse.2018.09.006>, 2018.
- 1044 Myneni, R. B., Hoffman, S., Knyazikhin, Y., Privette, J. L., Glassy, J., Tian, Y., Wang, Y., Song, X., Zhang, Y.,  
1045 Smith, G. R., Lotsch, A., Friedl, M., Morisette, J. T., Votava, P., Nemani, R. R., and Running, S. W.: Global  
1046 products of vegetation leaf area and fraction absorbed PAR from year one of MODIS data, *Moderate*  
1047 *Resolut. Imaging Spectroradiometer MODIS New Gener. Land Surf. Monit.*, 83, 214–231,  
1048 [https://doi.org/10.1016/S0034-4257\(02\)00074-3](https://doi.org/10.1016/S0034-4257(02)00074-3), 2002.
- 1049 Nakhavali, M. A., Mercado, L. M., Hartley, I. P., Sitch, S., Cunha, F. V., di Ponzio, R., Lugli, L. F., Quesada,  
1050 C. A., Andersen, K. M., Chadburn, S. E., Wiltshire, A. J., Clark, D. B., Ribeiro, G., Siebert, L., Moraes, A. C.  
1051 M., Schmeisk Rosa, J., Assis, R., and Camargo, J. L.: Representation of the phosphorus cycle in the Joint  
1052 UK Land Environment Simulator (vn5.5\_JULES-CNP), *Geosci. Model Dev.*, 15, 5241–5269,  
1053 <https://doi.org/10.5194/gmd-15-5241-2022>, 2022.
- 1054 O’Sullivan, M., Spracklen, D. V., Batterman, S. A., Arnold, S. R., Gloor, M., and Buermann, W.: Have  
1055 Synergies Between Nitrogen Deposition and Atmospheric CO<sub>2</sub> Driven the Recent Enhancement of the  
1056 Terrestrial Carbon Sink?, *Glob. Biogeochem. Cycles*, 33, 163–180,  
1057 <https://doi.org/10.1029/2018GB005922>, 2019.
- 1058 Peng, J., Wang, Y. P., Houlton, B. Z., Dan, L., Pak, B., and Tang, X.: Global Carbon Sequestration Is Highly  
1059 Sensitive to Model-Based Formulations of Nitrogen Fixation, *Glob. Biogeochem. Cycles*, 34,  
1060 e2019GB006296, <https://doi.org/10.1029/2019GB006296>, 2020.
- 1061 Peoples, M. B., Giller, K. E., Jensen, E. S., and Herridge, D. F.: Quantifying country-to-global scale  
1062 nitrogen fixation for grain legumes: I. Reliance on nitrogen fixation of soybean, groundnut and pulses,  
1063 *Plant Soil*, 469, 1–14, <https://doi.org/10.1007/s11104-021-05167-6>, 2021.
- 1064 Phillips, R. P., Brzostek, E., and Midgley, M. G.: The mycorrhizal-associated nutrient economy: A new  
1065 framework for predicting carbon-nutrient couplings in temperate forests, *New Phytol.*, 199, 41–51,  
1066 <https://doi.org/10.1111/nph.12221>, 2013.
- 1067 Poggio, L., de Sousa, L. M., Batjes, N. H., Heuvelink, G. B. M., Kempen, B., Ribeiro, E., and Rossiter, D.:  
1068 SoilGrids 2.0: producing soil information for the globe with quantified spatial uncertainty, *SOIL*, 7, 217–  
1069 240, <https://doi.org/10.5194/soil-7-217-2021>, 2021.

- 1070 Poorter, H., Niklas, K. J., Reich, P. B., Oleksyn, J., Poot, P., and Mommer, L.: Biomass allocation to leaves,  
 1071 stems and roots: Meta-analyses of interspecific variation and environmental control, *New Phytol.*, 193,  
 1072 30–50, <https://doi.org/10.1111/j.1469-8137.2011.03952.x>, 2012.
- 1073 Reed, S. C., Cleveland, C. C., and Townsend, A. R.: Functional Ecology of Free-Living Nitrogen Fixation: A  
 1074 Contemporary Perspective, *Annu. Rev. Ecol. Evol. Syst.*, 42, 489–512, <https://doi.org/10.1146/annurev-ecolsys-102710-145034>, 2011.
- 1076 Reed, S. C., Yang, X., and Thornton, P. E.: Incorporating phosphorus cycling into global modeling efforts:  
 1077 A worthwhile, tractable endeavor, *New Phytol.*, 208, 324–329, <https://doi.org/10.1111/nph.13521>,  
 1078 2015.
- 1079 Reick, C. H., Gayler, V., Goll, D., Hagemann, S., Heidkamp, M., Nabel, J. E., Raddatz, T., Roeckner, E.,  
 1080 Schnur, R., and Wilkenskield, S.: JSBACH 3-The land component of the MPI Earth System Model:  
 1081 documentation of version 3.2, 2021.
- 1082 Rödenbeck, C., Zaehle, S., Keeling, R., and Heimann, M.: How does the terrestrial carbon exchange  
 1083 respond to inter-annual climatic variations? A quantification based on atmospheric CO<sub>2</sub> data,  
 1084 *Biogeosciences*, 15, 2481–2498, <https://doi.org/10.5194/bg-15-2481-2018>, 2018.
- 1085 Santoro, M., Beaudoin, A., Beer, C., Cartus, O., Fransson, J. E. S., Hall, R. J., Pathe, C., Schmullius, C.,  
 1086 Schepaschenko, D., Shvidenko, A., Thurner, M., and Wegmüller, U.: Forest growing stock volume of the  
 1087 northern hemisphere: Spatially explicit estimates for 2010 derived from Envisat ASAR, *Remote Sens.*  
 1088 *Environ.*, 168, 316–334, <https://doi.org/10.1016/j.rse.2015.07.005>, 2015.
- 1089 Seiler, C., Melton, J., Arora, V., and Wang, L.: CLASSIC v1.0: the open-source community successor to the  
 1090 Canadian Land Surface Scheme (CLASS) and the Canadian Terrestrial Ecosystem Model (CTEM) – Part 2:  
 1091 Global Benchmarking, *Geosci. Model Dev.*, 14, 2371–2417, <https://doi.org/10.5194/gmd-2020-294>,  
 1092 2021.
- 1093 Seiler, C., Melton, J. R., Arora, V. K., Sitch, S., Friedlingstein, P., Anthoni, P., Goll, D., Jain, A. K., Joetzjer,  
 1094 E., Lienert, S., Lombardozzi, D., Luyssaert, S., Nabel, J. E. M. S., Tian, H., Vuichard, N., Walker, A. P., Yuan,  
 1095 W., and Zaehle, S.: Are Terrestrial Biosphere Models Fit for Simulating the Global Land Carbon Sink?, *J.*  
 1096 *Adv. Model. Earth Syst.*, 14, e2021MS002946, <https://doi.org/10.1029/2021MS002946>, 2022.
- 1097 Shi, M., Fisher, J. B., Brzostek, E. R., and Phillips, R. P.: Carbon cost of plant nitrogen acquisition: Global  
 1098 carbon cycle impact from an improved plant nitrogen cycle in the Community Land Model, *Glob. Change*  
 1099 *Biol.*, 22, 1299–1314, <https://doi.org/10.1111/gcb.13131>, 2016.
- 1100 Shu, S., Jain, A. K., Koven, C. D., and Mishra, U.: Estimation of Permafrost SOC Stock and Turnover Time  
 1101 Using a Land Surface Model With Vertical Heterogeneity of Permafrost Soils, *Glob. Biogeochem. Cycles*,  
 1102 34, e2020GB006585, <https://doi.org/10.1029/2020GB006585>, 2020.
- 1103 Smith, B., Wårlind, D., Arneeth, A., Hickler, T., Leadley, P., Siltberg, J., and Zaehle, S.: Implications of  
 1104 incorporating N cycling and N limitations on primary production in an individual-based dynamic  
 1105 vegetation model, *Biogeosciences*, 11, 2027–2054, <https://doi.org/10.5194/bg-11-2027-2014>, 2014.
- 1106 Soper, F. M., Taylor, B. N., Winbourne, J. B., Wong, M. Y., Dynarski, K. A., Reis, C. R. G., Peoples, M. B.,  
 1107 Cleveland, C. C., Reed, S. C., Menge, D. N. L., and Perakis, S. S.: A roadmap for sampling and scaling



- 1108 biological nitrogen fixation in terrestrial ecosystems, *Methods Ecol. Evol.*, 2021, 1–16,  
 1109 <https://doi.org/10.1111/2041-210X.13586>, 2021.
- 1110 Stocker, B. D., Prentice, I. C., Cornell, S. E., Davies-Barnard, T., Finzi, A. C., Franklin, O., Janssens, I.,  
 1111 Larmola, T., Manzoni, S., Näsholm, T., Raven, J. A., Rebel, K. T., Reed, S., Vicca, S., Wiltshire, A., and  
 1112 Zaehle, S.: Terrestrial nitrogen cycling in Earth system models revisited, *New Phytol.*, 210, 1165–1168,  
 1113 <https://doi.org/10.1111/nph.13997>, 2016.
- 1114 Sullivan, B. W., Smith, W. K., Alan, R., Nasto, M. K., Reed, S. C., and Chazdon, R. L.: Spatially robust  
 1115 estimates of biological nitrogen (N) fixation imply substantial human alteration of the tropical N cycle,  
 1116 *Proc. Natl. Acad. Sci.*, 111, 8101–8106, <https://doi.org/10.1073/pnas.1511978112>, 2014.
- 1117 Sun, Y., Goll, D. S., Chang, J., Ciais, P., Guenet, B., Helfenstein, J., Huang, Y., Lauerwald, R., Maignan, F.,  
 1118 Naipal, V., Wang, Y., Yang, H., and Zhang, H.: Global evaluation of the nutrient-enabled version of the  
 1119 land surface model ORCHIDEE-CNP v1.2 (r5986), *Geosci. Model Dev.*, 14, 1987–2010,  
 1120 <https://doi.org/10.5194/gmd-14-1987-2021>, 2021.
- 1121 Terrer, C., Prentice, I., Jackson, R., Keenan, T., Kaiser, C., Vicca, S., Fisher, J., Reich, P., Stocker, B.,  
 1122 Hungate, B., Penueles, J., McCallum, I., Soudzilovskala, N., Cernusak, L., Talhelm, A., Van, S. K., Piao, S.,  
 1123 Newton, P., Hovenden, M., Blumenthal, D., Liu, Y., Muller, C., Winter, K., Field, C., Viechtbauer, W., Van,  
 1124 L. C., Hoosbeek, M., Watanabe, M., Koike, T., Leshyk, V., Polley, W., and Franklin, O.: Nitrogen and  
 1125 phosphorus constrain the CO<sub>2</sub> fertilization of global plant biomass, *Nat. Clim. Change*, 9, 684–689,  
 1126 <https://doi.org/10.1038/s41558-019-0545-2>, 2019.
- 1127 Thomas, R. Q., Brookshire, E. N. J., and Gerber, S.: Nitrogen limitation on land: How can it occur in Earth  
 1128 system models?, *Glob. Change Biol.*, 21, 1777–1793, <https://doi.org/10.1111/gcb.12813>, 2015.
- 1129 Tian, H., Chen, G., Lu, C., Xu, X., Hayes, D. J., Ren, W., Pan, S., Huntzinger, D. N., and Wofsy, S. C.: North  
 1130 American terrestrial CO<sub>2</sub> uptake largely offset by CH<sub>4</sub> and N<sub>2</sub>O emissions: toward a full accounting of the  
 1131 greenhouse gas budget, *Clim. Change*, 129, 413–426, <https://doi.org/10.1007/s10584-014-1072-9>, 2015.
- 1132 Tian, H., Yang, J., Lu, C., Xu, R., Canadell, J. G., Jackson, R., Arneeth, A., Chang, J., Chen, G., Ciais, P.,  
 1133 Gerber, S., Ito, A., Huang, Y., Joos, F., Lienert, S., Messina, P., Olin, S., Pan, S., Peng, C., Saikawa, E.,  
 1134 Thompson, R. L., Vuichard, N., Winiwarter, W., Zaehle, S., Zhang, B., Zhang, K., and Zhu, Q.: The Global  
 1135 N<sub>2</sub>O Model Intercomparison Project (NMIP), *Bull. Am. Meteorol. Soc.*, 99, 1231–1251,  
 1136 <https://doi.org/10.1175/BAMS-D-17-0212.1>, 2018.
- 1137 Tian, H., Xu, R., Canadell, J. G., Thompson, R. L., Winiwarter, W., Suntharalingam, P., Davidson, E. A.,  
 1138 Ciais, P., Jackson, R. B., Janssens-Maenhout, G., Prather, M. J., Regnier, P., Pan, N., Pan, S., Peters, G. P.,  
 1139 Shi, H., Tubiello, F. N., Zaehle, S., Zhou, F., Arneeth, A., Battaglia, G., Berthet, S., Bopp, L., Bouwman, A. F.,  
 1140 Buitenhuis, E. T., Chang, J., Chipperfield, M. P., Dangal, S. R. S., Dlugokencky, E., Elkins, J. W., Eyre, B. D.,  
 1141 Fu, B., Hall, B., Ito, A., Joos, F., Krummel, P. B., Landolfi, A., Laruelle, G. G., Lauerwald, R., Li, W., Lienert,  
 1142 S., Maavara, T., MacLeod, M., Millet, D. B., Olin, S., Patra, P. K., Prinn, R. G., Raymond, P. A., Ruiz, D. J.,  
 1143 Werf, G. R. van der, Vuichard, N., Wang, J., Weiss, R. F., Wells, K. C., Wilson, C., Yang, J., and Yao, Y.: A  
 1144 comprehensive quantification of global nitrous oxide sources and sinks, *Nature*, 586, 248–256,  
 1145 <https://doi.org/10.1038/s41586-020-2780-0>, 2020.
- 1146 Tian, H., Bian, Z., Shi, H., Qin, X., Pan, N., Lu, C., Pan, S., Tubiello, F. N., Chang, J., Conchedda, G., Liu, J.,  
 1147 Mueller, N., Nishina, K., Xu, R., Yang, J., You, L., and Zhang, B.: History of anthropogenic Nitrogen inputs

- 1148 (HaNi) to the terrestrial biosphere: a 5 arcmin resolution annual dataset from 1860 to 2019, *Earth Syst.*  
1149 *Sci. Data*, 14, 4551–4568, <https://doi.org/10.5194/essd-14-4551-2022>, 2022.
- 1150 Todd-Brown, K. E. O., Randerson, J. T., Post, W. M., Hoffman, F. M., Tarnocai, C., Schuur, E. A. G., and  
1151 Allison, S. D.: Causes of variation in soil carbon simulations from CMIP5 Earth system models and  
1152 comparison with observations, *Biogeosciences*, 10, 1717–1736, [https://doi.org/10.5194/bg-10-1717-](https://doi.org/10.5194/bg-10-1717-2013)  
1153 2013, 2013.
- 1154 Townsend, P. A., Serbin, S. P., Kruger, E. L., and Gamon, J. A.: Disentangling the contribution of biological  
1155 and physical properties of leaves and canopies in imaging spectroscopy data, *Proc. Natl. Acad. Sci.*, 110,  
1156 E1074–E1074, <https://doi.org/10.1073/pnas.1300952110>, 2013.
- 1157 Verger, A., Baret, F., and Weiss, M.: Near Real-Time Vegetation Monitoring at Global Scale, *IEEE J. Sel.*  
1158 *Top. Appl. Earth Obs. Remote Sens.*, 7, 3473–3481, <https://doi.org/10.1109/JSTARS.2014.2328632>,  
1159 2014.
- 1160 Vicca, S., Stocker, B. D., Reed, S., Wieder, W. R., Bahn, M., Fay, P. A., Janssens, I. A., Lambers, H.,  
1161 Peñuelas, J., Piao, S., Rebel, K. T., Sardans, J., Sigurdsson, B. D., Sundert, K. V., Wang, Y. P., Zaehle, S., and  
1162 Ciais, P.: Using research networks to create the comprehensive datasets needed to assess nutrient  
1163 availability as a key determinant of terrestrial carbon cycling, *Environ. Res. Lett.*, 13, 125006,  
1164 <https://doi.org/10.1088/1748-9326/aaeae7>, 2018.
- 1165 Vitousek, P. M., Menge, D. N., Reed, S. C., and Cleveland, C. C.: Biological nitrogen fixation: rates,  
1166 patterns and ecological controls in terrestrial ecosystems, *Philos. Trans. R. Soc. B Biol. Sci.*, 368,  
1167 20130119, <https://doi.org/10.1098/rstb.2013.0119>, 2013.
- 1168 Vuichard, N., Messina, P., Luysaert, S., Guenet, B., Zaehle, S., Ghattas, J., Bastrikov, V., and Peylin, P.:  
1169 Accounting for carbon and nitrogen interactions in the global terrestrial ecosystem model ORCHIDEE  
1170 (trunk version, rev 4999): multi-scale evaluation of gross primary production, *Geosci Model Dev*, 12,  
1171 4751–4779, <https://doi.org/10.5194/gmd-12-4751-2019>, 2019.
- 1172 Walker, A. P., Beckerman, A. P., Gu, L., Kattge, J., Cernusak, L. A., Domingues, T. F., Scales, J. C.,  
1173 Wohlfahrt, G., Wullschlegel, S. D., and Woodward, F. I.: The relationship of leaf photosynthetic traits -  
1174  $V_{cmax}$  and  $J_{max}$  - to leaf nitrogen, leaf phosphorus, and specific leaf area: A meta-analysis and modeling  
1175 study, *Ecol. Evol.*, 4, 3218–3235, <https://doi.org/10.1002/ece3.1173>, 2014.
- 1176 Wang, R., Goll, D., Balkanski, Y., Hauglustaine, D., Boucher, O., Ciais, P., Janssens, I., Penuelas, J., Guenet,  
1177 B., Sardans, J., Bopp, L., Vuichard, N., Zhou, F., Li, B., Piao, S., Peng, S., Huang, Y., and Tao, S.: Global  
1178 forest carbon uptake due to nitrogen and phosphorus deposition from 1850 to 2100, *Glob. Change Biol.*,  
1179 23, 4854–4872, <https://doi.org/10.1111/gcb.13766>, 2017.
- 1180 Wang, S., Zhang, Y., Ju, W., Chen, J. M., Ciais, P., Cescatti, A., Sardans, J., Janssens, I. A., Wu, M., Berry, J.  
1181 A., Campbell, E., ..., and Penuelas, J.: Recent global decline of CO<sub>2</sub> fertilization effects on vegetation  
1182 photosynthesis, *Science*, 370, 1295–1300, <https://doi.org/10.1126/science.abg4420>, 2020a.
- 1183 Wang, Y. P., Law, R. M., and Pak, B.: A global model of carbon, nitrogen and phosphorus cycles for the  
1184 terrestrial biosphere, *Biogeosciences*, 7, 2261–2282, <https://doi.org/10.5194/bg-7-2261-2010>, 2010.

- 1185 Wang, Z., Tian, H., Yang, J., Shi, H., Pan, S., Yao, Y., Banger, K., and Yang, Q.: Coupling of Phosphorus  
1186 Processes With Carbon and Nitrogen Cycles in the Dynamic Land Ecosystem Model: Model Structure,  
1187 Parameterization, and Evaluation in Tropical Forests, *J. Adv. Model. Earth Syst.*, *12*, e2020MS002123,  
1188 <https://doi.org/10.1029/2020MS002123>, 2020b.
- 1189 Wieder, W.: RegridDED Harmonized World Soil Database v1.2,  
1190 <https://doi.org/10.3334/ORNDAAC/1247>, 2014.
- 1191 Wieder, W., Cleveland, C., Lawrence, D., and Bonan, G.: Effects of model structural uncertainty on  
1192 carbon cycle projections: Biological nitrogen fixation as a case study, *Environ. Res. Lett.*, *10*, 044016,  
1193 <https://doi.org/10.1088/1748-9326/10/4/044016>, 2015a.
- 1194 Wieder, W., Cleveland, C. C., Smith, W. K., and Todd-Brown, K.: Future productivity and carbon storage  
1195 limited by terrestrial nutrient availability, *Nat. Geosci.*, *8*, 441–444, <https://doi.org/10.1038/ngeo2413>,  
1196 2015b.
- 1197 Wieder, W., Lawrence, D. M., Fisher, R. A., Bonan, G. B., Cheng, S. J., Goodale, C. L., Grandy, A. S., Koven,  
1198 C. D., Lombardozzi, D. L., Oleson, K. W., and Thomas, R. Q.: Beyond Static Benchmarking: Using  
1199 Experimental Manipulations to Evaluate Land Model Assumptions, *Glob. Biogeochem. Cycles*, *33*, 1289–  
1200 1309, <https://doi.org/10.1029/2018GB006141>, 2019.
- 1201 Wiltshire, A. J., Burke, E. J., Chadburn, S. E., Jones, C. D., Cox, P. M., Davies-Barnard, T., Friedlingstein, P.,  
1202 Harper, A. B., Liddicoat, S., Sitch, S., and Zaehle, S.: JULES-CN: a coupled terrestrial carbon–nitrogen  
1203 scheme (JULES vn5.1), *Geosci Model Dev*, *14*, 2161–2186, <https://doi.org/10.5194/gmd-14-2161-2021>,  
1204 2021.
- 1205 Wright, S. J., Turner, B. L., Yavitt, J. B., Harms, K. E., Kaspari, M., Tanner, E. V. J., Bujan, J., Griffin, E. A.,  
1206 Mayor, J. R., Pasquini, S. C., Sheldrake, M., and Garcia, M. N.: Plant responses to fertilization  
1207 experiments in lowland, species-rich, tropical forests, *Ecology*, *99*, 1129–1138,  
1208 <https://doi.org/10.1002/ecy.2193>, 2018.
- 1209 Yang, X., Thornton, P. E., Ricciuto, D. M., and Post, W. M.: The role of phosphorus dynamics in tropical  
1210 forests - A modeling study using CLM-CNP, *Biogeosciences*, *11*, 1667–1681, [https://doi.org/10.5194/bg-](https://doi.org/10.5194/bg-11-1667-2014)  
1211 [11-1667-2014](https://doi.org/10.5194/bg-11-1667-2014), 2014.
- 1212 Zaehle, S. and Dalmonech, D.: Carbon-nitrogen interactions on land at global scales: Current  
1213 understanding in modelling climate biosphere feedbacks, *Curr. Opin. Environ. Sustain.*, *3*, 311–320,  
1214 <https://doi.org/10.1016/j.cosust.2011.08.008>, 2011.
- 1215 Zaehle, S. and Friend, A. D.: Carbon and nitrogen cycle dynamics in the O-CN land surface model: 1.  
1216 Model description, site-scale evaluation, and sensitivity to parameter estimates, *Glob. Biogeochem.*  
1217 *Cycles*, *24*, <https://doi.org/10.1029/2009GB003521>, 2010.
- 1218 Zaehle, S., Medlyn, B. E., Kauwe, M. G. D., Walker, A. P., Dietze, M. C., Hickler, T., Luo, Y., Wang, Y. P., El-  
1219 Masri, B., Thornton, P., Jain, A., Wang, S., Warlind, D., Weng, E., Parton, W., Iversen, C. M., Gallet-  
1220 Budynek, A., Mccarthy, H., Finzi, A., Hanson, P. J., Prentice, I. C., Oren, R., and Norby, R. J.: Evaluation of  
1221 11 terrestrial carbon-nitrogen cycle models against observations from two temperate Free-Air CO<sub>2</sub>  
1222 Enrichment studies, *New Phytol.*, *202*, 803–822, <https://doi.org/10.1111/nph.12697>, 2014.

- 1223 Zaehle, S., Jones, C. D., Houlton, B., Lamarque, J. F., and Robertson, E.: Nitrogen availability reduces  
1224 CMIP5 projections of twenty-first-century land carbon uptake, *J. Clim.*, 28, 2494–2511,  
1225 <https://doi.org/10.1175/JCLI-D-13-00776.1>, 2015.
- 1226 Zechmeister-Boltenstern, S., Keiblinger, K. M., Mooshammer, M., Peñuelas, J., Richter, A., Sardans, J.,  
1227 and Wanek, W.: The application of ecological stoichiometry to plant-microbial-soil organic matter  
1228 transformations, *Ecol. Monogr.*, 85, 133–155, <https://doi.org/10.1890/14-0777.1>, 2015.
- 1229 Zhang, Y. and Liang, S.: Fusion of Multiple Gridded Biomass Datasets for Generating a Global Forest  
1230 Aboveground Biomass Map, *Remote Sens.*, 12, 2559, <https://doi.org/10.3390/rs12162559>, 2020.
- 1231 Zhang, Y., Xiao, X., Wu, X., Zhou, S., Zhang, G., Qin, Y., and Dong, J.: A global moderate resolution dataset  
1232 of gross primary production of vegetation for 2000–2016, *Sci. Data*, 4, 1–13,  
1233 <https://doi.org/10.1038/sdata.2017.165>, 2017.
- 1234 Zheng, M., Zhou, Z., Luo, Y., Zhao, P., and Mo, J.: Global pattern and controls of biological nitrogen  
1235 fixation under nutrient enrichment: A meta-analysis, *Glob. Change Biol.*, 25, 3018–3030,  
1236 <https://doi.org/10.1111/gcb.14705>, 2019.
- 1237 Zheng, M., Zhou, Z., Zhao, P., Luo, Y., Ye, Q., Zhang, K., Song, L., and Mo, J.: Effects of human disturbance  
1238 activities and environmental change factors on terrestrial nitrogen fixation, *Glob. Change Biol.*, 26,  
1239 6203–6217, <https://doi.org/10.1111/gcb.15328>, 2020.
- 1240